Accepted Manuscript

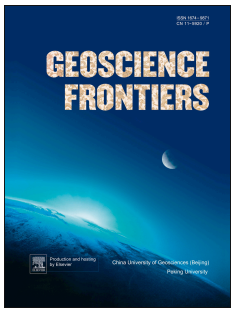

Deep-seated xenoliths and xenocrysts from Sytykanskaya pipe: evidence for the evolution of the mantle beneath Alakit, Yakutia, Russia

Dr. I.V. Ashchepkov , A.M. Logvinova , T. Ntaflos , L.F. Reimers , Z.V. Spetsius , N.V. Vladykin , D.S. Yudin , A.V. Travin , H. Downes , V.S. Palesskiy

PII: S1674-9871(14)00127-3

DOI: 10.1016/j.gsf.2014.08.005

Reference: GSF 322

To appear in: *Geoscience Frontiers*

Received Date: 21 May 2014

Revised Date: 31 July 2014

Accepted Date: 4 August 2014

Please cite this article as: Ashchepkov, I.V., Logvinova, A.M., Ntaflos, T., Reimers, L.F., Spetsius, Z.V., Vladykin, N.V., Yudin, D.S., Travin, A.V., Downes, H., Palesskiy, V.S., Deep-seated xenoliths and xenocrysts from Sytykanskaya pipe: evidence for the evolution of the mantle beneath Alakit, Yakutia, Russia, *Geoscience Frontiers* (2014), doi: 10.1016/j.gsf.2014.08.005.

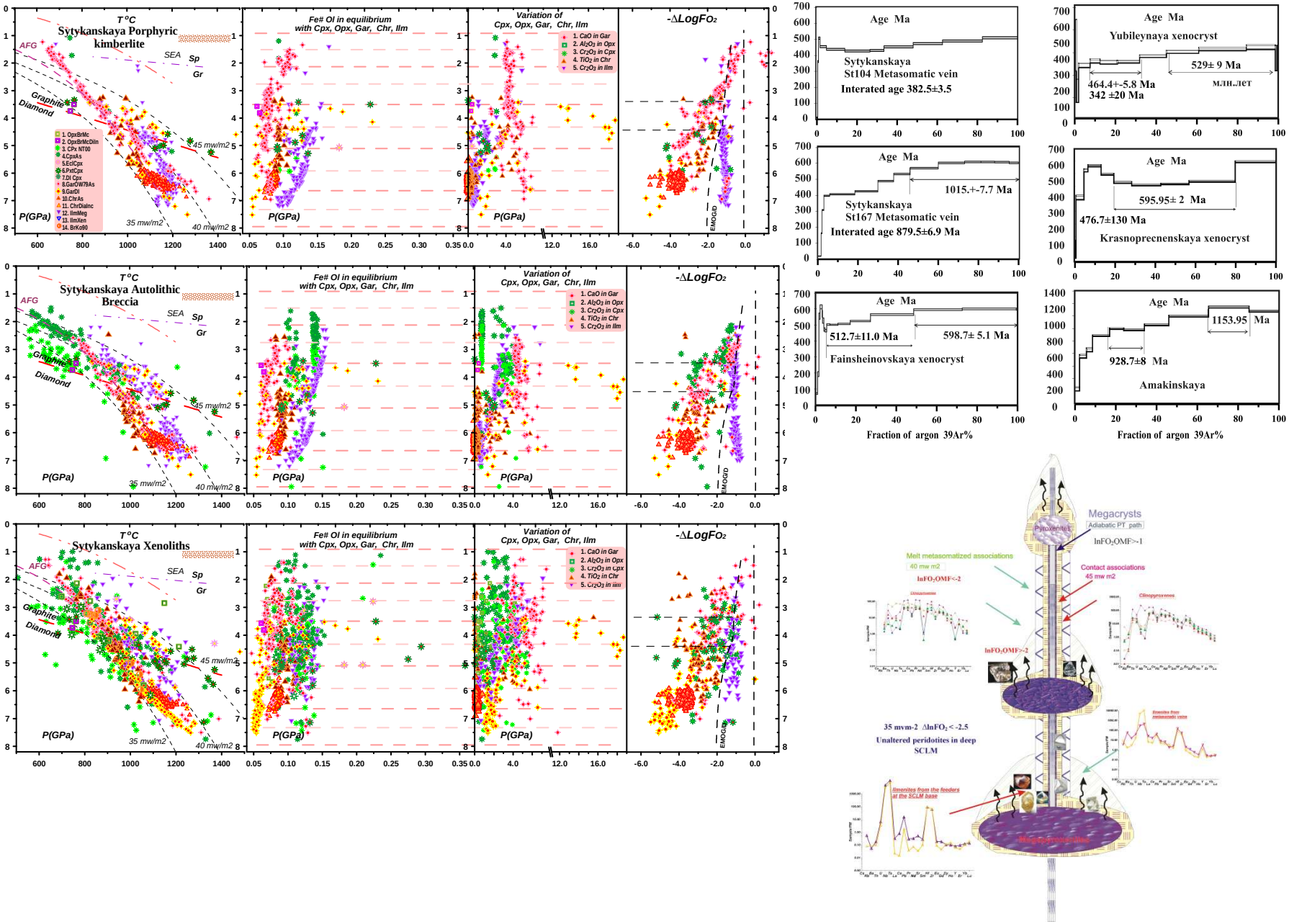

Deep-seated xenoliths and xenocrysts from Sytykanskaya pipe: evidence for the evolution of the mantle beneath Alakit, Yakutia, Russia

Ashchepkov I.V. (1), Logvinova A.M. (1), Ntaflos T. (2), Reimers L.F. (1), Spetsius Z.V. (3), Vladykin N.V. (4), Yudin D.S. (1,5), Travin A.V.(1,5,6), Downes H.(7), Palesskiy V.S. (1),

[1]*Institute of Geology and Mineralogy SD RAS, Koptyug ave 3, Novosibirsk, Russia*

[2]*University of Vienna, Austria*

[3]*Alrosa Stock Company, Mirny, Russia*

[4]*Institute of Geochemistry SD RAS, Irkutsk, Russia*

[5]*National Research Novosibirsk State University*

[6]*National Research Tomsk State University*

[7]*Department of Earth and Planetary Sciences, Birkbeck University of London, London, UK*

Word count: 14715

Display items: 18 Figures

Supplementary files 3

Submitted 21 may 2014

*Corresponding Author: Dr. Ashchepkov Igor Victorovich

Sobolev's Institute of Geology and Mineralogy SD RASc

academician V.A. Koptyug avenue 3.

63090 Novosibirsk, Russia

e- mails: Igor.Ashchepkov@igm.nsc.ru; garnet@igm.nsc.ru; igora57@mail.ru

phone (fax): 007-950-5918327

fax institute: 007 -383-2332792

Abstract

Heavy mineral concentrate and xenoliths from late autolithic breccia and porphyritic kimberlite of the Sytykanskaya pipe (Alakit field, Yakutia, Russia) were studied by EPMA and LA-ICPMS methods to obtain PTXfO_2 diagrams. Trends in P- Fe# - CaO - fO_2 for minerals from the porphyritic kimberlite show greater discontinuities than xenocrysts from the breccia. Xenoliths show the widest variation at all pressures. Protokimberlite systems are marked by ilmenite PT points that range from the lithosphere base (7.5 GPa) to a pyroxenite lens situated at intermediate depths (5 - 3.5 GPa) with increasing Cr because of AFC that formed two metasomatic groups with differing Fe#Ol (~ 10-12 and 13-15).

The first Opx-Gar-based mantle geotherm for the Alakit field based on 10 mineral associations is close to the 35 mW/m^2 geotherm at 6.5 GPa and 600^{o}C, i.e. near to the Moho. The oxidation state for the megacrystalline ilmenites in the lithosphere base is higher than for other kimberlites in Yakutia.

Calculated parental melts for clinopyroxene and garnet by xenocrysts from the breccia show highly inclined linear REE patterns with deep HFSE troughs similar to differentiated protokimberlite magmas. Melts calculated for metasomatic xenoliths have less inclined slopes without troughs in spider diagrams. Garnets reveal S-shaped REE patterns. Calculated melts for garnets from graphite-bearing Cr-websterites located mainly in middle part of the mantle column show slightly inclined convex REE patterns and Ba-Sr troughs with variable enrichment in Nb-Ta-U. The calculated parental melts for clinopyroxenes have inclined REE spectra with a depression in HFSE. Metasomatic clinopyroxenes have enriched patterns with Ba, Zr peaks.

^{40}Ar-^{39}Ar analyses of dispersed phlogopites from the Alakit mantle xenoliths yield a Proterozoic (1154 Ma) age, corresponding to continental arc metasomatism. Alkaline and Ti-rich veins with alkali amphiboles close to richterite formed at ~1015 Ma and mark a plume event in

Rodinia mantle. The~600-550 Ma stage relates to Rodinia break-up. The last metasomatic event near 385 Ma is related to the protokimberlite.

Keywords: kimberlites, mantle lithosphere, mantle xenoliths, thermobarometry, pyropes, ilmenites, geochemistry.

1. Introduction

The Alakite field occurs within the East Daldyn granulite-orthogneiss terrane which is related to the Anabar collision Paleoproterozoic belt including typical ancient island arc complexes (Smelov & Zaitsev, 2013; Rosen et al., 2006). In this field the basement is covered by Cambrian limestones dolomites with evaporates and later Permo - Triassic dolerites, revering to Siberian superplume event. Dating of basement sampled by drill holes and mantle xenoliths of the kimberlite pipes by Sm–Nd and Rb–Sr methods show three stages of development of the belt: 2200–2100 Ma, 1940–1760 Ma, and 1710–1630 Ma (Rosen et al ., 2006). Low crust mantle xenoliths are mainly granulates or gneisses (basic cumulates) containing in various proportions garnet - plagioclase and K- feldspar, clinopyroxenes (and orthopyroxenes) , amphiboles and biotites similar to those described in Udachnaya pipe (Koreshkova et al., 2009).

. There are distinct differences in the compositions of the minerals of mantle xenoliths from Alakite and Daldyn field as well as in the structures of the mantle columns (Ashchepkov et al 2010, 2013a; 2014).

The Sytykanskaya kimberlite pipe in the Yakutian kimberlite province is located near the boundary of the Daldyn and Alakite fields (Fig.1A) in the upper stretches of the Sytykan creek (Fig.1B) (Ashchepkov et al., 2010; Sobolev, 1977; Spetsius and Serenko, 1990).
It is buried by dolerite sills up to 70 m in thickness.

The pipe is composed of two independent bodies: the main northeast one consisting of early breccia and porphyritic kimberlite (PK) and late autolithic kimberlite breccia (ABK), and a

south-west body formed entirely of breccia. There are three phases of the kimberlite intrusion. All kimberlites types in Sytykanskaya pipes are richer in ilmenites and pyropes than other pipes from the Daldyn-Alakit region. The main ABK body contains a smaller proportion of pyrope and higher amounts of picroilmenite than the PK and early breccia. Pyrope content is lower in breccia from the south-west body than in the main north-eastern body. Mantle xenoliths are rare in the south-west body, but form up to 3.5 volume% in ABK in the central part where ultramafic xenoliths prevail and some diamondiferous eclogites were also found (Ponomarenko and Spetsius, 1976; Koptil et al., 1975; Lazko et al., 1982; Spetsius, 2007; Spetsius and Koptil, 2008). The ABK differs from the north-eastern PK in having a higher amount of dunites and garnet-spinel lherzolites. The early phases contain some cataclastic lherzolites, ilmenite-bearing peridotites and granular-grained garnet lherzolites, as well as Cr-diopside pyroxenites. Sytykanskaya pipe shows a sharp difference in diamond grade and different typomorphic features of diamonds in different kimberlite portions. Diamond grade in early breccia and PK of north-eastern body is seven-times lower compared with those of the ABK (Spetsius and Koptil, 2008; Spetsius and Serenko, 1990). The kimberlite in this pipe is now completely excavated and can be examined in spoil heaps near the excavation. The diamond grade is not very high compared with other large pipes in the Alakit field but some large diamonds up to 340 carats were discovered.

Among the kimberlites from Alakit field, the Sytykanskaya pipe is characterized by a large amount of deep-seated xenoliths which contain relics of fresh minerals, e.g. clinopyroxenes (CPx), garnets (Gar), olivines (Ol), phlogopites (Phl) , amphiboles (Amph), chromites (Chr), ilmenites (Ilm) and some other rare phases.

In this work we give the characteristics of the deep-seated xenoliths and xenocrysts from this pipe using mainly EPMA and ICP MS analyses and compare these results with the data for the concentrates from ABK and PK on the variation and PTXfO_2 diagrams. The xenocrysts of

ABK, PK and minerals from xenoliths were analyzed and plotted separately to see if there are any differences and to investigate the evolution of the mantle roots and feeder systems of the protokimberlites. Comparison of the compositional fields for the minerals from xenoliths and concentrates in variation diagrams allows us to recognize the details of the variations and grouping and find out their origin, which is also useful for estimation of potential diamond grade.

2. Methods and data

Minerals from the concentrates of ABK (~500) and PK (~400) from Sytykanskaya pipe were analyzed by electron probe microanalysis (EPMA). About 160 peridotite xenoliths of lherzolite, mainly veined lherzolites and enriched harzburgite type, half of which contain veins with phlogopites and other metasomatic minerals, and 10 pyroxenites and several eclogites mostly from the breccia were also analyzed with Camebax Micro microprobe using the methods described by Lavrent'ev et al. (1987) using a variety natural reference minerals and synthetic glasses for calibration. The accelerating voltage was 15 kV and a focused beam of 15 or 20 nA was used. Reduction procedure using "Karat program" (Lavrent'ev and Usova, 1994) was applied to the analyses. The relative standard deviation does not exceed 1.5%, the precision was close to 0.02-0.015% for minor elements. The most interesting xenoliths (15) were analyzed in detail in the University of Vienna in thin section using Cameca100 SX microprobe by utilizing wavelength-dispersive spectrometers with similar beam and voltage parameters but with a longer counting time (4 minutes) giving higher precision of analyses.

To compile the diagrams, we also used compositions of minerals from ~50 xenoliths and ~200 diamond inclusions analyzed by the same technique from the dissertation of Reimers (1994) and published data for the diamond-bearing eclogite associations (Spetsius, 2007; Spetsius and Koptil, 2008) (supplement 3).

Analyses of trace elements for three types of inclusions (xenocrysts from the breccia concentrate, metasomatic and veined xenoliths and garnet websterites) were obtained by LAM ICP MS methods using FinniganElement mass spectrometer and laser ablation system Nd YAG: UV NewWave in the Analytic Center of IGM SD RAS.

Phlogopite grains from xenoliths and xenocrysts from kimberlites were analyzed for $^{40}Ar/^{39}Ar$ age using the method described in detail by Travin et al. (2009). Quartz ampoules with samples were irradiated in the Cd-coated channel of a reactor (BBP-K type) at the Tomsk Polytechnic Institute. The gradient of the neutron flux did not exceed 0.5% of the sample size. Step-heating experiments were carried out in a quartz reactor with an external heater. The blank for ^{40}Ar (10 min at 1200°C) was no higher than 5×10^{-10} ncm^3. Ar was purified using Ti and ZrAl SAES getters. The isotopic composition of Ar was measured on a Micromass Noble Gas 5400 mass spectrometer.

3. Petrography

A collection of about 300 xenoliths was used to determine the variations of the petrographic groups in the mantle section beneath the Sytykanskaya pipe. The xenoliths include slightly depleted garnet lherzolites (Fig.2A, B, I, N) (35%) and harzburgites (10%) (Fig.2E, 2F), Sp lherzolites (10%) (Fig.2G), deformed peridotites (3%) (Fig.2C), Ilm-bearing peridotites where Ilm is a rock-forming mineral (Fig.2J, O), garnet phlogopite-ilmenite veined peridotite xenoliths (Fig.2F, G, L, I) (15%), garnet (Fig.2G) and Chr dunites (4%), garnet pyroxenites (Fig.3A-D) with ilmenites, graphite and mica (7%), Phl-Amph-Ilm-Cpx metasomatic veins (glimmerites) (8%) (Fig.2C), and a relatively small amount of eclogite (Fig.3E-F) (<0.2%). The percentage of rock types among the xenoliths is similar to those reported in previous studies (Bobrievich et al., 1959; Spetsius and Serenko, 1990; Manakov, 2005).

Most of the peridotite xenoliths contain phlogopite (Fig.2E-O) as do pyroxenites and eclogites. It is found as sporadic grains dispersed in the rocks and also as micro- and macro-veins, commonly with Cr-diopsides and more rarely garnet or chromite. Phlogopites commonly form coronas on garnets (Fig.2D, K) or together with pyroxenes and chromites totally replace garnet grains, forming symplectites or complex intergrowths of Cpx, Phl Chr (Fig.2C, K) and rarely secondary garnets (Fig.2K) (see supplement file 1) (sf1). Veins of Ilm-Phl-Cr-diopsides form stockworks in the peridotite matrix (Fig.2L) and cut through large porphyroclasts of olivine and garnets. Sometimes they are very thin and even dispersed. But in other cases the ilmenites form up to 5-10 % of rock volumes (Fig.2O) which happens commonly near the contacts with the megacrystalline associations. Some Ilm-Cpx or monomineral ilmenite veins cut large garnet porphyroclasts. Rare xenoliths of fine-grained dunite contain intergranular Ilm and ulvospinel grains as well as Cr-diopsides (Cr-Di) and garnet relics. They are relatively low temperature analogs of the deformed peridotites (Agashev et al., 2013; Boyd et al., 1997; Ionov et al., 2010). Eclogite xenoliths, which occur in other Yakutian kimberlite pipes (Snyder et al., 1997; Sobolev et al., 1984; Spetsius and Serenko, 1990; Pearson et al., 2005; Misra et al., 2004; Pernet-Fisher et al., 2014), are rare but we have two analyzed in our collection (Fig 3.E, F); though some diamond-bearing eclogites were discovered in this pipe (Spetsius and Serenko, 1990). Some of them also contain kyanite (Koptil et al., 1975). Several practically fresh garnet pyroxenites - websterites which also contain mica and chromites, were found in the PK facies (Fig 3A-D). Some of them contain significant amounts of graphite (Fig.4C).

The megacryst association is composed mainly of ilmenite (sf 1, fig.2A) and pyrope garnets. Several large ilmenite nodules represent large monocrystals cemented by fine Ilm grains and, in the outer contact, these aggregates contain Cr-Di and olivines typical for peridotites. These types of xenoliths are close to the contacts of the ilmenite polycrystalline nodules with deformed peridotites (Moore and Lock, 2001).

4. Mineralogy

Pyrope compositions on the diagram for the breccia and xenoliths (Fig.4A) and porphyritic kimberlites and pyroxenites (Fig.4B) show similarity in the configuration of the clusters and close interval of Cr_2O_3 variations to 13wt %. The total amount of sub-Ca garnets in the PK facies (Pokhilenko et al., 1991; Sobolev, 1977; Sobolev et al., 2003; 2004) is higher. The largest fraction of Ti-rich garnets plots in the low-Cr part but the increase in Cr-Ti can also be seen in Cr-rich part of the diagram for PK xenocrysts. Garnets from ABK and xenoliths show higher TiO_2 enrichment forming two separate levels. The pyroxenitic increase in both Cr and Ca and FeO enrichment is found in the diagram for garnets from metasomatic xenoliths (Fig.4A). In the P-Fe# and P-CaO diagrams (Figs. 10-11), the trends for garnets from the ABK and metasomatic xenoliths are more complex than for those from PK, possibly due to significant interaction during metasomatism. Garnets from PK reveal straighter and more stepped trends in all diagrams. Sub-calcic garnets dominate among the diamond inclusions and their amount is higher in the concentrates from PK compared to those from ABK

Cr-diopsides (Cr-Di) on the variation diagrams (Fig.5) fall into three intervals according to FeO content. Most of them belong to the low-Fe type (1-2.5% wt FeO) and low contents of all minor components including Cr which slightly increases with FeO; these come from enriched harzburgites and lherzolites. The Cr-Di varieties showing greatest variability in Na, Cr, Al, and Ti represent metasomatic veins in the peridotites from the middle part of the diagram (2-3.5 wt% FeO). The highest values are shown by Cr-Di from essentially micaceous glimmerites with alkali amphibole close to richterite (Hawthorne and Oberti, 2007). Garnet websterites with mica contain clinopyroxenes with Cr_2O_3 <2 wt%. The Fe-rich part corresponds to Ilm-bearing metasomatites which have quite different Al_2O_3 and TiO_2 contents.

Chromites are mostly Cr-rich varieties (Fig. 6). The fraction with Cr_2O_3>62 wt% that are located within the diamond window (Pokhilenko and Sobolev, 1995; Sobolev et al., 1973) is higher in the ABK and slightly less in the PK due to lower number of analyzed grains. But chromites from concentrates are enriched in TiO_2, compared to grains from xenoliths. The amount of such chromites is higher in the metasomatic xenoliths. The Al_2O_3 - Cr_2O_3 chromite plot does not show the common linear correlation but instead creates a cloud of points in the Cr-rich part which can be explained by a high degree of metasomatism. Only harzburgitic chromites from xenoliths form the common Al_2O_3 - Cr_2O_3 trend showing less metasomatic enrichment.

Imenites from Sytykanskaya pipe show the greatest variations (Fig.7A, B) and most complicated trends among those studied in the Yakutian province (Ashchepkov et al., 2010; 2013), showing wide variations in Cr and Al and other minor components. For ilmenites from the PK there are three main levels of Cr_2O_3 enrichment (Fig. 7B). In the Daldyn region three levels of Cr_2O_3 are common (Amshinsky and Pokhilenko, 1984; Kostrovitsky et al., 2006) but the Cr content in general is much lower than in Sytykanskaya and other Alakit pipes. The trend with ~ 0.5 wt % TiO_2 parallel to the FeO axis is formed by the uncontaminated protokimberlite melts. There is abrupt linear increase in this component from 2 to 3 wt% in the middle part of the TiO_2 trend. A further two levels at ~3.5 and 5 wt% Cr_2O_3 in the middle part of the TiO_2-Cr_2O_3 trends belong to the phlogopite-bearing metasomatites and glimmerite with alkali amphiboles which have very high Cr contents. In the left low-Ti part of the trend, there are also several levels of Cr-enrichment.

The ilmenite trends from the ABK and xenoliths (Fig. 7A) nearly coincide and reveal a division into the same clusters and trends with close Cr_2O_3 levels but the trends are more dispersed. Mg-rich low-Cr (group 1) ilmenites from Sytykanskaya pipe which are also found in some Ilm dunites show Cr decreases together with TiO_2. The MnO content is also decreasing in

general. The Cpx-bearing Ilm rocks are commonly richer in Cr, but those with Phl are most Cr-enriched. Ilmenites with low TiO_2 and MgO are relatively rare among the xenoliths.

Amphiboles in the Sytykanskaya pipe occur in the veins with phlogopites and ilmenites. Only those found in alkaline glimmerites are close to richterites (Hawthorne and Oberti, 2007). They are not as high pressure as those obtained in experiments at 7.0-9.0 GPa (Konzett and Ulmer, 1999), but they are similar to the K-Na type which was obtained in experiments at 3-4 GPa (Sweeney et al., 1993 a, b). Similar amphiboles were found in harzburgites from Udachnaya pipe (Solov'eva et al., 1997; Ashchepkov et al., in preparation). Amphiboles from Sytykanskaya xenoliths are more Cr-rich compared with richterites from MARIDs (Dawson and Smith, 1977; 1992; Boyd, 1990; Konzett et al., 2000; 2013) but are close to those in South Africa kimberlites (Dawson and Smith, 1980; Gregoire et al., 2002; 2003). Most amphiboles from veined xenoliths from Sytykanskaya are Cr-pargasite and one is pargasitic hornblende, similar to those found in the northern parts of Yakutia (Ashchepkov et al., 2004). The silica content of amphiboles correlates with pressure (Niida and Green, 1999). Only one pargasite from an ilmenite-bearing vein shows a high Ti content (Fig.8).

Phlogopites from Sytykanskaya xenoliths are highly variable in composition (Fig. 9). For the low-Fe varieties, two levels of Cr_2O_3 enrichment are visible: 0.5 and 2 wt % Cr_2O_3. Phlogopites with FeO>4 wt% and Cr_2O_3 close to 4-5 wt % are from the ilmenite-bearing veins. The Na_2O content is also up to 0.8 wt %, being lower in the middle part of the trend and high for the ilmenite-bearing associations. In the middle part of the diagram the TiO_2 level is highest ~ 2-5 wt %. Amounts of the minor components in phlogopites are accompanied by a decrease in SiO_2. The rise of Ti, Na and Cr corresponds to the increase of the Al/ (Al+Si) or eastonite component which corresponds to a pressure decrease (Arai, 1984; Mitchell, 1995).

5. PTX diagrams and variation of the oxygen fugacity conditions.

For the calculations of the PTfO_2 conditions we used combinations of the common thermobarometric methods (Brey and Kohler, 1990; Nimis and Taylor, 2000) and monomineral methods for garnets (Gar), clinopyroxenes (Cpx), chromites (Chr) and ilmenites (Ilm) (Ashchepkov et al., 2010; 2012; 2013a,b) calculated in the slightly modified PT program (see sf3). The thermobarometers for Cpx and Gar were checked using experimental data sets for peridotite (950) and eclogite systems (530). New corrections were introduced into Gar, Chr and Ilm barometers to increase the agreement between the calculated PT values and the experimental conditions (Ashchepkov et al., 2011; 2014 submitted).

PT conditions for garnet xenocrysts from PK (Fig. 10A) create nearly linear trends close to 600^{o}C at the Moho and decreasing to the 35 mW/m^2 geotherm at 6.5 GPa where there is an inflection corresponding to the convective branch, determined in many other mantle sections (Boyd, 1973; Rudnick et al., 1998; Kopylova et al., 1999). A similar geotherm can be calculated by Gar-Opx thermobarometry (Brey and Kohler, 1990) (Fig.11). The convective branch is marked by the high temperature trends for ilmenites and diamond inclusions of chromites and garnets. A pronounced inflection of ilmenites and diamond inclusions of eclogitic Cpx and Garnets is determined at 3.5 - 4 GPa along the graphite – diamond transition line (Kennedy and Kennedy, 1976) corrected to the lower pressures (Day, 2012). This explains the position of most diamond inclusions above the diamond stability field. Double geothermal arrays are detected between 4 and 6 GPa which probably corresponds to picroilmenite veins formed by protokimberlite melts. Such geothermal trends with a deviation from the conductive geotherms in the upper part were determined in the continental mantle of many regions worldwide (Dawson, 1980; Batumike et al., 2009; Boyd et al., 1997; Rudnick et al., 1998; Ashchepkov et al., 2013). Eclogitic Cpx from the diamond inclusions (Logvinova et al., 2005; Logvinova and Ashchepkov, 2008; Spetsius and Koptil, 2008; Efimova and Sobolev, 1977; Sobolev et al., 2004) show a wide range of geothermal conditions in the middle and lower part of the mantle section.

Opx inclusions together with Gar yield the lowest temperature cluster near 3.5 GPa, which is common for other mantle sections (Ashchepkov et al., 2013a). Chromite diamond inclusions form a compact cloud which deviates to the high temperature part of the diagram for deformed garnet peridotite and ilmenite megacrysts in the 7 - 5.5 GPa interval. Cpx diamond inclusions mostly trace the diamond – graphite line from the lowest temperature conditions for the Cr-poor varieties to high temperature branch for the eclogites of Cr-bearing hybrid type.

In this interval the Fe-content of garnets increased from the lithosphere base in 6 intervals from 7.5 to 1.5 GPa and rapidly rises from 2.5 GPa. The PT estimates for chromite and ilmenite coincide in pressure, but chromites mark relatively lower temperature conditions and show lower Fe# but mostly higher than garnets. Formation of this mineral probably occurred at the outer contacts of the protokimberlite melt feeders and in metasomatic veins.

Kinks in P-Fe# are observed near 3.2, 2.8 and 1.6 GPa. At the bottom of the chart (Fig. 10A), which presents the PTX estimates for inclusions in diamonds, there are four pressure intervals where CaO content in garnets is rather stable. The CaO content in garnets fluctuates in certain pressure intervals and abruptly splits near 4.5 and 5.0 GPa. Very high CaO is typical for garnets from pyroxenites and some eclogites from the middle pyroxenite lens (Pokhilenko et al., 1999) which is detected in most mantle sections beneath the Daldyn and Alakit fields (Ashchepkov et al., 2010; 2013a).

The ilmenite P-fO_2 trend of Sytykanskaya reveals comparatively oxidized conditions in the lithosphere base and then becomes less oxidized. This differs from the other mantle sections in Yakutia (Ashchepkov et al., 2004-2013), where it usually traces the dividing line of the stability of carbonatite melt and diamond (Stagno et al., 2010; 2013) which is close to the diamond stability field found by McCommon et al. (2001). The variations of oxidizing conditions defined for garnet and chromite are limited by this line on the left. Above 4.0 GPa oxidizing conditions for all minerals increase drastically.

For the xenocrysts found in ABK, the general variations of the P-Fe# trends are similar. However, skew and curved trends appears to be higher for the xenoliths and ABK xenocrysts, probably due to the influence of several branched systems of melts derived from kimberlites in different levels.

Picroilmenites formed by protokimberlite melt (More and Lock, 2001; Dawson et al., 1980; Ashchepkov et al., 2010) form two large clusters in the mantle column. Ilmenites and their parental melts in the lithosphere base are low in Cr_2O_3 and become significantly enriched in Cr_2O_3 near 4.5-3.5 GPa. The CaO and FeO trends for garnet at each level have formed separate trends which are similar to those from the PK but are more dispersed.

Clinopyroxenes from the ABK reveal mostly low pressure conditions. Deviations to HT conditions for Cr-bearing Cpx from peridotites occur at several levels, ranging from 6.5 to 3.5 GPa, which corresponds also to the metasomatites marked mainly by ilmenite PT points. Clinopyroxenes with Fe#Ol ~ 0.15 are close in Fe# to the most Fe-rich varieties of ilmenites which were formed from the latest and most fractionated derivatives of protokimberlite melt systems that, after crystallization of ilmenite-diopside systems, created significant amounts of diopside-phlogopite veins at the top of the mantle section. Associations with Fe#Ol ~ 0.11 -0.12 were formed by another more magnesian system that created polymineral Cpx-Gar-Ilm associations.

The arrays on the P-fO_2 diagrams look more stable in separate pressure intervals. For the chromite oxidation stage variations are similar to those from the PK but the amount of chromites in the deepest levels is higher.

PTX diagrams for the xenoliths (Fig.11) show a different configuration of trends and clusters in P-Fe#, X diagrams for some minerals, reflecting variations of peridotite associations in each mantle level. PT conditions for the most commonly used thermobarometry for 10 different associations (Brey and Kohler, 1990) nearly repeat the garnet geotherm from 6.5 to 2.0

GPa. This is the first polymineral geotherm for the mantle beneath the Alakit field. The PT estimates based on clinopyroxenes (Ashchepkov et al., 2010; 2012; 2013a,b; Nimis and Taylor, 2000) give a somewhat similar but broader range, reflecting high-temperature and low-temperature branches. The combined geotherms show a step deviation to 35 mW/m^2 conductive branch, similar to those for the mantle beneath Udachnaya pipe (Boyd et al., 1997; Ionov et al., 2010; Doucet et al., 2011; Goncharov et al., 2012; Ashchepkov et al 2010; 2013a, b). Clinopyroxene geotherms for Sytykanskaya are similar to those determined beneath the Daldyn field, and quite different from those determined for the mantle beneath Yubileynaya pipe (Ashchepkov et al., 2004).

The high pressure part of the ilmenite trend is formed by the uncontaminated low-Cr varieties but in the upper part the Cr-content increases. However, at the level of 4.0 GPa, it increases abruptly.

Some variations in the high-temperature part of the diagram (Fig. 11) near ~ 3.5 and 4.0 GPa corresponds to the metasomatites, thus marking the positions of the fluid-saturated melts as in South Africa (Gregoire et al., 2002; 2003; Gibson et al., 2008; Lazarov et al., 2012). The highest temperature conditions are defined by orthopyroxenes and ilmenites and clinopyroxene diamond inclusions which could be formed from protokimberlite melt derivatives.

Almost linear trends of Fe# for the pyroxenes and chromite in the middle part of the mantle columns correspond to the three types of evolving magmatic system responsible for the existence of at least three separate types of metasomatites. The highest Fe# (0.14-0.15) was for the Cpx and Ilm at depths of 5.5-6.5 GPa and slightly above, which corresponds to the Ilm peridotites. Two varieties with Fe#Ol 11 -0.12 were generated within the 5.5 to 3.7 GPa interval.

Two Gar-Cpx-Ilm sub-trends between Fe#Ol ~0.6-0.9 show the primary layering in the mantle. In the lower part of the mantle column, mantle inclusions create an evolving Fe-trend from the garnets to chromite diamond inclusions. Variation of CaO for the garnets from

xenoliths is higher than for xenocrysts. Variations of Cr-clinopyroxene of the xenoliths are also higher and vary in each level of the mantle column.

Very wide variations of oxidizing conditions are characteristic for the pyroxenes and garnets from xenoliths in each level of the P-fO_2 diagram (Fig.11) for xenoliths, which may correspond to intrusions of different melt portions and metasomatic gradients near the contacts. The widest variations of P- Fe#, fO_2 appear near the pyroxenite lens (Pokhilenko et al., 1999). Veins with phlogopite, ilmenites and alkali amphiboles were formed there as well as websterites with graphite and phlogopite. The most Fe#Ol-rich metasomatic clinopyroxenes, ilmenite and phlogopites occur in the middle part of the section. The most Cr-rich varieties are located at 3.0 GPa.

6. **Variations of trace elements of xenocrysts and xenolith minerals**

Rare earth element patterns in minerals were analyzed for three types of samples including xenocrysts from the ABK, metasomatic xenoliths, and glimmerites xenolith with alkaline amphiboles and garnet websterites with graphite.

There are systematic variations for trace elements (TRE) in each group. For Cr-diopsides from the ABK (Fig.12A) there are two major types of patterns. Samples with the highest La/Yb_n ratios (~400) and La/Ce_n ratios ~ 1 correspond to relatively low pressures. Others with La/Yb_n (45- 10) ratios high La/Ce_n and less inclined and nearly linear spectra are more deep-seated. These two types of Cpx patterns both show rather deep Ta, Nb and smaller Zr troughs. The most enriched Cpx pattern has La ~500xC1 and reveals no minimum of high field strength (HFSE) and elevated Ba and U. One Cpx pattern with a V-type shape is close to depleted Gar-free harzburgites of front- or back-arc settings (Ionov et al., 2013).

Garnets also reveal flattened REE patterns without strong HFSE depressions and as usual are dominated by the HREE. Some garnets have S-shaped spectra. But sharp dips in Sr and high

peaks in Pb and U, which are common for some lithospheric mantle peridotites (Ionov et al., 2010; Doucet et al., 2012), were not found. Instead they show elevated Th, U contents and even Ta, Nb and some also Zr-Hf.

There are two types of ilmenite REE patterns. The first one shows flattened patterns, typical for the most Mg-rich ilmenites (Clarke and Mackay, 1990). The other type reveals highly inclined patterns, enriched in LREE. All of them have HFSE maxima and are enriched in Y which increases along with the level of REE.

Clinopyroxenes from the metasomatic peridotites (Fig.12B) are also generally characterized by the slightly lower inclination of REE patterns, with La/Ce_n and $La/Pr_n<1$. This means that the melting degrees for the parental melts were higher than for the previous group, and the Gar/Cpx ratios in the source were lower. The level of Zr depletion is quite high. For many garnets, especially from deep part of the mantle column, deep troughs of MREE or S-spectra are found.

Ilmenites from xenoliths are characterized by inclined REE patterns and HFSE peaks slightly lower than the ilmenites of the first group with the low REE content. The difference between the Ta-Nb and Zr-Hf is also smaller, compared with the megacrystalline ilmenites. Phlogopites have characteristic patterns that resemble those for clinopyroxenes due to the high inclination of Gd/Yb_n. But the LREE part is flattened. This is typical of phlogopite patterns from peridotites in picrite basalts from the Vitim plateau (Ashchepkov et al., 2011).

The clinopyroxenes from glimmerites display inclined patterns with a small hump in LREE (Fig. 13 shaded area). Some of them also shows dips in Ta and Nb. One garnet (Fig. 13) marked by star has higher HREE level and a deep Ta-Nb trough.

A series of clinopyroxenes from garnet Cr-bearing pyroxenites (Fig. 13 marked by triangles) show different enrichments in REE highly inclined and straight line patterns and deep

troughs in Ba and varying enrichment in Nb-Ta-U which are lower than REE. Those with lower TRE levels reveal Zr-Hf dips.

Garnets from the pyroxenites show more straight line patterns than those from common lherzolites and pyroxenites from alkali basalts (Ashchepkov et al., 2011). They are characterized by deep troughs of Ba, Sr, and small Pb, U, small dips in Zr and Hf and quite different levels of Ta, Nb with general enrichment.

One phlogopite from glimmerites vein (Fig.13) show rather low REE level ~1xC1 and slightly inclined REE pattern with an inflection in Gd. It is enriched also in Ba, Th and slightly less in U, Ta and Nb. As with most phlogopites, it is characterized by a high concentration of Pb. Ulvospinel from the same vein displays rather low concentration of REE and a concave downward type pattern with the inflection in Gd similar to ilmenites. In the spider diagram the peaks in Ta-Nb and Zr-Hf are smaller than for the ilmenites but the dip in Y is lower. The ilmenites from pyroxenites show very high peaks in HFSE except Y. In general the geochemical features of the minerals from metasomatic glimmeritic veins and Cr-bearing pyroxenites look similar or supplementary.

7. ^{40}Ar-^{39}Ar ages of phlogopites

Compared with phlogopite ages of mantle peridotites from Daldyn field that mainly relate to Archean events, magmatic and metasomatic events in the Alakit region relate to the middle and late Proterozoic events and the Proterozoic– Phanerozoic boundary. One of the most ancient ^{40}Ar-^{39}Ar ages in the mantle of Alakit is given by xenocrysts from Amakinskaya pipe (1154 Ma). Ti-and alkali-rich veins with alkali amphiboles in the Sytykanskaya pipe give 1015 Ma (integrated 879 Ma) (Fig.14). Several phlogopite xenocrysts from other pipes in the Alakit field are close to 600-530 Ma (Fig.14). The latest event at 382 Ma is close to the beginning of the Late Devonian plume event. Similar ages are also noted in other isotopic systems (Griffin et al., 1999;

Pearson et al., 1997; Snyder et al., 1977; Smelov and Zaitsev, 2013). As a rule it is separated from appearance of the main kimberlite by an interval of about 25 -30 Ma.

8. Discussion.

8.1 Variations structure and evolution of the mantle section.

Comparison of three $PTfO_2$ diagrams for ABK, PK (Fig.10 A, B) and xenoliths (Fig.11) shows that the diagram for the ABK is more complex and probably more complete than that of the PK. Some additional trends for garnets are visible in the middle part of the section and the Chr also shows more complex and extending arrays. But the major difference is in the abundance of the Cpx which in the lower part corresponds mainly to the ilmenite PT conditions and Ilm-bearing mineral associations.

Commonly the thickness of the lithosphere beneath cratons is close to 200-250 km and eclogites are mainly found in the lower part of the mantle section (Kopylova and Caro, 2004; Heaman et al., 2006; Smit et al., 1997; Snyder et al ., 1997; Ashchepkov et al., 2011). Eclogites from Sytykanskaya pipe (Koptil et al., 1975; Lazko et al., 1982; Spetsius and Koptil, 2008) occur near 5 GPa close to the diamond – graphite transition. The cluster from 4 to 3.5 GPa with Fe# 0.09 -0.12 corresponds to metasomatites and hybrid eclogites. But the upper part of SCLM Cpx trends nearly coincides with the PT estimates for the low pressure ilmenite trend which probably traces the developing protokimberlite channels and fractionation of the protokimberlite magma. There are two sub-trends for the CPx extending to the Moho and probably reflecting the large vein associations (Fe# 0.13-0.15) and accompanying metasomatites in peridotites.

The $PTfO_2$ diagram for the xenoliths shows a stepped structure of the mantle column, especially on P – Fe# - fO_2 diagrams where several nearly isobaric levels are found from 3.5 GPa to the base of the SCLM. Garnets together with Opx and most Chr and some Cpx estimates show rather low-T geothermal branch which is close to the average Arkhangelsk geotherm (Afanasiev

et al., 2013) determined by the method used by Mather et al. (2011) which cuts the conductive geotherms and is close to 35 mWm^{-2} at 6.5 GPa and is close to 600^{o}C near Moho. A similar geotherm has been determined for 10 different Opx-Gar mineral associations. Different configurations of the PT and P-CaO, FeO, TiO_2 etc. arrays are detected for each mineral type. Garnets show three trends of P-Fe#: a primary one in which Fe#=0.6-0.7 and two stages of melt percolation with Fe#0.8-0.9 and 0.11. The more Fe-rich associations within the pyroxenite layer coincide with the Ilm metasomatites and hybrid eclogites and probably reflect a different metasomatic event that took place in Rodinia (Santosh et al., 2009) mantle, with the last event relating to the formation of protokimberlites. They show several joint trends for the Ilm and Cpx in Fe, with Fe# ~0.11 and 0.13 which increases in the upper part up to the pyroxenite layer.

Garnet diamond inclusions yield PT estimates and a P-Fe stepped trend that reflects primary mantle layering consisting of at least 6 intervals in the lower part of SCLM starting from 3.5GPa. They are also visible on the P- fO_2 diagrams where there are several lines of equal pressures but different fO_2.

The diamonds inclusions of different type mark different levels within mantle column. Most peridotitic garnet diamond inclusions of sub-calcic type relate to cold ancient geotherms (Griffin et al., 2002; 2009; Pearson and Wittig, 2014; Taylor and Anand, 2004) and mark five levels from the lithosphere base to the pyroxenite layer. A few garnet diamonds inclusion are more Fe-rich and coincide with PT conditions determined for chromite diamond inclusions and partly overlie hot branch produced ilmenites related to protokimberlites. They reveal pyroxenitic enrichment in CaO and show higher Fe#Ol values~ 0.07- 0.09.

Cr-bearing pyroxene diamond inclusions (Fe#=0.1-0.15) and some diamond eclogites which were found within the depth range of 3.5 -4 GPa refer mainly to the 40-45 mW/m^2 geotherm. These high-MgO varieties are related to pyroxenites and trace an interval from the lithosphere base to pyroxenite lens, like those found beneath the Jericho pipe in Canada (Smart

et al., 2009) at 5 -5.5 GPa and probably reflect primary mantle stratification. The omphacite diamond inclusions and kyanite eclogites which are similar to CaO-rich eclogites from Canada (Heaman et al., 2006) show different heating degrees ~ 35-45 mW/m^2. The latter probably reflect interaction with protokimberlite melts. High variations of compositions and PT conditions of pyroxenes associated with diamonds is explained by interaction with different magmas that produced different types of pyroxenites (Gonzaga et al., 2010) including hybrid Cr-bearing and kyanite eclogites (Spetsius and Koptil, 2008).

Cr-bearing garnet with graphite websterites are located in different levels within 4.0-5.0 GPa and some of them near the Moho. A few pyroxenites are found at pressures of 6.0-6.5 GPa. Their position and geothermal conditions are similar to those found beneath Mir (Roden et al., 2006) and Udachnaya pipe (Pokhilenko et al., 1999; Snyder et al., 1997; Sobolev, 1977).

The metasomatic horizon where the alkaline amphiboles are located judging from the thermobarometry lies within the lower part of the pyroxenite layer (4-4.5GPa) and, judging by the high alkalinity and TiO_2 content, should be related to the plume event which took place at the early stage of Rodinia (Condie, 2004; Santosh et al., 2009).

The ilmenite trend for the ABK stage is more extensive than for the PK stage and probably reflects the transfer of protokimberlite melts to the upper part of the mantle section. The abrupt linear increase in this component from 2 to 3 wt % Cr_2O_3 probably relates to formation of melt channels in the mantle column, which was accompanied by dissolution of minerals from country rocks, mainly chromite and Cr-diopsides. Compared with the PK, ilmenites from the upper part of SCLM are more Cr-rich. In the upper part the oxidation state of the ilmenites and accompanying metasomatites increase which probably corresponds to an increase of differentiation of protokimberlites and metasomatism under the influence of melt systems.

The complex configuration of the ilmenite trends for both stages reflects the complex structure of the feeder system for the protokimberlite melts which in general is divided into two levels. This TiO_2-Cr_2O_3 configuration is quite different compared with the situation in South Africa where Cr-enrichment is common for the low- and high-Mg ilmenite varieties (Haggerty, 1975). It is related to the metasomatites located in the upper and lower parts of the protokimberlite system. The most alkaline and Ti-enriched glimmerite veins refer to the middle of SCLM near the pyroxenite layer.

Ilmenites from xenoliths also mark sheared peridotites which mostly belong to the lower part of the mantle section but several PT estimates like in the SCLM beneath Dalnyaya pipe (Rodionov et al., 1991) also mark intermediate levels between 6.5 and 3.5 GPa similar to the mantle section beneath the Kimberly pipe in South Africa (Katayama et al., 2009). This corresponds probably to interaction with highly volatile-rich melts which decrease the mechanical properties of peridotites (Karato, 2010). Location of the clusters of Ilm-bearing metasomatites in different levels probably corresponds to primary mantle layering. Possibly their location was determined by the conditions of the rising protokimberlite melt with periodic boiling near the boundaries which are traced by the magma bodies. Probably the combined phenomena and dynamic of the melts upwelling was determined by the primary mantle banding. Some Ilm-bearing peridotites show rather wide compositional range of ilmenites as is also common for the polymict breccias (Giuliani et al., 2013)

The Ilm- Gar wehrlites in the lithosphere base are similar to those found in the beginning of the fractionation trend for protokimberlites beneath the Dalnyaya pipe (Rodionov et al., 1988). The accompanying metasomatites could be diamond-bearing like those found beneath the Udachnaya pipe (Pokhilenko et al., 1976) because some ilmenites were found as inclusions in diamonds (Reimers, 1994).

The difference of the $PTXfO_2$ configurations produced by the xenocrysts from PK and ABK concentrates and layering reconstructed by xenoliths is explained by the fact that xenocrysts in kimberlites are mainly from the wall rocks and contact zones of the feeding channels which were influenced by the protokimberlites forming the channels of the melt path. Rather smooth PT trends with the several inflections reflect the evolution of the protokimberlite melts. This also explains the variations of xenocrysts from the PK and ABK. They reflect mainly the evolution of the contact association of protokimberlites in two stages.

The rather long Ilm-Cpx and Gar P-Fe# trends may mark not only the contact associations but also the direct melt percolation through the mantle columns (Foley et al., 1992). But carbonate-like and relatively oxidized melts should crystallize near the graphite – diamond transition (Tappe et al, 2006).

8.2 Trace element evidences for magmatic and metasomatic events in mantle column beneath Sytykanskaya pipe

Geochemical features of the xenocrysts from the PK and ABK also reflect the characteristics the melts which reacted with the peridotite wall rocks. To determine the primary features we reconstructed the melts using partition coefficients (KD) for Cpx (Hart and Dunn, 1993; Bedard, 2006), Gar (Hauri et al, 1994; Green et al., 2000) and for ilmenites (Zack and Brumm, 1998) (Fig.15 A, B).

The parental melts for Cpx from concentrates have two types of highly inclined patterns probably produced under the influence of the protokimberlites which show slightly lower incompatible elements relative to REE similar to megacrysts from the Sloan pipe in Colorado (Ashchepkov et al., 2013b). Ta and Nb are much lower than the REE which results from co-precipitation of ilmenite. The decoupling of the Ta-Nb and Zr-Hf seen in glimmerites (Fig.16)

may be influenced by rutile. The dips in Zr correspond to zircon precipitation. Two types of REE and TRE patterns with different $(La/Yb)_n$ ratios are produced by melts which precipitated (were in equilibrium) different amounts of garnet and were probably derived from protokimberlite melts at different depths. The dips in Pb show that these melts precipitated sulfides; the only sample that has Pb, U peaks and lower REE probably results from the admixture of partial melts derived from peridotite material. The sample with the highest TRE level probably was derived from the most fractionated fluid-saturated melt which did not precipitate Ilm.

Garnets from the concentrates show hybrid features which may be seen in the inflected patterns with minima in HMREE and elevated LREE. The HFSE-enrichment commonly results from fertilization by carbonatite melts (Griffin et al., 1999b; Burgess and Harte, 2004; Ashchepkov et al., 2013; Marchesi et al., 2013). We did not study zonation in TRE but this is a possible explanation (Howarth et al., 2013) of the systematic difference in TRE geochemistry between the ABK xenocrysts and minerals from xenoliths.

Many veined peridotite xenoliths from Sytykanskaya pipe show inflected patterns with HREE minima. Contamination of wall rocks and dissolution of some minerals in the metasomatic veins may be the reason for the inflected REE patterns. Modeling of melting and fractionation (Fig.17A) shows that most pyroxenes in concentrates cannot be produced by partial melts of garnet peridotites with common 1-0.5% melting degree and realistic Ga/Cpx ratios < 1. Commonly such melts have humped REE patterns with $(La/Sm)_n$ <1. The linear inclined patterns could be a result of very low degree ~0.01% melting of already enriched peridotites (Fig.17B). Thus, most Cpx parental melts result from a high degree of protokimberlite differentiation.

The garnet parental melts show sometimes major U maxima but also Th and Ba enrichment, which are a relic subduction signature visible in some Udachnaya peridotites (Doucet et al., 2013), but some elevated LILE components and Th are a result of metasomatism,

produced by carbonatite-type melts Zr minima are more typical for H_2O than for carbonatite type of metasomatism. Such melts may be found in back-arc settings (Fig. 15A, B).

The patterns of the melts parental for phlogopites show a flattened hump in the MLREE part. This is a result of crystallization from melts which had already crystallized clinopyroxenes with patterns that are humped in the LREE part. The same feature was found for phlogopites and some clinopyroxenes in Vitim pyroxenites (Ashchepkov et al., 2011)

Metasomatites and pyroxenites show similar signs of metasomatism with elevated HFSE (Fig. 16) components which commonly imply carbonatite-related metasomatism. The parental melts for the minerals from glimmerites with alkali amphibole show significant LILE enrichment which suggests a fluid-rich environment.

Series of clinopyroxenes from garnet pyroxenites (Fig. 16) with graphite generally show a cognate origin possibly formed by the different melting degree accompanied by melt differentiation and precipitation of minor ilmenite and rutile. Most parental melts for clinopyroxenes show inclined and concave downward patterns which are not common for alkaline melts formed in the garnet facies. The lack of Sr, Pb, U anomalies shows that peridotite did not undergo fluid flux from a subducted slab subjected to the typical oceanic metasomatism. Garnet and clinopyroxene parental melts from pyroxenites reveal disequilibria in most cases. Garnet parental melts have flatter patterns but higher U, Th peaks.

The origin of the pyroxenites may be complex. The inclination of the REE patterns for garnets is close to those of the subduction-related eclogites (Snyder et al., 1997). Possibly they were produced by the hybridization of Ti-bearing plume melts with subduction-related eclogites causing also the straight-line REE patterns for garnets and pyroxenes with inflections at Gd.

The parental melts of the ilmenites are quite different in TRE (Fig. 15 A, B). The low concentrations are typical for the dunite veins in the base of the SCLM and possibly accompanying metasomatites. The inclined patterns with the linear REE are typical for

protokimberlite melts formed in the lower and middle part of mantle column. Patterns that are highly enriched in TRE are typical for the metasomatic Gar-bearing associations enriched in HFSE to different degrees. They also show inflections that can possibly be explained by dissolution of separate minerals by highly differentiated volatile-enriched melts.

The dips in Ta-Nb for the melts parental for ilmenites (Fig 15) are characteristic of ilmenites derived from protokimberlite melts that have crystallized a large amount of ilmenites and garnets. The convex REE tendencies are characteristic of the final crystallization of melts that precipitated phases with convex REE distributions. Such patterns are common for phlogopites. Phlogopite in this same vein shows a more pronounced tilt in HREE and the LMREE.

8.3 *Stages of the metasomatism*

8.3.1. Ancient metasomatism. The ^{40}Ar-^{39}Ar age of 1015 Ma suggests that the mantle beneath Alakit contains ancient metasomatites which appear to be associated mainly with water-bearing highly alkaline melts, together with relatively young metasomatites which were produced by differentiated carbonatite-type melts. The latter are younger than those found in mantle column beneath Udachnaya pipe (Pokhilenko et al., 2012). The first stage was probably influenced by back-arc melts (Pearson et al., 1997) with relatively high Ba, Sr, Pb, Sr, K and Na and HFSE anomalies. Presence of rutile supports this idea. In our case the scattered phlogopites suggest the influence of K-rich fluids within a continental margin environment which should be accompanied by lamproite magmatism. But the rarity of HFSE anomalies for common xenoliths means relatively reduced conditions.

More ancient events were not found yet in Sytykanskaya but may be suggested because of age for the xenocryst from Amakinskaya pipe. Signs of primary depletion by fluid-rich melts forming sinusoidal garnet REE patterns are quite common for the metasomatized mantle

peridotites. Garnet parent melts are commonly not in equilibrium with those calculated for the clinopyroxenes (Fig. 15) even in the same xenoliths (Fig. 16). Relatively low alkalinity and Fe # are characteristic for pyroxenes from this stage. The abundance of carbon may be a sign of subduction processes but graphite carbon isotope values are close to average mantle values.

Formation of websterites with phlogopite and graphite which may be complementary to the ancient metasomatites with fluctuations of U, Ta, Nb and low LILE may relate to this time. Presence of such pyroxenites in different levels within 6 – 4 GPa interval suggests pervasive melt percolation (Griffin and O'Reilly, 2007). This type of metasomatite is located in the low-Fe part of the variation diagrams for phlogopites (Fig.9) and pyroxenes (Fig.5). Judging by the abundance of S-type garnets (Fig. 2), almost the entire lithospheric mantle column under the Sytykanskaya pipe was subjected to large-scale phlogopite metasomatism which probably corresponds to the earliest ages about 1153 Ma (Fig. 17).

The formation of highly alkaline and Ti metasomatic veins with richterite ~1015 Ma ago may relate to large-scale plume-related melt percolation in the lithospheric mantle beneath Rodinia (Santosh et al ., 2009). Similarly in the South African mantle, phlogopite metasomatism dated at 1100 Ma is associated with the plume-generated Bushveld intrusion (Hopp et al., 2008). The superplume events commonly show the nearly coincidence of the all ages for Phl in mantle and low crust (Eccles et al., 2010). Kimberlites and lamproites in India (Rao et al., 2013) and Australia have nearly the same age, close to 1100 M, so this event took place worldwide.

Most of the pyroxenes from the concentrates show the protokimberlite features and fractionation patterns which have HFSE and Pb dips (Fig. 15A). Typical partial melts from peridotites commonly show lower inclination of REE pattern and smoother TRE spider diagrams (Fig. 15B). Most of the metasomatic associations reveal transitional features between these two end members.

8.3.2. Plume event referring to the Rodinia supercontinent breakdown

The largest event shown in the lithosphere under many Alakit pipes took place ~ 600-550 Ma ago, close to the Proterozoic –Phanerozoic boundary. Such an event is close to the time of melilite carbonatite magmatism in the Sayan Foothills and the Baikal area (Travin et al., 2002). This should correspond to the Ti-rich carbonatite-type metasomatism.

7.3.3 Protokimberlite stage. High-Fe and Ti metasomatic ilmenite veins are related to the protokimberlite melts. The amount of ilmenites in the pipe is rather high. It seems that protokimberlite melts could dissolve early metasomatites in the base of mantle column. An essentially oxide liquid may have formed a separate phase due to immiscibility with the silicate melt (Clarke and Mackay, 1990) and may have formed an intrusive phase. Almost monomineral ilmenite veinlets in peridotites cut the large porphyroclasts of garnets in some xenoliths.

Furthermore, metasomatites related to the ilmenites are much more Fe-rich than usual in peridotites. The influence of ilmenite metasomatism appears to be widespread in the xenoliths, although scattered Phl metasomatism dominates. It is not clear to what extent the protokimberlite melts influenced the lithospheric mantle. Did they cause changes only near the conducting channels or was it more widespread? An answer could be given by the study of xenoliths of other small pipes of this field.

The time gap of 25 -30 Ma between the beginning of plume activity and mantle metasomatism and the appearance of major kimberlitic explosions is documented also by other isotopic systems (Smelov and Zaitsev, 2013). However, it is not possible to discount the presence of excess argon, which can produce a more ancient age, measured only by the ^{40}Ar-^{39}Ar method. However, the dating of kimberlite by this method gives acceptable results (Agashev et al., 2004).

8.4. Structure of the feeder systems and the explanations

It is necessary to emphasize that many of the associations of mantle xenoliths from Sytykanskaya pipe show signs of disequilibria (Reimers, 1994; Reimers et al., 1998) like those detected in xenocrysts and intergrowths from Zagadochnaya pipe (Nimis et al., 2007; Ziberna et al., 2013). They are visible in the veins and veinlets and in rims on garnets and other reaction products which could be explained by multistage metasomatism. There are also coronas on garnets (Fig.2, Sf1) sometimes monomineralic consisting of phlogopites or ilmenites, sometimes polymineralic together with pyroxenes and chromites or ulvospinels. Some aggregates after garnets consist of symplectites of Phl together with Cpx, Ilm or Chr. Many garnets show reaction alteration or complete substitution which may be not only the result of reactions and dissolution but also a sign of mantle diapirism which is proved by thermobarometry.

There are several possibilities to explain the wide variation of the fO_2 conditions and geochemistry of mantle xenocrysts. The internal zones for the feeders and magmatic chambers should represent the geochemistry of pure protokimberlite melts highly enriched in fluids (Moore & Lock, 2001; Kopylova et al., 2009) for the low-Cr or Cr-free associations (Ol, Cpx, Ilm , Gar) showing signs of fractionation. The outer rims should consist of the zones of the Cr-bearing associations of relatively coarse Ti-enriched Cpx, with elevated Cr content. The geochemistry of the grains should be close to the protokimberlite melts. Such pyroxenes are found not only in Sytykanskaya but also are typical for Sloan (USA). In the outer contacts the influence of the direct intrusions should be less. But the small veinlets produced by fluid-enriched melts which could be of quite variable compositions and produce dispersed intergranular Phl or ilmenites or veins of monomineral or mostly polymineral associations.

8.5. Influence of mantle metasomatism on diamond grade.

Among the diamond inclusions of Sytykanskaya pipe, chromites dominate (Manakov, 2001) as in many other pipes from the Alakit field (Sobolev et al., 2002). Another widely distributed group is sub-Ca pyropes. In a subordinate quantity the high-temperature Cr-pyroxene, apparently related to the proto-kimberlite, and usual Fe-enriched Cr-diopsides from metasomatites are found. Sub-calcic pyropes (Pokhilenko and Sobolev, 1995; Sobolev et al., 1973; Sobolev, 1977) undoubtedly came from the ancient giant-grained dunites (Pokhilenko et al., 1991), which form veins and lenses in the lithospheric mantle. The age of such garnets by analogy with others may be 3.5-2.7 Ga. But the majority of garnets are slightly younger and thus peridotites have undergone to the ancient metasomatism (Malkovets et al., 2012). The situation in SCLM beneath the Alakit field may be similar. The chromite diamond inclusions form an individual group. They are sometimes associated with the pyropes and differ in PT conditions. It seems that they are closer in conditions to the ilmenites and some high-temperature and relatively Fe-rich pyropes. The giant-grained dunite veins with pyropes (Pokhilenko et al., 1995) and chromites have a different genesis; however, they both served as conduits of melts like dunites in ophiolites (Batanova &Savelieva, 2009). Chromite dunites could be formed with the participation of the high-temperature fluid-rich melts, which, as a rule, relate to a separate stage of the protokimberlitic process. Thus, if this is correct, then a particularly large part of the diamonds of the Sytykanskaya pipe and Alakit field as a whole is connected with the protokimberlite stage. From other side the presence of the highly depleted substratum in the lower part of the lithospheric mantle is also a contributory factor for an increased diamond grade.

However, judging by the oxidation states for the ilmenites, protokimberlitic melts beneath the Sytykanskaya pipes were strongly oxidized, by 1 log unit higher than the diamond stability line (McCommon et al., 2001).This possibly served as the reason for the dissolution of many diamonds (Fedortchouk et al., 2005). Variations of the oxygen fugacity even in one xenolith may be very high (Solov'eva et al., 2012). Reduction of the metasomatic carbonatite melts on

peridotites may be the reason for the diamond growth. The opposite significant influence of oxidized melts or fluid is the reason for diamond dissolution. It is likely that the inner and outer contact zones of the protokimberlite melt bodies are subjected to the interaction in different degree. The simplified model of such zonation (Fig.18) suggests differentiation of the protokimberlites in the intermediate magmatic chambers and during melt movement in feeders and reaction with wall rock peridotites.

Conclusions

1. The mantle column beneath the Sytykanskaya pipe experienced multistage plume-related metasomatism corresponding to the early and mainly to the late stages of Rodinia supercontinent.
2. Signs of ancient arc or subduction-related events are recognized in several mineral associations, but most minerals suggest reactions with plume-related melts.
3. Trace element features of garnets and clinopyroxenes indicate disequilibrium in their parental melts
4. Comparison of the concentrates from porphyritic kimberlites and breccia show an increase of the metasomatic associations and evolution of the mantle column.
5. Metasomatism of the mantle column and relatively high oxidation stage is probably the reason of the relatively low diamond grade of this kimberlite pipe.

Acknowledgements

The work is supported by RBRF grants 05-05-64718, 03-05-64146; 08-05-00524; 11-05-00060; 11-05-91060-PICS and joint research projects of IGM SB RAS and ALROSA Stock company 77-2, 65-03, 02-05. We are grateful to the ALROSA Stock Company for help in sample collecting.

References

Afanasiev, V.P., Ashchepkov, I.V., Verzhak, V.V., O' Brien, H., Palessky, S.V. 2013. PT conditions and trace element variations of picroilmenites and pyropes from the Arkhangelsk region. Journal of Asian Earth Sciences 70–71, 45-63

Agashev A.M., Pokhilenko N.P., Tolstov A.V., Polyanichko N.P., Mal'kovets V.G., Sobolev N.V. 2004 New data on age of kimberlites from Yakutian kimberlite province. Doklady Earth sciences RAN 399,95-99

Agashev, A. M., Ionov, D. A., Pokhilenko, N. P., Golovin, A. V., Cherepanova,Yu, Sharygin, I. S., 2013. Metasomatism in lithospheric mantle roots: Constraints from whole-rock and mineral chemical composition of deformed peridotite xenoliths from kimberlite pipe Udachnaya. Lithos 160-161, 201-215.

Amshinsky, A.N., Pokhilenko, N.P. 1983 Peculiarities of the pycroilmenite compositions from Zarnitsa kimberlite pipe (Yakutia). Russian Geology and Geophysics 24/11, 116-119.

Arai, S. 1984.Pressure-temperature dependent compositional variation of phlogopitic micas in upper mantle peridotites. Contributions to Mineralogy and Petrology 87, 260-264.

Artemieva I M. 2009.The continental lithosphere: Reconciling thermal, seismic, and petrologic data. Lithos 109, 23-46.

Ashchepkov, I.V., Vladykin, N.V., Nikolaeva, I.V., Palessky, S. V., Logvinova, A.M., Saprykin, A.I., Khmel'nikova, O. S., Anoshin, G.N.2004.Mineralogy and Geochemistry of Mantle Inclusions and Mantle Column Structure of the Yubileinaya Kimberlite Pipe, Alakit Field, Yakutia. Doklady Earth sciences RAN395 (4), 517–523.

Ashchepkov, I.V., Pokhilenko, N.P., Vladykin, N.V., Logvinova, A.M., Kostrovitsky, S.I., Afanasiev, V.P., Pokhilenko, L.N., , Kuligin, S.S., Malygina, L.V., Alymova, N.V., Khmelnikova, O.S., Palessky, S.V., Nikolaeva, I.V., Karpenko, M.A., Stagnitsky, Y.B. 2010.

Structure and evolution of the lithospheric mantle beneath Siberian craton, thermobarometric study.Tectonophysics, 485, 17-41.

Ashchepkov, I.V., André, L., Downes, H., Belyatsky, B.A. 2011. Pyroxenites and megacrysts from Vitim picrite-basalts (Russia): Polybaric fractionation of rising melts in the mantle? Journal of Asian Earth Sciences, 42, 14-37.

Ashchepkov, I.V., Rotman, A.Y., Somov, S.V., Afanasiev, V.P., Downes, H., Logvinova, A.M., Nossyko, S. Shimupi, J., Palessky, S.V., Khmelnikova, O.S., Vladykin, N.V.2012. Composition and thermal structure of the lithospheric mantle beneath kimberlite pipes from the Catoca cluster, Angola. Tectonophysics530–531, 128-151

Ashchepkov, I.V., Vladykin, N.V., Ntaflos, T., Downes, H., Mitchel, R., Smelov, A.P. Rotman,A.Ya., Stegnitsky, Yu., Smarov, G.P, Makovchuk, I.V., Nigmatulina, E.N., Khmelnikova, O.S.2013a. Regularities of the mantle lithosphere structure and formation beneath Siberian craton in comparison with other cratons. Gondwana Research 23, 4-24.

Ashchepkov, I.V., Ntaflos, T., Kuligin, S.S., Malygina, E.V., Agashev, A.M., Logvinova, A.M., Mityukhin, S.I., Alymova, N.V., Vladykin, N.V., Palessky, S.V., Khmelnikova, O.S. 2013b. Deep-Seated Xenoliths from the Brown Breccia of the Udachnaya Pipe, Siberia. D. G. Pearson et al. (eds.), Proceedings of 10th International Kimberlite Conference, V1, Special Issue of the Journal of the Geological Society of India,v.1, 59-74.

Ashchepkov, I.V., Downes, H., Mitchell, R., Vladykin, N.V., Coopersmith, H., Palessky, S.V. 2013c. Wyoming Craton Mantle Lithosphere: Reconstructions Based on Xenocrysts from Sloan and Kelsey Lake Kimberlites. Proceedings of 10th International Kimberlite Conference. - New Delhi: Springer India, v. 1. p. 13-27

Ashchepkov, I. V., Vladykin, N. N., Ntaflos, T., Kostrovitsky, S. I., Prokopiev, S. A.. Downes, H., Smelov, A. P., Agashev, A. M., Logvinova, A. M., Kuligin, S. S., Tychkov, N. S., Salikhov, R. F., Stegnitsky, Yu. B., Alymova, N. V., Vavilov, M. A., Minin, V. A., Babushkina,

S. A., Ovchinnikov, Yu. I., Karpenko, M. A., Tolstov, A. V., Shmarov, G.P. Layering of the lithospheric mantle beneath the Siberian Craton: Modeling using thermobarometry of mantle xenolith and xenocrysts, Tectonophysics, 2014. DOI: 10.1016/j.tecto.2014.07.017

Ashchepkov, I.V. 1980. Picroilmenites from Zarnitsa kimberlite pipe. Diploma thesis. Novosibirsk state University. Pokhilenko N.P. supervisor. Novosibirsk state University. 65 p.

Aulbach, S., Pearson, N.J., O'Reilly, S.Y., Doyle, B.J., 2007.Origins of Xenolithic Eclogites and Pyroxenites from the Central Slave Craton, Canada. Journal of Petrology 48, 1843-1873.

Batanova, V., Savelieva, G., 2009. Melt migration in the mantle beneath spreadingzones and formation of replacive dunites: a review. Russian Geology and Geophysics 50, 763–778.

Batumike, J.M., Griffin, W.L., O'Reilly, S.Y. 2009.Lithospheric mantle structure and the diamond potential of kimberlites in southern D.R. Congo. Lithos 112 S1, 166-176.

Bedard, J. H., 2006. A catalytic delamination-driven model for coupled genesis of Archaean crust and sub-continental lithospheric mantle. Geochimica et Cosmochimica Acta 70, 1188-1214.

Bobrievich, A.P., Bondarenko, M.N., Gnevushev, M.A, Krasov, A.M., Smirnov, G.I. and Yurkevich, R.K. (1959). The diamond deposits of Yakutia. Moscow: Gosgeoltekhizdat, 527 p. (in Russian).

Boyd, F.R., Pokhilenko, N.P., Pearson, D.G., Mertzman S.A., Sobolev, N.V., Finger, L.W. 1997. Composition of the Siberian cratonic mantle: evidence from Udachnaya peridotite xenoliths. Contributions to Mineralogy and Petrology 128, 228-246.

Boyd, F.R. 1973. A pyroxene geotherm. Geochimica et Cosmochimica Acta, 37, 2533-2546.

Boyd, F.R., 1990. Mantle Metasomatism: Evidence from a MARID–Harzburgite Compound Xenolith. Carnegie Institution Washington, Yearbook, 90, pp. 18–23.

Brey, G.P., Kohler, T. 1990.Geothermobarometry in four-phase lherzolites. II. New thermobarometers, and practical assessment of existing thermobarometers.Journal of Petrology 31, 1353-1378.

Clarke, D.B, Mackay, R.M 1990. An Ilmenite-Garnet-Clinopyroxene nodule from Matsoku: Evidence of Oxide-Rich liquid Immiscibility in Kimberlites? Canadian Mineralogist 28, 229-239

Burgess, S.R., Harte, B. 2004. Tracing lithosphere evolution through the analysis of heterogeneous G9-G10 garnets in peridotite xenoliths, II: REE chemistry.Journal of Petrology 45, 609-634

Condie K.C. 2004. Supercontinents and superplume events: distinguishing signals in the geologic record Physics of the Earth and Planetary Interiors 146, 319-332

Dawson J. B. Kimberlites and their xenoliths.Springer-Verlag, Berlin. 1980. 252p.

Dawson, J.B., Smith, J.V., 1977. The MARID (mica–amphibole–rutile–ilmenite–diopside) suite of xenoliths in kimberlite. Geochimica et Cosmochimica Acta 41, 309–323.

Dawson, J.B., Smith, J.V., 1982. Mantle amphiboles - a review. Mineralogical Magazine. 45, 35-46.

Day H.W. 2012. A revised diamond-graphite transition curve. American Mineralogist, 97, 52–62.

Doucet, L. S., Ionov, D. A., Golovin, A.V. & Pokhilenko, N. P. 2012. Depth, degrees and tectonic settings of mantle melting during craton formation: inferences from major and trace element compositions of spinel harzburgite xenoliths from the Udachnaya kimberlite,central Siberia. Earth and Planetary Science Letters 359-360, 206-218.

Eccles, D.R., Simonetti, S.S., Cox, R. 2010. Garnet pyroxenite and granulite xenoliths from or the astern Alberta: Evidence of ~1.5 Ga lower crust and mantle in western Laurentia. Precambrian Research 177, 339-354.

Efimova, E. S., Sobolev, N.V. 1977. Abundance of crystalline inclusions in Yakutian diamonds. Doklady Akademii Nauk SSSR 237,1475-1478 (in Russian).

Fedortchouk,Y., Canil, D., Carlson, J.A. 2005. Dissolution forms inLac de Gras diamonds and their relationship to the temperatureand redox state of kimberlite magma. Contributions to Mineralogyand Petrology 150, 54-69.

Foley, S.F., Yaxley, G.M., Rosenthal, A., Buhre, S., Kiseeva, E.S., Rapp, R.P., Jacob, D.E. 2009. The composition of near-solidus melts of peridotite in the presence of CO_2 and H_2O between 40 and 60 kbar. Lithos 112, S1, 274-283

Foley, S.F., 1992.Vein-plus-wallrock melting mechanism in the lithosphere and the origin of potassic alkaline magmas. Lithos 28, 435–453.

Gibson, S.A., Malarkey, J., Day, J.A., 2008. Melt depletion and enrichment beneath the western Kaapvaal Craton: evidence from Finsch peridotite xenoliths. Journal of Petrology 49, 1817-1852.

Gregoire, M., Bell, D. R. & Le Roex, A. P. 2002.Trace element geochemistryof phlogopite-rich mafic mantle xenoliths: their classificationand their relationship to phlogopite-bearing peridotites andkimberlites revisited. Contributions to Mineralogy and Petrology 142, 603 -625.

Gregoire, M., Bell, D. R. & Le Roex, A. P. 2003. Garnet lherzolites from the Kaapvaal Craton (South Africa): trace element evidencefor a metasomatic history. Journal of Petrology 44, 629-657.

Goncharov, A. G., Ionov, D. A., Doucet, L. S. & Pokhilenko, L. N. 2012. Thermal state, oxygen fugacity and C-O-H fluid speciation in cratonic lithospheric mantle: New data on peridotite xenoliths from the Udachnaya kimberlite, Siberia. Earth and Planetary Science Letters 357-358, 99-110.

Griffin, W. L., Ryan, C. G., Kaminsky, F. V., O'Reilly, S. Y., Natapov, L. M., Win, T. T.,

Kinny, P.D., Ilupin, I. P. 1999a. The Siberian lithosphere traverse: Mantle terranes and the assembly of the Siberian Craton. Tectonophysics 310, 1-35.

Griffin, W.L., Shee, S.R., Ryan, C.G., Win, T.T., Wyatt, B.A. 1999b. Harzburgite to lherzolite and back again: metasomatic processes in ultramafic xenoliths from the Wesselton kimberlite, Kimberley, South Africa. Contributions to Mineralogy and Petrology 134, 232-250

Griffin, W. L., O'Reilly, S.Y., Afonso, J.C., Begg, G.C., 2009. The Composition and Evolution of Lithospheric Mantle: A Reevaluation and Its Tectonic Implications, Journal of Petrology 50, 1185–1204

Griffin, W.L., Spetsius, Z.V., Pearson, N.J., O'Reilly, S.Y. 2002. In-situ Re-Os analysis of sulfide inclusions in kimberlite olivine: New constraints on depletion events in the Siberian lithospheric mantle. Geochemistry, Geophysics, Geosystems, 3, (11), 1069, doi:10.1029/2001GC000287.

Griffin, W. L., O'Reilly, S.Y. 2007. Cratonic lithospheric mantle: Is anything subducted? Episodes, 30, 43-53

Green, T.H., Blundy, J.D., Adam, J., Yaxley, G.M., 2000. SIMS determination of trace element partition coefficients between garnet, clinopyroxene and hydrous basaltic liquids at 2–7.5 GPa and 1080–1200 °C. Lithos 53, 165–187.

Hauri, E.H., Wagner, T.P., Grove, T.L., 1994. Experimental and natural partitioning of Th, U, Pb and other trace elements between garnet, clinopyroxene and basaltic melts. Chem. Geol. 117, 149–166.

Hart, S. R., Dunn, T., 1993 Experimental cpx/melt partitioning of 24 trace elements. Contributions to Mineralogy and Petrology 113, 1-8.

Harte, B., Kirkley, M.B., 1997. Partitioning of trace elements between clinopyroxene and garnet: data from mantle eclogites. Chemical Geology 136, 1-24.

Grutter, H.S., 2009. Pyroxene xenocryst geotherms.Techniques and application. Lithos 112, 1167-1178.

Giuliani, A., Kamenetsky, V.S., Kendrick, M.A., Phillips, D., Wyatt, B.A., Maas, R. 2013 Oxide, sulphide and carbonate minerals in a mantle polymict breccia: Metasomatism by proto-kimberlite magmas, and relationship to the kimberlite megacrystic suite. Chemical Geology, 353, 30, 4-18.

Gonzaga, R.G., Lowry, D., Jacob, D.E., LeRoex, A., Schulze, D., Menzies, M.A. 2010 Eclogites and garnet pyroxenites: Similarities and differences. Journal of Volcanology and Geothermal Research 190, 235-247.

Dawson, J. B. 1984. Contrasting types of upper mantle metasomatism. In: Kornprobst, J. (ed.) Kimberlites II. The Mantle and Crust - Mantle Relationships. Amsterdam: Elsevier, 289-294.

Dawson, J. B. 1980. Kimberlites and their Xenoliths. Berlin: Springer.210 p.

Haggerty, S.E.1975. The chemistry and genesis of opaque minerals in kimberlite. Physics and chemistry of the Earth. 9, 227-243.

Hawthorne, F.C., Oberti, R., 2007. Classification of the Amphiboles. In: Rosso, J.J. (Ed.), Amphiboles: Crystal Chemistry, Occurrence, and Health Issues. Reviews in Mineralogy and Geochemistry, vol. 67. Mineralogical Society of America and The Geochemical Society, Washington, DC, pp. 55–88.

Heaman, L.M., Creaser, R.A., Cookenboo, H.O., Chacko, T. 2006. Multistage modification of the northern slave mantle lithosphere evidence from zircon- and diamond-bearing eclogite xenoliths entrained in Jericho Kimberlite, Canada. Journal of Petrology 47, 821-858.

Howarth, G.,H. Barry,P.H,. Pernet-Fisher, J.F., Baziotis, I. P., Pokhilenko, N.P., Pokhilenko, L.N., Bodnar, R.J., Taylor, L.A., Agashev A.M. 2014. Superplume metasomatism: Evidence from Siberian mantle xenoliths. Lithos, 184–187, 209-224.

Horn, I., Foley, S.F.,Jackson, S.E., Jenner,G.A. 1994.Experimentally determined partitioning of high field strength- and selected transition elements between spinel and basaltic melt. Chemical Geology, 117, 193–218.

Hopp, J., Trieloff, M., Brey, G.P., Woodland A.B., Simon N.S.C., Wijbrans J.R., Siebel W., Reitter E. 2008. $^{40}Ar/^{39}Ar$-ages of phlogopite in mantle xenoliths from South African kimberlites: Evidence for metasomatic mantle impregnation during the Kibaran orogenic cycle. Lithos, 106, 351-364.

Ionov, D.A., Doucet, L.S., Ashchepkov I.V. 2010. Composition of the Lithospheric Mantle in the Siberian Craton: New Constraints from Fresh Peridotites in the Udachnaya-East Kimberlite. Journal of Petrology, 51, 2177-2210.

Ionov, D.A., Doucet, L.S., Carlson, R.W., Pokhilenko, N.P., Golovin, A.V., Ashchepkov, I.V. 2011. Peridotite xenolith inferences on the formation and evolution of the central Siberian cratonic mantle. Goldschmidt Conference Abstracts. 1085.

Ionov, D.A., Bénard, A., Plechov, P.Yu., Shcherbakov, V.D. 2013. Along-arc variations in lithospheric mantle compositions in Kamchatka, Russia: First trace element data on mantle xenoliths from the Klyuchevskoy Group volcanoes. Journal of Volcanology and Geothermal Research 263, 122-131.

Karato, S. 2010. Rheology of the Earth's mantle: A historical review. Gondwana Research 18, 17-45

Kargin, A.V., Golubeva, Yu.Yu., Kononova V.A. 2011. Kimberlites of the Daldyn-Alakit region (Yakutia): Spatial distribution of the rocks with different chemical characteristics. Petrology. 19/5, 496-520

Kennedy, C.S., Kennedy, G.C., 1976. The equilibrium boundary between graphite and diamond. Journal of Geophysical Research 81, 2467-2470

Konzett, J., Armstrong, R.A., Günther, D., 2000. Modal metasomatism in the Kaapvaal craton lithosphere: constraints on timing and genesis from U–Pb zircon dating of metasomatized peridotites and MARID-type xenoliths. Contributions to Mineralogy and Petrology 139, 704-719

Konzett, J., Ulmer, P. 1999. The Stability of Hydrous Potassic Phases in Lherzolitic Mantle - an Experimental Study to 9·5 GPa in Simplified and Natural Bulk Compositions. Journal of Petrology 40, 629-652

Konzett, J., Wirth, R., Hauzenberger, C., Whitehouse, M. 2013. Two episodes of fluid migration in the Kaapvaal Craton lithospheric mantle associated with Cretaceous kimberlite activity: Evidence from a harzburgite containing a unique assemblage of metasomatic zirconium-phases. Lithos 182–183, 165-184.

Koptil, V.I., Las'ko, E.E., Serenko V.P.1975. Diamond kyanite eclogites from Sytykanskaya kimberlite pipe – first finding in USSR. Doklady Earth Sciences SSSR, 225/4, 924-927.

Kostrovitsky, S.I., Morikiyo, T., Serov, I.V., Yakovlev, D.A., Amirzhanov, A.A. 2007. Isotope-geochemical systematics of kimberlites and related rocks from the Siberian Platform. Russian Geology and Geophysics 48, 272-290.

Kostrovitsky, S.I., Alymova, N.V., Yakovlev, D.A., Serov, I.V., Ivanov, A.S., Serov, V.P. 2006. Specific features of picroilmenite composition in various diamondiferous fields of the Yakutian province. Doklady Earth Sciences, 406, 19-23.

Kopylova, M.G., Caro, G. 2004. Mantle xenoliths from the Southeastern Slave craton: Evidence for chemical zonation in a thick, cold lithosphere. Journal of Petrology 45, 1045-1067.

Kopylova, M.G., Russell, J.K., Cookenboo, H. 1999. Petrology of peridotite and pyroxenite xenoliths from the Jericho kimberlite: Implications for the thermal state of the mantle beneath the Slave craton, northern Canada. Journal of Petrology. 40, 79-104.

Kopylova, M. G., Nowell, G. M., Pearson, D. G., Markovic, G. 2009. Crystallization of megacrysts from protokimberlitic fluids: Geochemical evidence from high-Cr megacrysts in the Jericho kimberlite. Lithos 112S, 284-295.

Koreshkova, M.Yu., Downes, H., Nikitina, L.P., Vladykin, N.V., Larionov, A.N., Sergeev, S.A. 2009. Trace element and age characteristics of zircons in granulite xenoliths from the Udachnaya kimberlite pipe, Siberia. Precambrian Research, 168, 197-212.

Lazko, E.E., Serenko, V.P., Koptil, V.I., Rudnizkaya, E.S., Zepin, V.I. 1982. Kyanite diamondiferous eclogites from the kimberlite pipe Sytykanskaya (Yakutia). Izvestiya AN SSSR, Ser. geol., 7, 55-69.

Katayama, I., Suyama, Y., Ando, S., Komiya, T. 2009. Mineral chemistry and P–T condition of granular and sheared peridotite xenoliths from Kimberley, South Africa: origin of the textural variation in the cratonic mantle. Lithos, 109, 333-340.

Lavrent'ev, Yu.G., Usova, L.V., Kuznetsova, A.I., Letov, S.V. 1987. X-ray spectral quant metric microanalysis of the most important minerals of kimberlites Russian Geology and Geophysics, 48 (5), 75–81.

Lazarov, M., Brey, G. P., Stefan Weyer, S. 2012. Evolution of the South African mantle — A case study of garnet peridotites from the Finsch diamond mine (Kaapvaal craton); part 1: Inter-mineral trace element and isotopic equilibrium. Lithos, 154, 193-209.

Logvinova, A.M., Taylor, L.A., Floss, C., Sobolev, N.V. 2005. Geochemistry of multiple diamond inclusions of harzburgitic garnets as examined in situ. International Geology Review. 47, 1223-1233.

Logvinova, A.M., Ashchepkov, I.V. 2008. Diamond inclusions and eclogites thermobarometry, Siberia. Goldschmidt Conference Abstracts. Geochimica et Cosmochimica Acta. Special Supplement. 72. 16S, A567

Mather, K.A., Pearson, D.G., McKenzie, D., Kjarsgaard, B.A., Priestley K. 2011. Constraints on the depth and thermal history of cratonic lithosphere from peridotite xenoliths, xenocrysts and seismology. Lithos 125, 729-742

McDonough, W.F., Sun, S.-S, 1995.The composition of the Earth. Chemical Geology 120, 223–253.

Malkovets, V.G., Griffin, W.L. , Pearson, N.J., Rezvukhin, D.I., O'Reilly, S.Y., Pokhilenko, N.P., Garanin, V.K., Spetsius, Z.V., Litasov, K.D. 2012. Late metasomatic addition of garnet to the SCLM: Os-isotope evidence. Goldschmidt Conference Abstracts 1315.

Malkovets, V.G., Griffin, W.L., Pearson, N.J., Rezvukhin, D.I., O'Reilly, S.Y., Pokhilenko, N.P., Garanin, V.K., Spetsius, Z.V., Litasov, K.D. 2012. Late metasomatic addition of garnet to the SCLM: Os-isotope evidence. 10th International Kimberlite Conference Long Abstarcts 10IKC-173.

Matusiak-Małek, M., Puziewicz, J., Ntaflos, T., Grégoire, M., Downes, H. 2010. Metasomatic effects in the lithospheric mantle beneath the NE Bohemian Massif: A case study of Lutynia (SW Poland) peridotite xenoliths. Lithos, 117, 49-60.

Manakov, A.V., 2001. Material models of the upper mantle of Yakutian diamond-bearing province. Herald of the Voronezh University 11, .46-54 (in russian)

Marchesi, C., Garrido, C.J., Bosch, D., Bodinier, J.-L., Gervilla, F., Hidas, K. 2013. Mantle refertilization by melts of crustal-derived garnet pyroxenite: Evidence from the Ronda peridotite massif, southern Spain Earth and Planetary Science Letters, 362, 66-75.

Mitchell, R.H., 1995. Kimberlites, Orangeites, and Related Rocks. Plenum Press, New York. 1-90.

Mitchell, R.H., Bergman, S.C., 1991.Petrology of Lamproites. Plenum Press, New York.

McCammon, C.A., Griffin, W.L., Shee, S.R., O'Neill, H.S.C. 2001. Oxidation during metasomatism in ultramafic xenoliths from the Wesselton kimberlite, South Africa: implications for the survival of diamond. Contributions to Mineralogy and Petrology 141, 287-296.

McGregor I.D.1974. The system MgO- SiO_2-Al_2O_3: solubility of Al_2O_3 in enstatite for spinel and garnet peridotite compositions. American Mineralogist 59, 110-119.

Misra, K.C., Anand, M., Taylor, L.A., Sobolev, N.V. 2004. Multi-stage metasomatism of diamondiferous eclogite xenoliths from the Udachnaya kimberlite pipe, Yakutia, Siberia. Contributions to Mineralogy and Petrology 146, 696-714

Moore, A.E., Lock, N.P., 2001. The origin of mantle-derived megacrysts and sheared peridotites-evidence from kimberlites in the northern Lesotho—Orange Free State (South Africa) and Botswana pipe clusters. South Africa Journal of Geology 104, 23-38.

Niida, K., Green, D. H. 1999. Stability and chemical composition of pargasitic amphibole in MORB pyrolite underupper mantle conditions. Contributions to Mineralogy and Petrology135, 18-40.

Nimis P., Taylor W. 2000. Single clinopyroxene thermobarometry for garnet peridotites.Part I. Calibration and testing of a Cr-in-Cpx barometer and an enstatite-in-Cpx thermometer. Contributions to Mineralogy and Petrology 139, 541-554.

Nimis P., Zanetti A., Dencker I., Sobolev N.V. 2009. Major and trace element composition of chromian diopsides from the Zagadochnaya kimberlite (Yakutia, Russia): Metasomatic processes, thermobarometry and diamond potential. Lithos 112, 397-412

O'Neill, H. St. C., Wall, V. J. 1987.The olivine orthopyroxene-spinel oxygen geobarometer, the nickel precipitation curve, and the oxygen fugacity of the Earth's upper mantle. Journal of Petrology28, 1169-1191.

O'Neill,H.St.C, Wood B.J.1979.A n experimental study of Fe-Mg- partitioning between

garnet and olivine and its calibration as a geothermometer. Contributions to Mineralogy and Petrology 70, 59-70.

Pearson, D.G. 1999. The age of continental roots. Lithos, 48, 171-194.

Pearson, D.G., Kelley, S.P., Pokhilenko, N.P., Boyd F.R. 1997. Laser 40Ar/39Ar analyses of phlogopites from southern African and Siberian kimberlites and their xenoliths: constraints on eruption ages, melt degassing and mantle volatile composition. Russian Geology and Geophysics, 38, 106-117.

Pearson, D.G., Wittig, N. 2014. The Formation and Evolution of Cratonic Mantle Lithosphere – Evidence from Mantle Xenoliths. Treatise on Geochemistry (Second Edition). Elsevier. 255–292.

Pearson, D.G. Snyder, G.A. Shirey, S.B. Taylor, L.A. Carlson, R.W. Sobolev N.V. 1995. Archaean Re-Os age for Siberian eclogites and constraints on Archaean tectonics. Nature, 374, 711-713.

Pernet-Fisher, J. F., Howarth, G.H., Liu, Y., Barry, P.H., Carmody, L., Valley, J.W., Bodnar, R.J., Spetsius, Z.V., Taylor L.A. 2014. Komsomolskaya diamondiferous eclogites: evidence for oceanic crustal protoliths. Contributions to Mineralogy and Petrology, 167:981. DOI 10.1007/s00410-014-0981-y

Pidgeon, R.T., Smith, C.B., Fanning, C.M., 1989. Kimberlite and lamproite emplacement ages in Western Australia. In: Ross, J., et al. (Eds.), Kimberlites and Related Rocks Volume 1: Their composition, Occurrence, Origin and Emplacement. Blackwell Scientific Publications, Carlton, (Geol. Soc. Aust. Special Publication) pp. 382–391.

Pokhilenko, N. P., Sobolev, N.V., Kuligin, S. S., Shimizu, N.1999. Peculiarities of distribution of pyroxenite paragenesis garnets in Yakutian kimberlites and some aspects of the evolution of the Siberian craton lithospheric mantle. Proceedings of the VII International Kimberlite Conference.The P.H. Nixon volume. 690-707.

Ponomarenko, A.I., Spetsius, Z.V. 1976. Diamondiferous eclogites from the kimberlite pipe Sytykanskaya. Geology and Geophysics, 6, 103-106.

Pokhilenko, N.P., Pearson, D.G., Boyd, F.R., Sobolev, N.V. 1991. Megacrystalline dunites: sources of Siberian diamonds. Carnegie Institute Washington.Yearbook. 90, 11-18.

Pokhilenko, N.P., Sobolev, N.V. 1995. Mineralogical criteria for kimberlite diamond grade. Kimberlites of Yakutia: Field guide book: Sixth International Kimberlite Conference. Novosibirsk, 1995. P. 79-81

Pokhilenko, N. P., Sobolev N.V., Sobolev V.S. and Lavrentiev Y.G. 1976. Xenoliths of diamond bearing ilmenite-pyrope lherzolites from the kimberlite pipe Udachnaya (Yakutia).) Doklady AN SSSR. 231, 438-442.

Pokhilenko, N. P., Sobolev, N.V., Kuligin, S. S., Shimizu, N., 1999. Peculiarities of distribution of pyroxenite paragenesis garnets in Yakutian kimberlites and some aspects of the evolution of the Siberian craton lithospheric mantle. Proceedings of the VII International Kimberlite Conference. The P.H. Nixon volume. P. 690-707.

Pokhilenko, L.N., Alifirova, T.A., Yudin, D.S. 2012. ^{40}AR/^{39}AR dating of phlogopite of mantle xenoliths from kimberlite pipes of Yakutia: evidence for deep ancient metasomatism of the Siberian platform. 10th International Kimberlite Conference: Long Abstracts. - Bangalore, 57.

Rao, C.N.V. Wu, F.-Y., Mitchell, R.H., Li, Q.-L., Lehmann, B. Mesoproterozoic U–Pb ages, trace element and Sr–Nd isotopic composition of perovskite from kimberlites of the Eastern Dharwar craton, southern India: Distinct mantle sources and a widespread 1.1 Ga tectonomagmatic event. Chemical Geology, 353, 3, 48-64.

Rosen, O.M., Levskii, L.K., Makeev, A.F., Zhuravlev, D.Z., Spetsius, Z.V., Rotman, A.Ya., Zinchuk, N.N., Manakov, A.V., Serenko, V.P. 2006. Paleoproterozoic accretion in the

Northeast Siberian craton: Isotopic dating of the Anabar collision system. Stratigraphy and Geological Correlation. 14, 581-601.

Rudnick, R.L., McDonough, W.F., O'Connell, R.J., 1998. Thermal structure, thickness and composition of continental lithosphere. Chemical Geology 145, 395-411

Reimers, L.F. 1994 Deep seated mineral associations of the kimberlites pipe Sytycanskaya (materials of the study of mantle rock and crystalline inclusions in diamonds). Institute of Geology and Geophysics. Novosibirsk. 258 p.

Reimers, L.F., Pokhilenko, N.P., Yefimova, E.S., Sobolev, N.V. 1998. Ultramafic Mantle Assemblages from Sytykanskaya Kimberlite Pipe (Yakutia) Seventh International Kimberlite Conference, Cape Town, April 1998: Extended Abstracts, Cape Town, 730-732

Roden, M.F., Patiño-Douce, A.E., Jagoutz, E., Laz'ko, E.E., 2006. High pressure petrogenesis of Mg-rich garnet pyroxenites from Mir kimberlite, Russia. Lithos, 90/1-2, 77-91.

Rodionov, A S , Amshinsky., Pokhilenko, N P., 1988. Ilmenite – Pyrope wehrlite – a new type of kimberlite xenoliths paragenesis. Russian Geol. Geophys. 19/7, 53-57

Rodionov, A.S., Sobolev, N.V., Pokhilenko, N.P., Suddaby, P., Amshinsky, A.N., 1991. Ilmenite-bearing peridotites and megacrysts from Dalnaya kimberlite pipe, Yakutia. Fifth International Kimberlite Conference: Extended abstracts, 339-341

Santosh, M., Maruyama, S., Yamamoto, A. 2009. The making and breaking of supercontinents: Some speculations based on superplumes, super downwelling and the role of tectosphere. Gondwana Research 15, 324-341

Smart, K.A., Heaman, M., Chacko,T.,Simonetti,A., Kopylova,M.,Mah,D., Daniels, D. 2009. The origin of high-MgO diamond eclogites from the Jericho Kimberlite, Canada. Earth and Planetary Science Letters, 284, 527-537

Smelov, A.P., Zaitsev, A.I. 2013. The Age and Localization of Kimberlite Magmatism in the Yakutian Kimberlite Province: Constraints from Isotope Geochronology—An Overview. D.

G. Pearson et al. (eds.), Proceedings of 10th International Kimberlite Conference, Volume 1, Special Issue of the Journal of the Geological Society of India, 225-234.

Smit, K.V., Stachel, T., Creaser, R.A., Ickert, R.B., DuFrane, S.A., Stern, R.A., Seller, M. 2014. Origin of eclogite and pyroxenite xenoliths from the Victor kimberlite, Canada, and implications for Superior craton formation. Geochimica et CosmochimicaActa 125, 308-337.

Snyder, M., TaylorL. A., Crozaz G., Halliday A.N., Beard B.L, Sobolev V.N.,Sobolev N.V. 1997. The origin of Yakutian eclogite xenoliths. Journal of Petrology 38, 85-113.

Snyder, D.B., Lockhart, G. 2009. Does seismically anisotropic subcontinental mantle lithosphere require metasomatic wehrlite–pyroxenite dyke stockworks? Lithos, 112/2, 961-965.

Sobolev, N.V., 1977. Deep-Seated Inclusions in Kimberlites and the Problem of the Composition of the Mantle. Amer. Geophys.Union, Washington, DC. 279 p.

Sobolev, N.V., Lavrentev, Y.G., Pokhilenko, N.P., Usova, L.V. 1973.Chrome-Rich Garnets from the Kimberlites of Yakutia and Their Parageneses. Contributions to Mineralogy and Petrology, 40, 39-52.

Sobolev, N.V., Pokhilenko, N.V., Efimova, E.S. 1984. Xenoliths of diamond bearing peridotites in kimberlites and problem of the diamond origin. Russian Geology and Geophysics, 25/12, 63-80.

Sobolev, N.V., Logvinova, A.M., Efimova, E.S. 2009. Syngenetic phlogopite inclusions in kimberlite-hosted diamonds: implications for role of volatiles in diamond formation. Russian Geology and Geophysics 50, 1234–1248.

Sobolev, N.V., Logvinova, A.M., Zedgenizov, D.A., Yefimova, E.S., Taylor, L.A., Promprated, P., Koptil, V.I., Zinchuk, N.N. 2003. Mineral Inclusions in Diamonds from Komsomolskaya and Krasnopresnenskaya Pipes, Yakutia: Evidence for Deep Lithospheric Heterogeneities in Siberian Craton. 8th International Kimberlite conference, Extended Abstracts, 2003, FLA_0141

Sobolev, N.V, Logvinova, A.M, Zedgenizov, D.A, Seryotkin, Y.V., Yefimova, E.S., Floss, C., Taylor, L.A., 2004. Mineral inclusions in microdiamonds and macrodiamonds from kimberlites of Yakutia: a comparative study. Lithos, 77, 225–242.

Solov'eva, L.V., Egorov, K.N., Markova, M.E., Kharkiv, A.D., Popolitov, K.E., Barankevich V.G. 1997. Mantle metasomatism and melting in deep-seated xenoliths from the Udachnaya pipe, their possible relationship with diamond and kimberlite formation. Russian Geology and Geophysics. 38/1, 172- 193

Solov'eva, L.V., Yasnygina, T.A., Egorov K.N. 2012. Metasomatic parageneses in deep-seated xenoliths from pipes Udachnaya and Komsomol'skaya-Magnitnaya as indicators of fluid transfer through the mantle lithosphere of the Siberian craton. Russian Geology and Geophysics, 53, 1304-1323.

Spetsius, Z.V. 2007. The nature of indicator minerals in kimberlites: a case from the mantle xenoliths studying. Plumes and their sources. Ed. by N.V. Vladykin Irkutsk. Institute of Geography. 90-108.

Spetsius, Z.V., Serenko ,V.P. 1990. Composition of the continental mantle and low crustbeneath the Siberian platform. Moscow, Nauka. 271 p (in Russian).

Spetsius, Z.V., Koptil V.I. 2008. Associations with the diamond from the kimberlite pipe Sytykanskaya, Yakutia. Geologiya I Razvedka, 23-28.

Stagno, V. Frost, D.J. 2010. Carbon speciation in the asthenosphere: experimental measurements of the redox conditions at which carbonate-bearing melts coexist with graphite or diamond in peridotite assemblages. Earth Planet. Sci. Lett. 300, 72-84,

Stagno, V., Ojwang, D.O., McCammon, C.A. Frost, D.J. 2013. The oxidation state of the mantle and the extraction of carbon from Earth's interior. Nature. 493, 84-88.

Sweeney, R.J., Thompson,A. B., Ulmer,P. 1993. Melting experiments were performed on a natural mica-amphibole-rutile-ilmenite-clinopyroxene (MARID) sample from the Kaapvaal

mantle lithosphere (AJE137) at 20 to 35 kbar and 800 to 1450°C. Contributions to Mineralogy and Petrology.115, 225-241.

Sweeney, R.J., Thompson, A.B., Ulmer, P., 1993. Phase relations of a natural MARID composition and implications for MARID genesis, lithospheric melting and mantle metasomatism. Contributions to Mineralogy and Petrology 115, 225-241.

Tappe, S., Pearson, D.G.,,Kjarsgaard, B.A., Nowell, G., Dowall, D. 2013. Mantle transition zone input to kimberlite magmatism near a subduction zone: Origin of anomalous Nd–Hf isotope systematics at Lac de Gras, Canada. Earth and Planetary Science Letters, 371–372, 235-251.

Taylor, L.A., Anand, M., 2004. Diamonds: time capsules from the Siberian Mantle. Chemie der Erde. 64, 1-74

Taylor, W.R., Kammerman, M., Hamilton, R.1998. New thermometer and oxygen fugasity sensor calibrations for ilmenite and chromian spinel-bearing peridotitic assemblages.7th International Kimberlite Conference.Extended abstracts. 891-901

Tappe, S., Foley, S.F., Jenner, G.A., Heaman L.M., Kjarsgaard B. A., Romer R. L., Stracke A., Joyce N., Hoefs J. 2006. Genesis of ultramafic lamprophyres and carbonatites at Aillik Bay, Labrador: a consequence of incipient lithospheric thinning beneath the North Atlantic craton Journal of Petrology 47, 1261-1315.

Travin, A.V., Aschepkov, I.V., Udin, D., Prostyakov, K. 2002. Laser and stepwise-heating $^{40}Ar/^{39}Ar$ dating of kimberlite-like rocks from Sayan Foothills and peripheral part of the Siberian platform. Geochimica et Cosmochimica Acta. Special Supplement.6 (15A), A783.

Travin, A.V., Yudin, D.S,. Vladimirov, A.G., Khromykh, S.V., Volkova, N.I., Mekhonoshin, A.S., Kolotilina, T.B.. 2009. Thermochronology of the Chernorud granulite zone, Ol'khon Region, Western Baikal area. Geochemistry International. 47(11), 1107-1124

Zack, T., Brumm, R. 1998. Ilmenite/liquid partition coefficients of 26 trace elements determined through ilmenite/clinopyroxene partitioning in garnet pyroxenite. In: Gurney, J.J., Gurney, J.L., Pascoe, M.D., Richardson, S.H. (Eds.), 7th International Kimberlite Conference. Red Roof Design, Cape Town, 986-988.

Ziberna, L, Nimis, P, Zanetti, A., Marzoli, A., Sobolev N.V. 2013. Metasomatic Processes in the Central Siberian Cratonic Mantle: Evidence from Garnet Xenocrysts from the Zagadochnaya Kimberlite. Journal of Petrology 54, 2379-2409.

Figure captions

Fig.1. (A). Location of Sytykanskaya pipe Alakit field and other kimberlite fields in Siberian platform

1. Siberian platform. 2 – Shields. Kimberlite fields: 3. Alakit field; Late Devonian fields; 4. Lower Triassic and Jurassic fields (Kostrovitsky et al., 2007).

(B) Geological scheme of the Alakite pipe and location of the kimberlite pipes. 1 .P_2-T_1 trap dolerites; 2.C_2-P_1 sandstones; 3.Cm_2-S_1; 4. Kimberlite pipes excavated (a) and buried (b)

Fig.2. Photo images of the mantle xenoliths from Sytykanskaya pipe.

A = Fine-grained granular garnet lherzolite. B. Coarse-grained granular garnet lherzolite. C. Deformed garnet peridotite. D. Details of garnet lherzolites: Cpx corona on garnet. E. ilmenite-bearing peridotite. F. Sp harzburgite. G. Garnet harzburgite with disseminated idiomorphic phlogopite. H. Garnet dunite. I Garnet harzburgite with Phl . J. Serpentinized garnet-bearing harzburgite with abundant intergranular Ilmenite. K. Details of substitution of garnet grains by Cpx-Phl-Ilm aggregates. L. Phl-Cpx-Ulvospinel-Ilm veinlets in peridotites. M. Garnet

harzburgite with garnet partly substituted by Phl and Cpx. N. Garnet harzburgite with disseminated Ilm and Phl. O. Deformed ilmenite peridotite.

Fig. 3. Images of scanned thin sections of pyroxenite and eclogite mantle xenoliths.

A. Garnet Cr-bearing websterite. B. Gar Cr-diopside websterite with Phl vein. C. Cr-diopside websterite with graphite. D phlogopite, ulvospinel, ilmenite in Ilmenite-bearing peridotite with Cr-diopside and relics of garnets. E. Bi-mineral eclogite. F. Eclogite with relics of Cpx and intergranular reaction products.

Fig. 4. Compositions of pyropes (a) from ABK (b) and PK from Sytykanskaya pipe. In addition in Fig 4a, compositions of garnets from analyzed xenoliths and diamond inclusions are shown. In Fig1b compositions of the garnets from veined metasomatites and pyroxenites analyzed by LAM ICP MS. The fields in Cr_2O_3- CaO diagram are after Sobolev et al. (1973).

Fig.5. Compositions of Cr- diopsides from ABK (A) and PK(B) from Sytykanskaya pipe.

Fig.6. Compositions of chromites from ABK (a) and PK(b) from Sytykanskaya pipe.

Fig.7. Compositions of ilmenites from ABK (a) and PK(b) from Sytykanskaya pipe

Fig.8. Compositions of amphiboles from ABK and mantle xenoliths from Sytykanskaya pipe. In comparison with those from those from concentrate of Yubileynaya pipe (Ashchepkov et al., 2004; 2010) and experimental data from MARIDS (Konzet et al., 1997).

Fig.9. Compositions of phlogopites from ABK and mantle xenoliths from Sytykanskaya pipe.

Fig.10. A) PTXfO_2 diagram for the concentrate from porphyritic kimberlite from Sytykanskaya pipe and diamond inclusions according to Spetsius and Koptil (2007).

Signs: 1. Opx: T^{o}C (Brey and Kohler, 1990)-P(GPa)(McGregor, 1974). 2. The same for diamond inclusions. Cpx: 3.T^{o}C-P(GPa)(Nimis and Taylor, 2000); 4.T^{o}C (Nimis and Taylor, 2000 modified)–P(GPa) (Ashchepkov et al ., 2010); 5.The same for eclogites; 6.The same for pyroxenites. 7. The same for diamond inclusions; Garnet (monomineral) 8.9.T^{o}C (O'Neill and Wood, 1979) -P(GPa) (Ashchepkov et al ., 2010), 10.The same for diamond inclusions.

Chromite 11.T^{o}C (O'Neill and Well, 1987)-P(GPa) (Ashchepkov et al., 2010); 12. The same for diamond inclusions. 13. Ilmenite megacrysts T^{o}C (Taylor et al., 1998)- P(GPa) (Ashchepkov et al., 2010); 14. The same for xenoliths; 15. T^{o}C-P(GPa) (Brey and Kohler, 1990). The compositions of the diamond inclusions is taken from (Logvinova et al., 2005; Sobolev et al., 2003;2004).

Field for diamond-bearing associations after Stagno et al. (2013). The horizontal dashed line at 3.5 and 4.5 GPa corresponds to the Graphite – Diamond boundary at 35 and 40 mWm^{-2} respectively.

B. PTXfO_2 diagram for the concentrate from ABK from Sytykanskaya pipe and diamond inclusions according to Spetsius and Koptil (2007). Symbols are the same as in Fig 10 A.

Fig. 11. PTXfO_2 diagram for the 160 xenoliths from our collection and 50 xenoliths and diamond inclusions from Reimers (1994). Symbols are the same as in Fig 10 A.

Fig. 12 A. REE and TRE spider diagrams for the minerals from concentrates ABK of Sytykanskaya pipe. Dashed lines is the range of kimberlite compositions for this pipe (Kostrovitsky et al., 2008; Kargin et al., 2011)

Fig. 12 B. REE patterns and TRE spider diagrams for the minerals from metasomatic xenoliths of Sytykanskaya pipe. Normalization to primitive mantle after McDonough and Sun (1995).

Fig. 13. REE patterns and TRE spider diagrams for the minerals from pyroxenite xenoliths and alkali amphibole-bearing glimmerites from Sytykanskaya pipe (marked by asterisks).

Fig. 14. Ages of phlogopites by ^{40}Ar-^{39}Ar method from xenoliths of Sytykanskaya pipe in comparison with ages for xenocrysts from Alakite kimberlite pipes

Fig. 15. REE and TRE spider diagrams for melts calculated for the minerals from concentrate ABK (A) and metasomatic xenoliths of Sytykanskaya pipe (B). Dashed pattern represents the range of kimberlite compositions in Sykanskaya pipe after Kargin et al. (2011).

Fig. 16. REE and TRE spider diagrams for melts parental for the minerals from pyroxenite xenoliths and amphibole-bearing glimmerites from Sytykanskaya pipe (marked by asterisks).

Fig. 17. A. Modeling of the partial melting of Udachnaya pipe peridotites with the bulk KD corresponding to the modal abundances (Doucet et al., 2013). B. Fractionation of the protokimberlite melts with the bulk KD corresponding to the association Ol =0,5, Ilm =0.15, Cpx=0.25, Gar =0.1. Partition coefficients from (Hart and Dunn, 1993; Hauri et al., 1994; Bedard, 2006; Green et al., 2000; Grove, 1994; Harte and Kirkley, 1997; Zack and Brumm, 1998).

Fig. 18. Scheme demonstrating the difference in conditions of the internal zones of magma chambers and feeder systems. The inner contact should be represented by essentially Cpx aggregates with garnet relics. The outer contacts should be represented by the veined peridotites.

Table 1. Compositions of the mantle xenocrysts from the Sytykan kimberlite pipes breccia

Number	S079	S052	S053	S054	S055	S056	S068	S640	S068	S067	S053	STK14	STK24	STK137	SG076	SG077	SG078	SG079	SG066	SG087	SG060	SG062	SG063	SG064	SI169	SI152	SI149	SI150	SI135	SI123	SI138
Element	Clinopyroxenes											Phlogopites			Garnets										Ilmenites						
SiO2	54.21	54.36	53.32	53.92	54.31	54.89	54.29	54.81	54.55	54.83	54.82	40.67	37.63	39.55	41.08	41.73	41.82	42.07	40.1	41.64	40.13	41.89	42.1	41.82							
TiO2	0.121	0.048	0.094	0.185	0.069	0.268	0.14	0.05	0.268	0.1	0.094	0.308	3.88	1.74	0.581	0.074	0.335	0.045	0.317	0.578	1.03	0.227	1.08	0.301	45.68	48.27	52.16	51.17	52.42	50.67	51.34
Al2O3	0.618	2.83	0.71	2.83	2.69	3.27	4.25	2.82	1.59	0.94	0.71	12.32	14.43	14.10	19.12	16.5	18.87	17.88	14.69	18.42	12.07	21.26	19.83	19.87	0.198	0.301	0.788	0.561	0.704	0.527	0.634
Cr2O3	2.26	3.01	2.61	0.788	3.35	0.681	3.51	3.37	4.09	3.53	2.61	0.323	0.46	1.89	4.16	9.87	5.76	8.11	10.23	5.25	12.37	2.68	1.89	4.79	2.52	2.41	0.528	0.468	0.744	0.578	0.547
FeO	2.22	2.18	2.04	3.25	1.9	4.3	2.07	2.31	2.39	2.36	2.04	4.73	5.18	5.22	9.21	6.7	7.14	7.01	8.54	7.36	7.43	8.42	9.32	7.15	42.59	40.37	33.83	36.64	34.21	37.85	34.91
MnO	0.067	0.1	0.046	0.068	0.101	0.142	0.075	0.086	0.102	0.062	0.046	0.035	0.063	0.06	0.471	0.449	0.416	0.422	0.453	0.282	0.38	0.391	0.313	0.387	0.284	0.289	0.42	0.227	0.286	0.213	0.244
MgO	16.06	14.27	15.63	14.67	13.93	17.57	13.22	13.92	14.75	14.86	15.63	24.71	23.27	23.16	17.79	22.65	20.79	22.81	15.85	20.41	17.91	20.28	20.95	20.85	7.66	8.97	12.47	10.07	12.23	10.37	12.18
CaO	21.24	18.96	21.2	20.3	18.55	14.69	16.96	18.12	17.64	19.84	21.2	0.044	0.052	0.01	6.75	1.59	4.56	1.57	9.05	5.47	7.82	4.56	4.74	4.52	0.063	0.105	0.157	0.096	0.158	0.087	0.148
Na2O	1.84	3.06	1.82	2.24	3.22	2.65	4.04	3.38	3.3	2.43	1.82	0.756	0.642	0.24	0.10	0.00	0.09	0.02	0.05	0.07	0.05	0.08	0.09	0.06	0.406	0.118	0.198	0.207	0.151	0.157	0.184
K2O	0.008	0.027	0.027	0.031	0.02	0.04	0.009	0	0.009	0.003	0.027	10.63	9.7	9.95	0.02	0.02	0.02	0.02	0.02	0.02	0.03	0.01	0.02	0.02							
Total	98.644	98.845	97.497	98.282	98.14	98.501	98.564	98.866	98.689	98.955	98.997	94.526	95.307	95.91	99.28	99.58	99.79	99.96	99.3	99.5	99.21	99.8	100.33	99.75	99.41	100.84	100.54	99.44	100.9	100.45	100.19
Ba	3.67	0.59	7.60	0.66	15.71	12.24	0.68	0.97	0.97	6.31	0.29	21546	16128	22.82	4.44	3.14	7.27	0.91	1.93	3.06	0.03	0.12	2.16	4.07	12.24	405	0.22	0.001	0.15	0.02	58.76
La	1.72	8.80	9.34	3.25	16.39	45.02	31.01	38.98	45.26	116.82	5.97	3.60	0.59	1.70	0.97	0.11	0.73	0.10	0.71	0.13	0.02	0.06	0.59	0.37	4.53	17.59	0.130	0.008	0.011	0.012	69.98
Ce	5.1	35.3	28.8	12.9	36.3	113.7	106.2	136.1	178.0	299.2	11.3	6.72	1.69	6.56	0.56	0.82	2.78	1.04	2.74	1.30	0.12	0.47	2.08	1.45	9.31	28.98	0.827	0.015	0.023	0.078	74.52
Pr	0.8	5.9	4.7	2.0	5.0	15.2	11.2	14.1	18.2	34.9	1.5	0.79	0.32	0.82	0.23	0.44	0.38	0.23	0.49	0.17	0.03	0.07	0.56	0.18	1.28	2.12	0.049	0.006	0.002	0.008	5.70
Nd	4.5	28.3	23.7	9.2	22.1	66.1	44.5	52.8	65.1	131.7	5.4	5.22	2.96	4.76	3.13	4.06	1.69	1.93	2.75	1.04	0.29	0.35	4.04	1.47	5.72	9.13	0.256	0.057	0.009	0.049	18.71
Sm	1.05	5.72	5.18	1.87	4.28	12.25	8.00	9.81	11.81	20.73	0.44	2.58	0.90	0.80	1.22	1.42	0.46	1.50	0.98	0.86	0.29	0.12	0.90	1.37	0.67	1.13	0.072	0.026	0.007	0.016	2.36
Eu	0.39	1.64	1.55	0.53	1.11	3.44	2.48	3.03	3.34	6.00	0.12	0.60	0.30	0.17	0.53	0.31	0.09	0.62	0.39	0.06	0.17	0.06	0.20	0.55	0.13	0.29	0.016	0.007	0.003	0.003	0.58
Gd	1.11	4.28	4.18	1.38	3.78	10.36	5.89	6.77	7.82	13.81	0.3	0.44	0.47	0.47	2.51	0.65	0.24	2.57	1.32	0.14	0.60	0.24	0.57	2.93	0.24	0.61	0.058	0.014	0.024	0.021	1.68
Tb	0.14	0.43	0.43	0.14	0.45	1.10	0.66	0.77	0.87	1.56	0.03	0.03	0.06	0.04	0.83	0.07	0.02	0.50	0.15	0.04	0.16	0.09	0.09	0.66	0.03	0.09	0.007	0.004	0.004	0.009	0.19
Dy	0.84	2.05	1.97	0.60	1.88	4.92	2.87	3.48	3.64	6.33	0.13	0.12	0.18	0.15	6.93	0.40	0.07	3.79	0.53	0.31	1.35	1.02	1.13	5.71	0.15	0.39	0.040	0.041	0.029	0.021	0.99
Ho	0.14	0.29	0.28	0.09	0.31	0.68	0.37	0.45	0.47	0.91	0.02	0.03	0.03	0.03	2.10	0.07	0.02	0.92	0.08	0.10	0.37	0.34	0.38	1.35	0.03	0.05	0.008	0.013	0.005	0.003	0.17
Er	0.34	0.65	0.56	0.18	0.71	1.08	0.70	0.82	0.84	1.57	0.03	0.08	0.05	0.23	5.37	0.17	0.09	2.72	0.20	0.39	1.06	1.49	1.61	4.69	0.08	0.11	0.024	0.012	0.016	0.019	0.41
Tm	0.04	0.06	0.06	0.02	0.08	0.12	0.06	0.08	0.09	0.18	0.003	0.02	0.02	0.02	0.75	0.05	0.01	0.41	0.04	0.07	0.19	0.27	0.29	0.74	0.01	0.03	0.003	0.005	0.003	0.008	0.06
Yb	0.22	0.40	0.31	0.10	0.48	0.66	0.32	0.38	0.44	0.83	0.011	0.06	0.11	0.36	5.40	0.28	0.23	3.06	0.38	0.81	1.40	2.17	2.98	5.85	0.10	0.10	0.032	0.026	0.034	0.022	0.45
Lu	0.03	0.04	0.03	0.01	0.06	0.06	0.04	0.04	0.05	0.09	0.002	0.01	0.04	0.08	0.85	0.11	0.03	0.49	0.12	0.15	0.23	0.39	0.59	0.88	0.02	0.02	0.005	0.007	0.007	0.005	0.05
Hf	0.56	2.43	3.14	1.04	5.70	6.93	1.92	2.35	2.42	4.43	0.37	0.35	0.22	0.17	0.70	0.26	0.13	2.26	0.64	0.11	0.57	0.11	0.54	1.96	28	45	17	17	28	26	37
Ta	0.03	0.11	0.17	0.02	0.34	0.15	0.03	0.04	0.20	4.06	0.002	0.61	3.77	1.12	0.01	0.07	0.05	0.06	0.05	0.11	0.01	0.02	0.21	0.09	431	18	269	183	377	364	373
Pb	2.84	0.29	0.71	0.33	10.44	5.86	2.77	3.72	4.12	4.77	0.8	9.96	1.92	1.73	0.77	0.84	1.75	0.35	0.73	1.05	0.22	0.27	1.73	2.83	6.36	7.88	1.67	0.18	0.99	0.59	14.02
Th	0.09	0.10	0.62	0.03	1.07	2.43	1.76	2.37	2.32	10.06	0.46	10.58	4.44	0.47	0.04	0.27	0.30	0.02	0.12	0.03	0.003	0.02	0.15	0.05	0.25	1.33	0.01	0.005	0.002	0.001	7.54
U	0.06	0.03	0.18	0.01	0.82	0.28	0.35	0.53	0.50	1.01	0.02	0.34	0.53	8.84	0.02	0.04	0.04	0.03	0.07	0.05	0.01	0.02	0.10	0.11	0.34	0.87	0.08	0.04	0.05	0.04	3.80
Sc	20	47	45	15	196	186	109	143	144	199	12	42	21	15	108	107	8	143	259	136	42	125	463	156	64.4	14.0	32.5	31.7	40.7	39.7	64.4
V	182	155	376	187	348	1084	1236	1649	1637	1462	141	1897	634	2151	217	102	1412	476	628	435	74	386	778	371	2826	1466	2110	1809	1801	1840	1994
Co	34	7	18	9	119	72	76	100	103	101	5	1023	490	539	41	23	408	93	106	68	22	71	107	118	331	42	270	222	196	202	272
Cu	5.46	0.18	6.56	1.05	52.71	16.51	2.53	6.42	2.16	11.66	0.3	33	18	13	180	202	78	3.3	7.5	14.1	1.0	0.7	10.1	23.4	59	34	55	47	34	30	84
Ni	434	114	317	126	2524	1014	957	1257	1253	1566	85	7548	4607	849	286	192	437	169	104	119	47	66	226	505	1370	329	1015	935	1030	1256	1958
Rb	0.73	0.04	0.63	0.05	3.81	0.32	0.01	0.02	0.07	0.40	0.03	7.56	3.38	7.35	0.05	0.10	3.50	0.01	0.14	0.52	0.06	0.11	0.15	0.39	5.22	2.37	0.21	0.03	0.33	0.14	28.21
Sr	102	247	253	119	415	968	770	979	1042	1318	133	50	21	389	0.00	2.56	194.57	1.75	126.61	3.90	1.32	0.54	8.42	11.78	70.8	38.3	6.4	0.4	0.5	0.5	147.4
Y	3.35	7.02	6.25	2.05	7.71	15.80	9.11	10.54	11.46	19.87	0.36	568	587	6	2.8	1.9	3.7	22.6	1.9	2.6	8.9	10.5	11.1	36.3	5.75	14.80	0.22	0.16	0.11	0.11	4.17
Zr	4.47	35.1	41.3	13.8	115.9	143.7	52.4	64.6	75.5	148.6	3.19	49	43	54	58.5	32.0	34.8	80.0	36.7	4.6	19.3	2.9	17.1	70.3	408	601	417	417	760	764	1009
Nb	0.26	0.73	2.24	0.18	3.57	3.04	1.30	1.78	5.29	168.22	0.03	4.3	69	14	2.71	2.03	1.70	0.58	0.69	1.26	0.05	0.31	1.74	0.72	3477	204	2005	1264	2708	2478	2929

Table 2. Compositions of the minerals from the peridotite mantle xenoliths of Sytykan kimberlite pipe

Element	S079	S052	S053	S054	S055	S056	S068	S640	S068	S067	S053	STK14	STK24	STK137	SG76	SG07	SG78	SG79	SG66	SG87	SG60	SG62	SG63	SG64	SI169	SI152	SI149	SI150	SI135	SI123	SI138
SiO2	54.89	55.25	55.29	54.55	55.90	55.43	52.72	55.48	54.90	55.13	55.46	42.70	42.35	42.75																	
TiO2	0.13	0.12	0.13	0.14	0.08	0.30	0.42	0.08	0.10	0.13	0.23	0.37	0.43	0.37	41.51	40.84	42.05	41.56	40.84	42.06	42.06	41.71	40.8	42.29							
Al2O3	2.03	0.43	0.70	0.74	3.22	3.31	2.51	0.78	0.54	2.37	1.64	11.02	11.98	10.84	0.193	0.161	0.232	0.218	0.161	0.678	0.678	0.15	0.133	0.064	53.69	49.38	50.68	49.18	49.13	46.73	53.09
Cr2O3	2.36	1.74	0.65	3.19	5.35	3.56	3.26	2.54	3.42	2.76	0.13	0.21	0.38	0.20	21.22	15.53	22.24	21.39	15.53	16.34	16.34	21.01	19.91	21.75	0.68	0.33	0.25	0.35	0.32	0.34	0.53
FeO	2.66	3.43	1.82	1.65	2.06	3.16	2.92	2.56	2.05	2.56	3.91	3.60	2.70	3.41	2.33	9.95	0.766	2.38	9.95	5.87	5.87	3.01	3.98	3.37	0.65	1.80	0.95	1.89	1.93	2.63	4.93
MnO	0.09	0.07	0.07	0.06	0.09	0.08	0.10	0.06	0.06	0.09	0.06	0.02	0.03	0.01	7.73	7.03	9.01	8.8	7.03	7.91	7.91	9.13	9.33	7.45	31.60	38.30	35.80	37.32	38.63	39.35	24.46
MgO	15.89	16.28	17.04	16.11	13.50	14.53	15.84	16.23	15.70	15.59	17.16	27.79	26.98	28.08	0.334	0.427	0.479	0.482	0.427	0.334	0.334	0.496	0.521	0.49	0.24	0.34	0.26	0.35	0.28	0.32	0.32
CaO	19.81	22.86	23.32	21.29	17.19	16.64	21.06	21.20	21.54	18.94	21.82	0.05	0.02	0.11	20.16	20.06	16.34	20.17	20.06	20.01	20.01	20.26	18.04	22.06	12.06	9.29	10.35	10.60	9.52	8.59	16.25
Na2O	2.71	1.69	0.58	1.81	4.46	4.21	1.99	2.19	2.23	3.09	1.40	0.18	0.12	0.13	4.74	4.86	8.17	3.92	4.86	4.59	4.59	3.74	6.02	2.97							
K2O												10.24	9.55	9.46	0.049	0.049	0.038	0.065	0.049	0.236	0.236	0.041	0.017	0.033							
Total	100.57	101.88	99.60	99.55	101.85	101.22	100.83	101.12	100.54	100.66	101.82	96.18	94.53	95.36	98.27	98.91	99.33	98.99	98.91	98.03	98.03	99.55	98.75	100.48	98.92	99.44	98.28	99.68	99.81	97.96	99.59
Ba	3.67	0.59	7.6	0.66	15.71	12.24	0.68	0.97	0.97	6.31	0.29	21546	16128	22.82	4.44	3.14	7.27	0.91	1.93	3.06	0.03	0.12	2.16	4.07	12.24	404.8	0.22	0	0.15	0.02	58.76
La	1.72	8.8	9.34	3.25	16.39	45.02	31.01	38.98	45.26	116.82	5.97	3.6	0.59	1.7	0.97	0.11	0.73	0.1	0.71	0.13	0.02	0.06	0.59	0.37	4.53	17.59	0.13	0.008	0.011	0.012	69.98
Ce	5.1	35.3	28.8	12.9	36.3	113.7	106.2	136.1	178	299.2	11.3	6.72	1.69	6.56	0.56	0.82	2.78	1.04	2.74	1.3	0.12	0.47	2.08	1.45	9.31	28.98	0.827	0.015	0.023	0.078	74.52
Pr	0.8	5.9	4.7	2	5	15.2	11.2	14.1	18.2	34.9	1.5	0.79	0.32	0.82	0.23	0.44	0.38	0.23	0.49	0.17	0.03	0.07	0.56	0.18	1.28	2.12	0.049	0.006	0.002	0.008	5.7
Nd	4.5	28.3	23.7	9.2	22.1	66.1	44.5	52.8	65.1	131.7	5.4	5.22	2.96	4.76	3.13	4.06	1.69	1.93	2.75	1.04	0.29	0.35	4.04	1.47	5.72	9.13	0.256	0.057	0.009	0.049	18.71
Sm	1.05	5.72	5.18	1.87	4.28	12.25	8	9.81	11.81	20.73	0.44	2.58	0.9	0.8	1.22	1.42	0.46	1.5	0.98	0.86	0.29	0.12	0.9	1.37	0.67	1.13	0.072	0.026	0.007	0.016	2.36
Eu	0.39	1.64	1.55	0.53	1.11	3.44	2.48	3.03	3.34	6	0.12	0.6	0.3	0.17	0.53	0.31	0.09	0.62	0.39	0.06	0.17	0.06	0.2	0.55	0.13	0.29	0.016	0.007	0.003	0.003	0.58
Gd	1.11	4.28	4.18	1.38	3.78	10.36	5.89	6.77	7.82	13.81	0.3	0.44	0.47	0.47	2.51	0.65	0.24	2.57	1.32	0.14	0.6	0.24	0.57	2.93	0.24	0.61	0.058	0.014	0.024	0.021	1.68
Tb	0.14	0.43	0.43	0.14	0.45	1.1	0.66	0.77	0.87	1.56	0.03	0.03	0.06	0.04	0.83	0.07	0.02	0.5	0.15	0.04	0.16	0.09	0.09	0.66	0.03	0.09	0.007	0.004	0.004	0.009	0.19
Dy	0.84	2.05	1.97	0.6	1.88	4.92	2.87	3.48	3.64	6.33	0.13	0.12	0.18	0.15	6.93	0.4	0.07	3.79	0.53	0.31	1.35	1.02	1.13	5.71	0.15	0.39	0.04	0.041	0.029	0.021	0.98
Ho	0.14	0.29	0.28	0.09	0.31	0.68	0.37	0.45	0.47	0.91	0.02	0.03	0.03	0.03	2.1	0.07	0.02	0.92	0.08	0.1	0.37	0.34	0.38	1.35	0.03	0.05	0.008	0.013	0.005	0.003	0.17
Er	0.34	0.65	0.56	0.18	0.71	1.08	0.7	0.82	0.84	1.57	0.03	0.08	0.05	0.23	5.37	0.17	0.09	2.72	0.2	0.39	1.06	1.49	1.61	4.69	0.08	0.11	0.024	0.012	0.016	0.019	0.41
Tm	0.04	0.06	0.06	0.02	0.08	0.12	0.06	0.08	0.09	0.18	0.003	0.02	0.02	0.02	0.75	0.05	0.01	0.41	0.04	0.07	0.19	0.27	0.29	0.74	0.01	0.03	0.003	0.005	0.003	0.008	0.06
Yb	0.22	0.4	0.31	0.1	0.48	0.66	0.32	0.38	0.44	0.83	0.011	0.06	0.11	0.36	5.4	0.28	0.23	3.06	0.38	0.81	1.4	2.17	2.98	5.85	0.1	0.1	0.032	0.026	0.034	0.022	0.45
Lu	0.03	0.04	0.03	0.01	0.06	0.06	0.04	0.04	0.05	0.09	0.002	0.01	0.04	0.08	0.85	0.11	0.03	0.49	0.12	0.15	0.23	0.39	0.59	0.88	0.02	0.02	0.005	0.007	0.007	0.005	0.05
Hf	0.56	2.43	3.14	1.04	5.7	6.93	1.92	2.35	2.42	4.43	0.37	0.35	0.22	0.17	0.7	0.26	0.13	2.26	0.64	0.11	0.57	0.11	0.54	1.96	28	45	17	17	28	26	37
Ta	0.03	0.11	0.17	0.02	0.34	0.15	0.03	0.04	0.2	4.06	0.002	0.61	3.77	1.12	0.01	0.07	0.05	0.06	0.05	0.11	0.01	0.02	0.21	0.09	431	18	269	183	377	364	373
Pb	2.84	0.29	0.71	0.33	10.44	5.86	2.77	3.72	4.12	4.77	0.8	9.96	1.92	1.73	0.77	0.84	1.75	0.35	0.73	1.05	0.22	0.27	1.73	2.83	6.36	7.88	1.67	0.18	0.99	0.59	14.02
Th	0.09	0.1	0.62	0.03	1.07	2.43	1.76	2.37	2.32	10.06	0.46	10.58	4.44	0.47	0.04	0.27	0.3	0.02	0.12	0.03	0.03	0.02	0.15	0.05	0.25	1.33	0.01	0.005	0.002	0.001	7.54
U	0.06	0.03	0.18	0.01	0.82	0.28	0.35	0.53	0.5	1.01	0.02	0.34	0.53	8.84	0.02	0.04	0.04	0.03	0.07	0.05	0.01	0.02	0.1	0.11	0.34	0.87	0.08	0.04	0.05	0.04	3.8
Sc	20	47	45	15	196	186	109	143	144	199	12	42	21	15	108	107	8	143	259	136	42	125	463	156	64.4	14	32.5	31.7	40.7	39.7	64.4
V	182	155	376	187	348	1084	1236	1649	1637	1462	141	1897	634	2151	217	102	1412	476	628	435	74	386	778	371	2826	1466	2110	1809	1801	1840	1994
Co	34	7	18	9	119	72	76	100	103	101	5	1023	490	539	41	23	408	93	106	68	22	71	107	118	331	42	270	222	196	202	272
Cu	5.46	0.18	6.56	1.05	52.71	16.51	2.53	6.42	2.16	11.66	0.3	33	18	13	180	202	78	3.3	7.5	14.1	1	0.7	10.1	23.4	59	34	55	47	34	30	84
Ni	434	114	317	126	2524	1014	957	1257	1253	1566	85	7548	4607	849	286	192	437	169	104	119	47	66	226	505	1370	329	1015	935	1030	1256	1958
Rb	0.73	0.04	0.63	0.05	3.81	0.32	0.01	0.02	0.07	0.4	0.03	7.56	3.38	7.35	0.05	0.1	3.5	0.01	0.14	0.52	0.06	0.11	0.15	0.39	5.22	2.37	0.21	0.03	0.33	0.14	28.2
Sr	102	247	253	119	415	968	770	979	1042	1318	133	50	21	389	0	2.56	194.57	1.75	126	3.9	1.32	0.54	8.42	11.78	70.8	38.3	6.4	0.4	0.5	0.5	147.4
Y	3.35	7.02	6.25	2.05	7.71	15.8	9.11	10.54	11.46	19.87	0.36	568	587	6	2.8	1.9	3.7	22.6	1.9	2.6	8.9	10.5	11.1	36.3	5.75	14.8	0.22	0.16	0.11	0.11	4.17
Zr	4.47	35.1	41.3	13.8	115.9	143.7	52.4	64.6	75.5	148.6	3.19	49	43	54	58.5	32	34.8	80	36.7	4.6	19.3	2.9	17.1	70.3	408	601	417	417	760	764	1009
Nb	0.26	0.73	2.24	0.18	3.57	3.04	1.3	1.78	5.29	168.22	0.03	4.3	69	14	2.71	2.03	1.7	0.58	0.69	1.26	0.05	0.31	1.74	0.72	3477	204	2005	1264	2708	2478	2929

Table 3. Compositions of the minerals from the pyroxenite mantle xenoliths of Sytykan kimberlite pipe

Element	STk135Ga	STk135Cp	STk55Gar	STk55Cpx	STk55Ilm	STk115Ga	STk115Cp	STk9Gar	STk9Cpx	STk75Gar	STk75Cpx	STk60Cpx	STk60Ilm	STk196Cp	STk189Phl	STk196Sp	STk167Cp	STk167Ga	STk250Cp	STk250Ga
SiO2	41.34	55.1	55.09	41.79		41.85	53.07	41.2	55.47	42.38	56.03	54.78		56.23	41.43		54.54	42.43	55.68	41.9
TiO2	0.104	0.046	0.218	0.168	48.37	0.034	0.96	0.094	0.044	0.239	0.119	0.249	48.37	0.157	0.17	0.38	0.082	0.245	0.3	0.174
Al2O3	19.87	0.772	2.7	22.76	0.5	20.66	1.57	19.88	0.802	21.95	1.03	3.38	0.43	1.95	13.15	8.77	1.34	21.99	4.96	21.14
Cr2O3	4.44	0.727	0.71	0.533	0.45	3.72	1.4	4.35	0.82	2.07	0.419	1.63	2.12	0.533	0.82	57.68	3.34	1.95	2.64	3.44
FeO	9.99	1.8	2.12	9.51	37.02	8.83	2.54	9.93	1.9	7.43	2.47	2.9	37.46	2.61	2.82	21.81	3.02	7.47	1.82	9.34
MnO	0.48	0.056	0.044	0.456	0.22	0.461	0.08	0.449	0.065	0.372	0.097	0.09	0.29	0.106	0.02	0.42	0.086	0.365	0.071	0.517
MgO	17.74	17.52	15.87	16.9	9.59	19.21	16.1	17.92	17.47	21.15	17.57	14.56	9.14	17.01	26.05	10.45	15.12	21.09	13.67	20.17
CaO	5.87	22.77	21.93	7.91		5.09	23.49	6.04	22.95	4.64	21.27	19.91		20.07	0		19.17	4.66	17.15	3.86
Na2O	0.009	0.576	1.67	0.046		0.005	0.58	0.007	0.604	0.045	1.28	2.75	0.08	1.85	0.53		2.95	0.026	3.94	0.074
K2O	0.008	0.017	0.008	0.01		0.004	0.01	0.005	0.018	0.005	0.024	0.01	0.01	0.022	9.57		0.011	0.009	0.015	0.011
Total	99.85	99.38	100.35	100.09		99.88		99.88	100.14	100.29	100.31	100.25		100.54	0.1		99.65	100.23	100.25	100.62
Ba	0.025	0.16	0.055	0.12	0.02	0.022	4.03	0.037	0.1	0.023	5.0	1.0	0.3	1.52	1644	0.044	0.24	0.017	0.376	0.621
La	0.155	2.39	0.136	5.20	0.13	0.13	7.04	0.14	3.20	0.14	7.35	4.61	0.3	33.5	0.70	0.13	5.80	0.13	6.52	0.12
Ce	0.21	4.16	0.17	12.33	0.12	0.15	12.3	0.22	5.07	0.24	15.7	13.41	0.2	94.2	1.64	0.14	18.6	0.27	26.60	0.21
Pr	0.05	0.44	0.05	1.89	0.01	0.02	1.43	0.037	0.51	0.05	2.13	2.57	0.0	16.2	0.20	0.01	3.79	0.06	4.17	0.05
Nd	0.37	1.60	0.51	7.78	0.06	0.21	5.35	0.41	1.8	0.33	5.9	14.8	0.1	82.9	0.90	0.05	17.09	0.37	18.03	0.49
Sm	0.18	0.18	0.518	1.64	0.01	0.11	0.837	0.24	0.23	0.24	1.0	3.312	0.0	15.7	0.23	0.01	4.13	0.34	4.80	0.84
Eu	0.08	0.05	0.26	0.45	0.01	0.05	0.17	0.11	0.1	0.151	0.3	0.97	0.01	3.81	0.11	0.01	0.98	0.20	1.32	0.51
Gd	0.49	0.17	1.16	1.02	0.07	0.22	0.45	0.59	0.19	0.76	0.76	3.02	0.07	11.2	0.22	0.05	2.97	1.00	3.93	3.00
Tb	0.12	0.02	0.25	0.07	0.01	0.074	0.04	0.14	0.02	0.19	0.08	0.43	0.01	1.15	0.04	0.01	0.36	0.21	0.48	0.83
Dy	1.25	0.10	1.79	0.30	0.03	0.82	0.17	1.63	0.10	1.68	0.37	2.34	0.03	6.12	0.19	0.01	1.69	1.99	2.49	7.52
Ho	0.40	0.02	0.40	0.033	0.005	0.24	0.03	0.48	0.02	0.42	0.06	0.41	0.01	0.89	0.04	0.00	0.27	0.55	0.33	1.74
Er	1.52	0.03	1.27	0.072	0.024	1.06	0.05	1.70	0.04	1.50	0.12	1.04	0.03	2.30	0.10	0.01	0.63	1.91	0.58	5.20
Tm	0.24	0.003	0.17	0.008	0.003	0.20	0.01	0.30	0.01	0.24	0.01	0.10	0.00	0.19	0.01	0.00	0.06	0.26	0.05	0.90
Yb	1.91	0.02	1.19	0.031	0.028	1.67	0.04	2.43	0.03	1.61	0.06	0.68	0.02	1.31	0.07	0.01	0.34	1.86	0.23	7.57
Lu	0.32	0.003	0.19	0.005	0.006	0.30	0.00	0.49	0.00	0.27	0.01	0.10	0.01	0.21	0.01	0.00	0.04	0.31	0.02	1.01
Hf	0.10	0.023	0.25	1.027	16.3	0.11	0.15	0.14	0.04	0.32	0.14	4.65	21.5	6.78	0.46	0.08	1.77	0.40	3.33	0.19
Ta	0.00	0.00	0.00	0.038	205	0.06	0.22	0.01	0.03	0.02	0.12	0.30	327	0.19	2.18	0.87	0.035	0.04	0.00	0.001
Pb	0.079	0.40	0.085	0.38	0.036	0.14	1.39	0.14	0.54	0.10	0.92	0.49	0.038	1.12	1.73	0.024	0.40	0.10	1.39	0.063
Th	0.029	0.105	0.005	0.528	0.004	0.007	0.48	0.024	0.17	0.07	0.23	0.27	0.013	0.55	8.07	0.003	0.057	0.013	0.19	0.007
U	0.02	0.016	0.007	0.079	0.05	0.009	0.091	0.023	0.018	0.019	0.031	0.025	0.04	0.057	0.89	0.004	0.011	0.023	0.006	0.003
Co	49.6	25.4	33.8	24.1	175	46.2	22.5	57.8	28.1	47.9	19.4	16.7	175	21.1	64.4	230	17.2	42.3	14.2	36.4
Cu	0.39	1.27	0.54	0.86	35	1.45	3.37	1.08	2.12	1.03	1.79	1.41	25.3	6.07	3.91	2.74	2.44	2.42	1.27	0.83
Ni	21	331	14	293	645	18	358	27	412	39	316	204	973	335	1484	613	284	36	201	12
Rb	0.24	0.21	0.333	0.215	0.16	0.202	1.06	0.21	0.19	0.194	1.25	0.15	0.14	1.21	395	0.40	0.11	0.11	0.30	0.39
Sr	0.4	40	0.1	196	0	0.3	222	0.1	50.3	0.1	120	147	1	527	25.1	0.2	241	0.2	891.1	0.4
Y	9.25	0.3	9.94	0.80	0.08	6.7	0.6	10.2	0.4	10.6	1.4	8.5	0.1	19.6	1.0	0.0	5.7	12.2	7.4	40.4
Zr	3.4	0.4	13.3	17.8	401	3.5	3.4	3.4	0.6	9.4	3.4	148	570	214	12.7	3.0	34.2	10.8	60.7	7.3
Nb	0.07	0.04	0.02	0.49	1620	0.62	3.54	0.13	0.34	0.29	1.46	1.21	2733	2.67	39.2	9.04	0.46	0.30	0.04	0.04

Fig.1

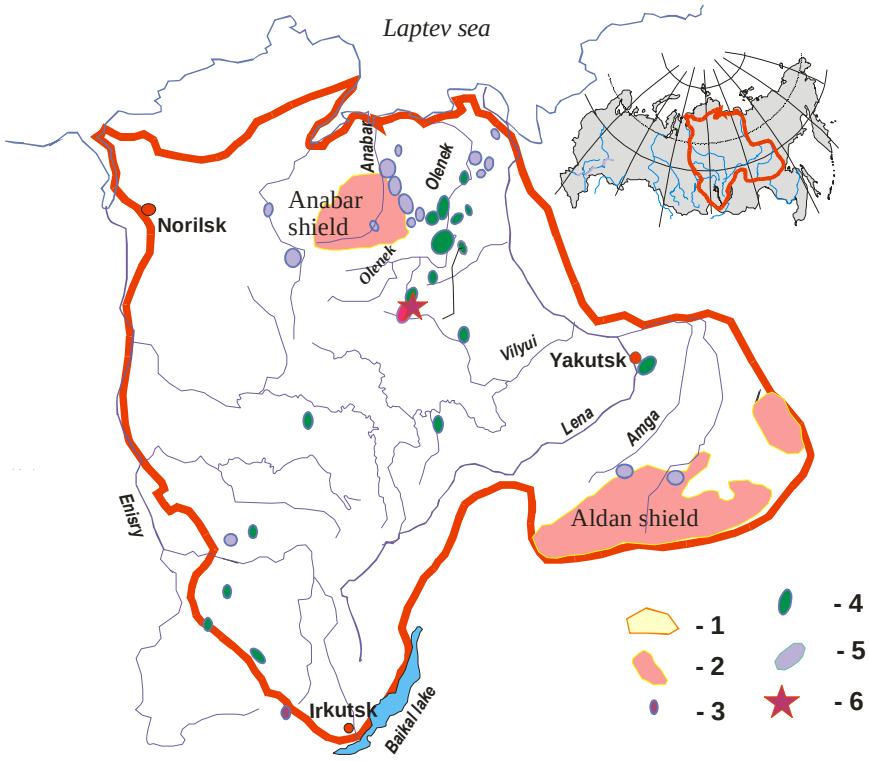
Laptev sea
Anabar
Olenek
Anabar shield
Norilsk
Olenek
Vilyui
Yakutsk
Lena
Amga
Aldan shield
Enisey
Irkutsk
Baikal lake
- 1
- 2
- 3
- 4
- 5
- 6

A.

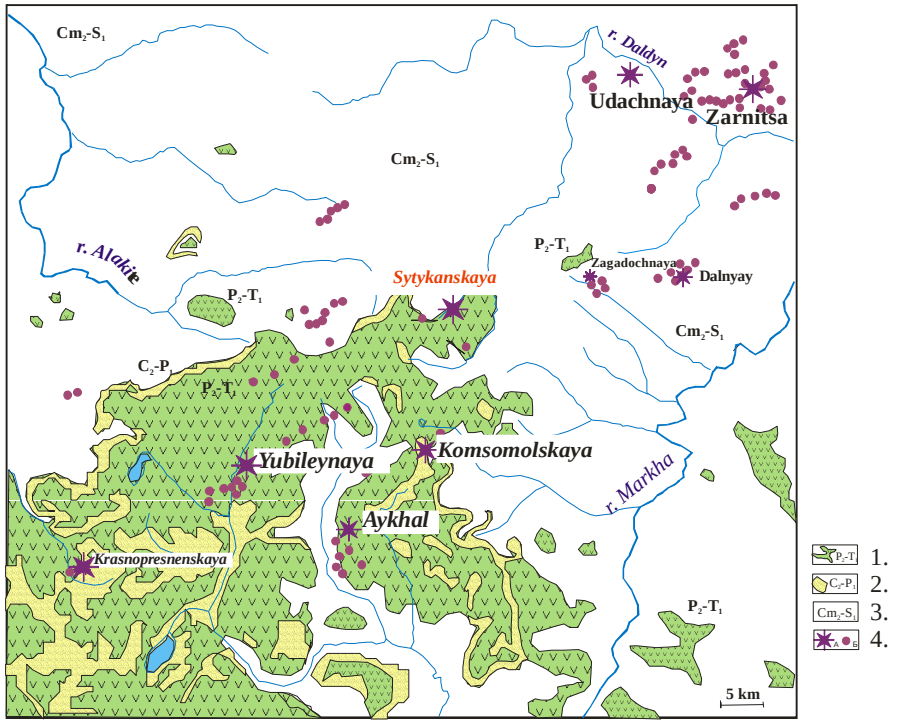
Cm2-S1
r. Daldyn
Udachnaya
Zarnitsa
Cm2-S1
r. Aldan
P2-T1
Zagadochnaya
Dalnyay
Sytykanskaya
P2-T1
Cm2-S1
C2-P1
P2-T1
Yubileynaya
Komsomolskaya
r. Markha
Aykhal
Krasnopresnenskaya
P2-T1
5 km
1.
2.
3.
4.

B.

Fig.2

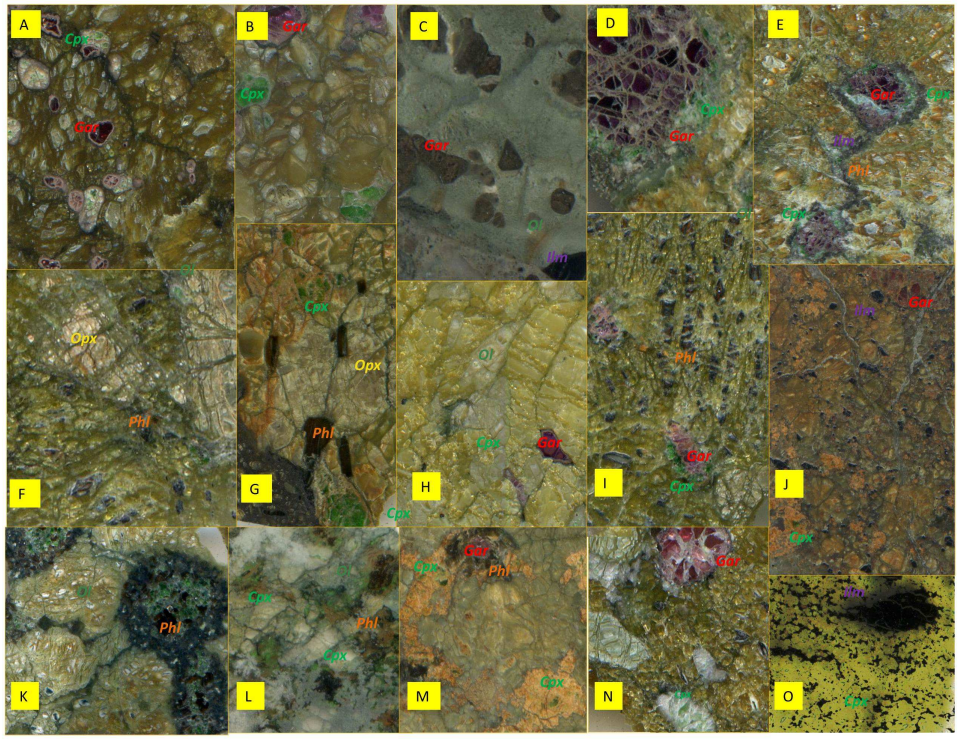

Fig.3

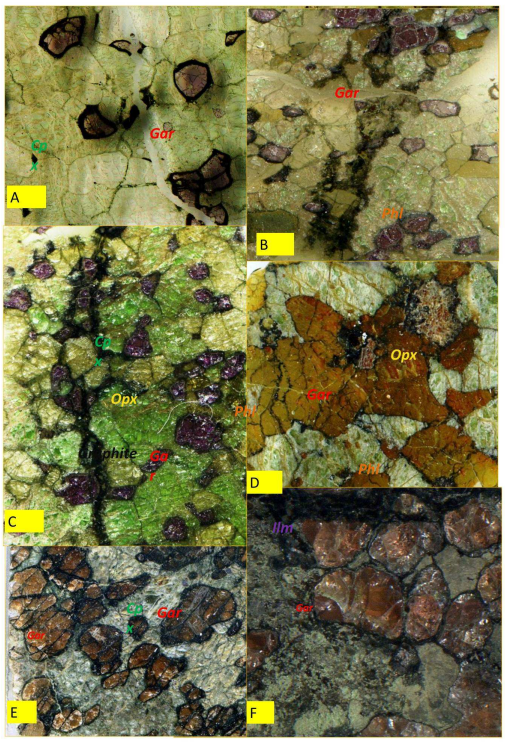

Fig.4

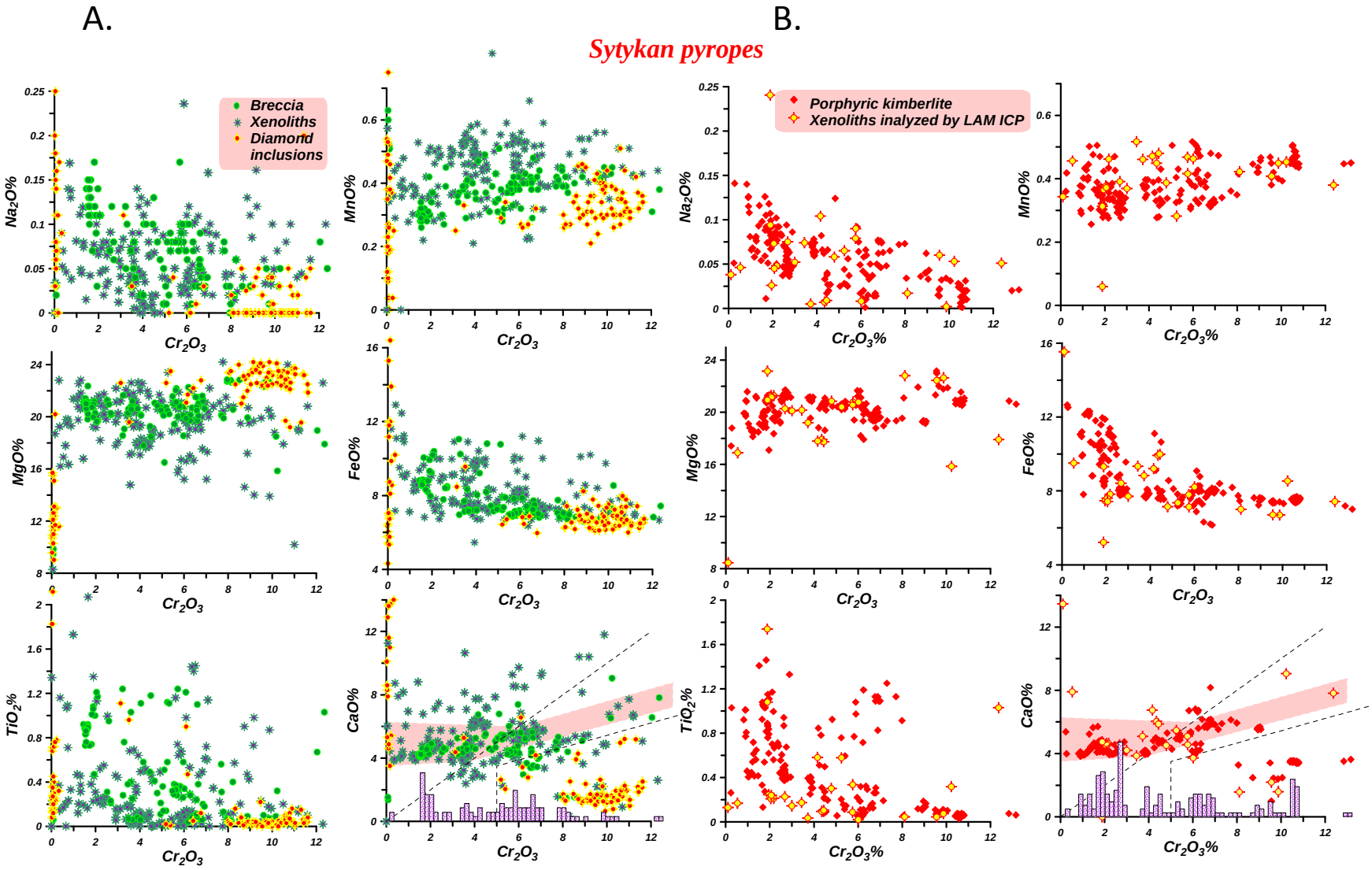
A.
B.
Sytykan pyropes
Breccia
Xenoliths
Diamond inclusions
Porphyric kimberlite
Xenoliths inalyzed by LAM ICP
Na2O%
MnO%
MgO%
FeO%
TiO2%
CaO%
Cr2O3
Cr2O3%

Fig.5

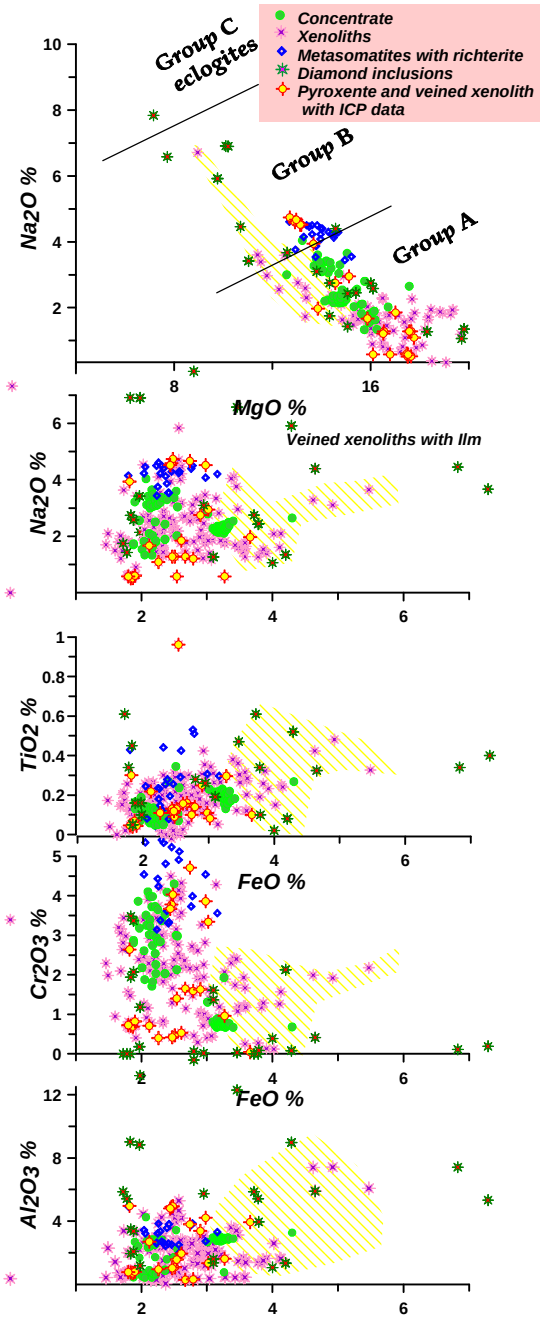
Concentrate
Xenoliths
Metasomatites with richterite
Diamond inclusions
Pyroxente and veined xenolith with ICP data
Group C eclogites
Group B
Group A
Na2O %
MgO %
Veined xenoliths with Ilm
Na2O %
TiO2 %
FeO %
Cr2O3 %
FeO %
Al2O3 %

Fig.6

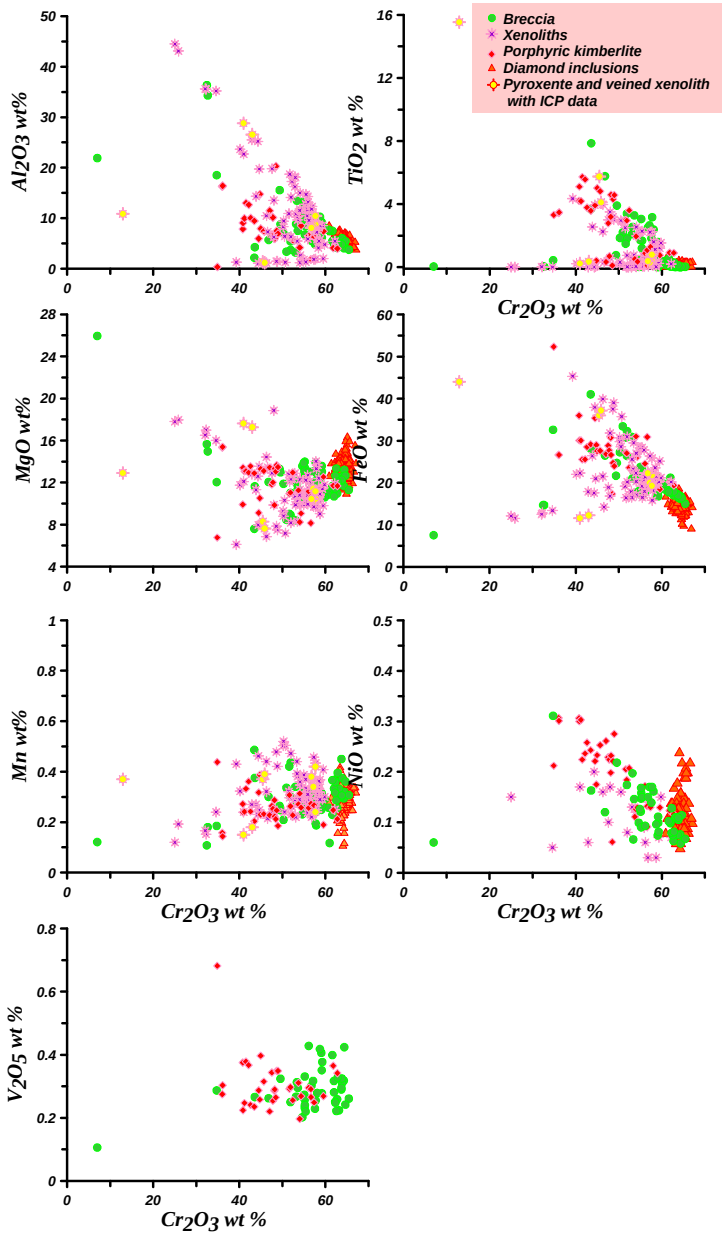
Breccia
Xenoliths
Porphyric kimberlite
Diamond inclusions
Pyroxente and veined xenolith with ICP data
Al2O3 wt%
TiO2 wt %
Cr2O3 wt %
MgO wt%
FeO wt %
Mn wt%
NiO wt %
V2O5 wt %

Fig.7

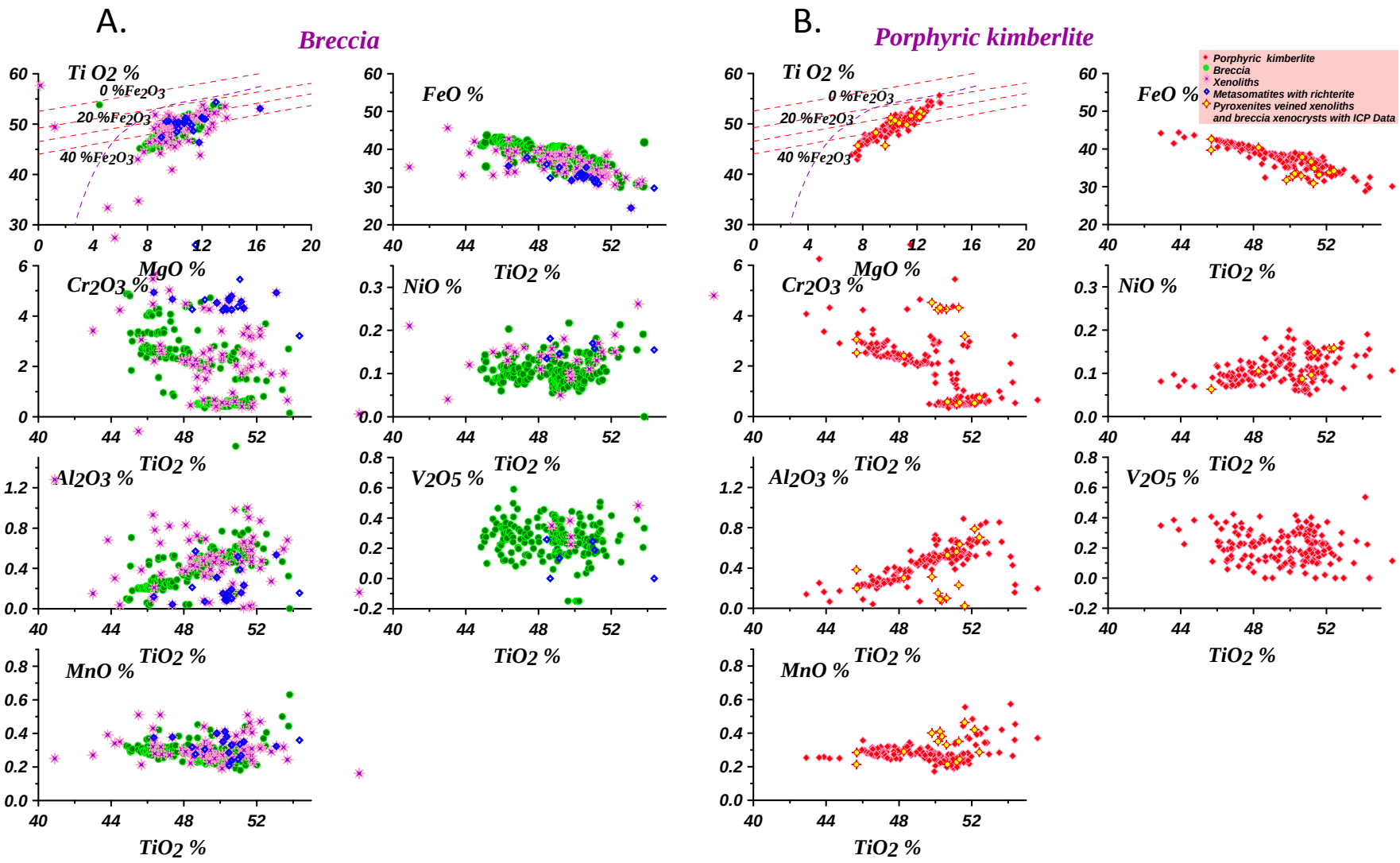
A.
Breccia
B.
Porphyric kimberlite
Ti O2 %
0 %Fe2O3
20 %Fe2O3
40 %Fe2O3
MgO %
FeO %
Cr2O3 %
TiO2 %
NiO %
Al2O3 %
V2O5 %
MnO %
Porphyric kimberlite
Breccia
Xenoliths
Metasomatites with richterite
Pyroxenites veined xenoliths
and breccia xenocrysts with ICP Data

Fig.8

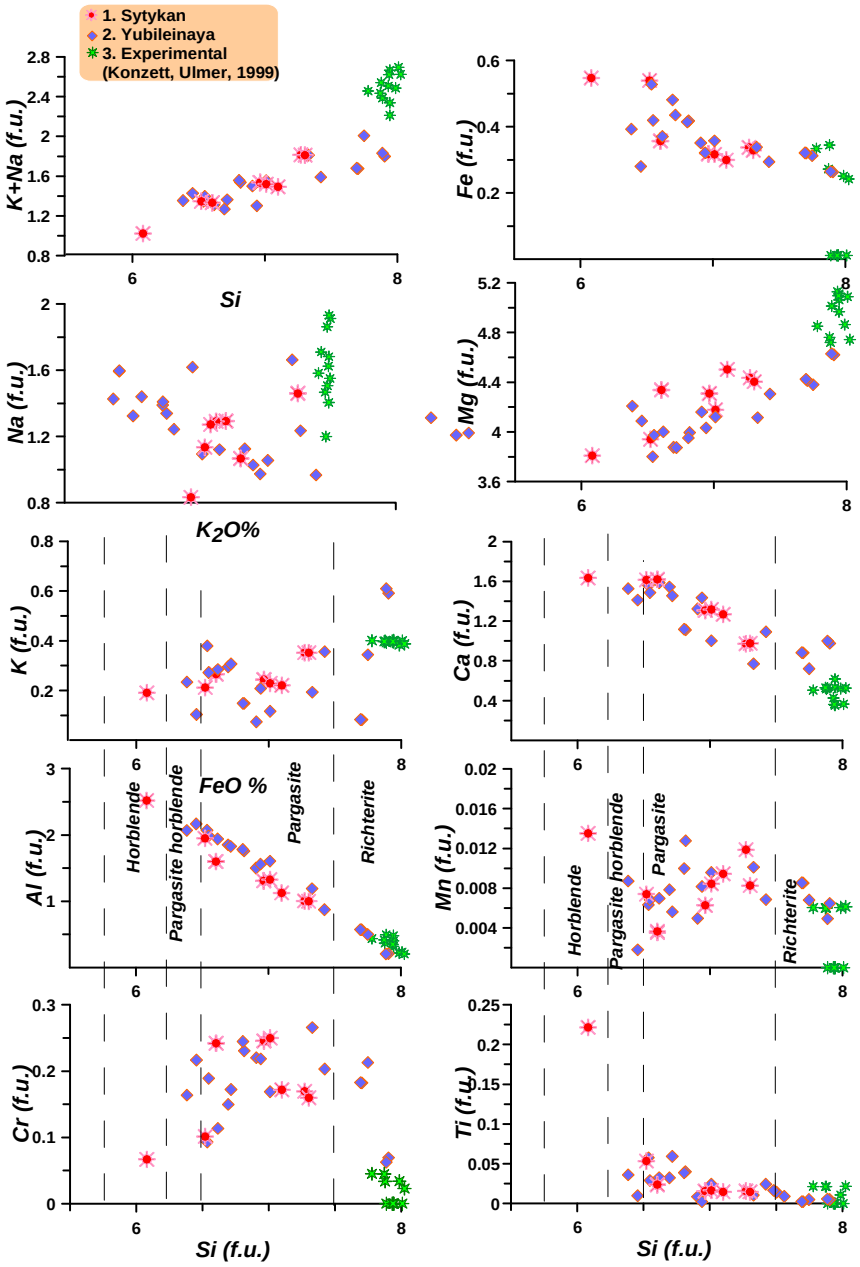
1. Sytykan
2. Yubileinaya
3. Experimental
(Konzett, Ulmer, 1999)
K+Na (f.u.)
Si
Fe (f.u.)
Na (f.u.)
Mg (f.u.)
K2O%
K (f.u.)
Ca (f.u.)
FeO %
Al (f.u.)
Horblende
Pargasite horblende
Pargasite
Richterite
Mn (f.u.)
Cr (f.u.)
Ti (f.u.)
Si (f.u.)

Fig.9

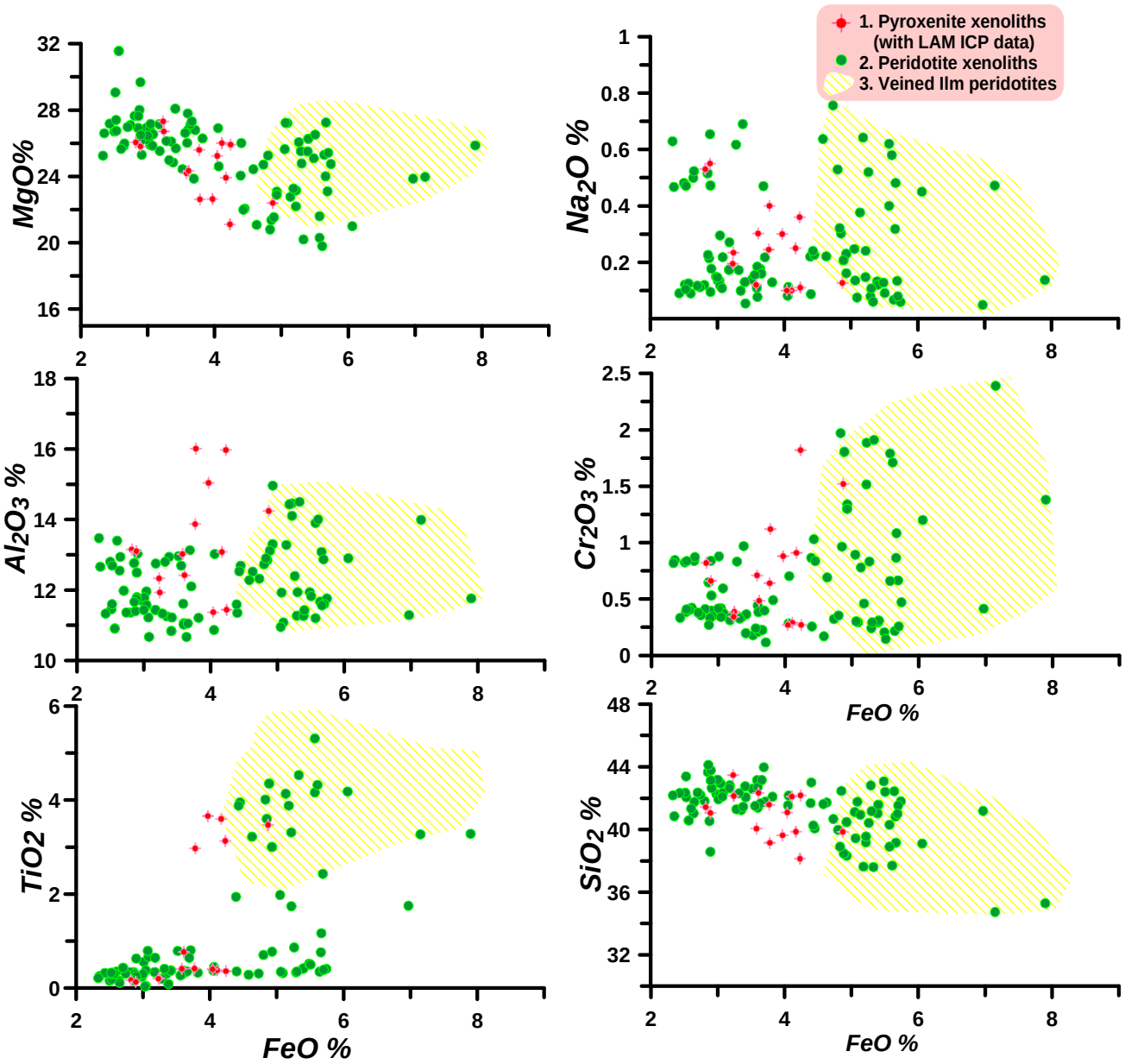
1. Pyroxenite xenoliths (with LAM ICP data)
2. Peridotite xenoliths
3. Veined Ilm peridotites
MgO%
Na2O %
Al2O3 %
Cr2O3 %
TiO2 %
SiO2 %
FeO %
FeO %

Fig.10

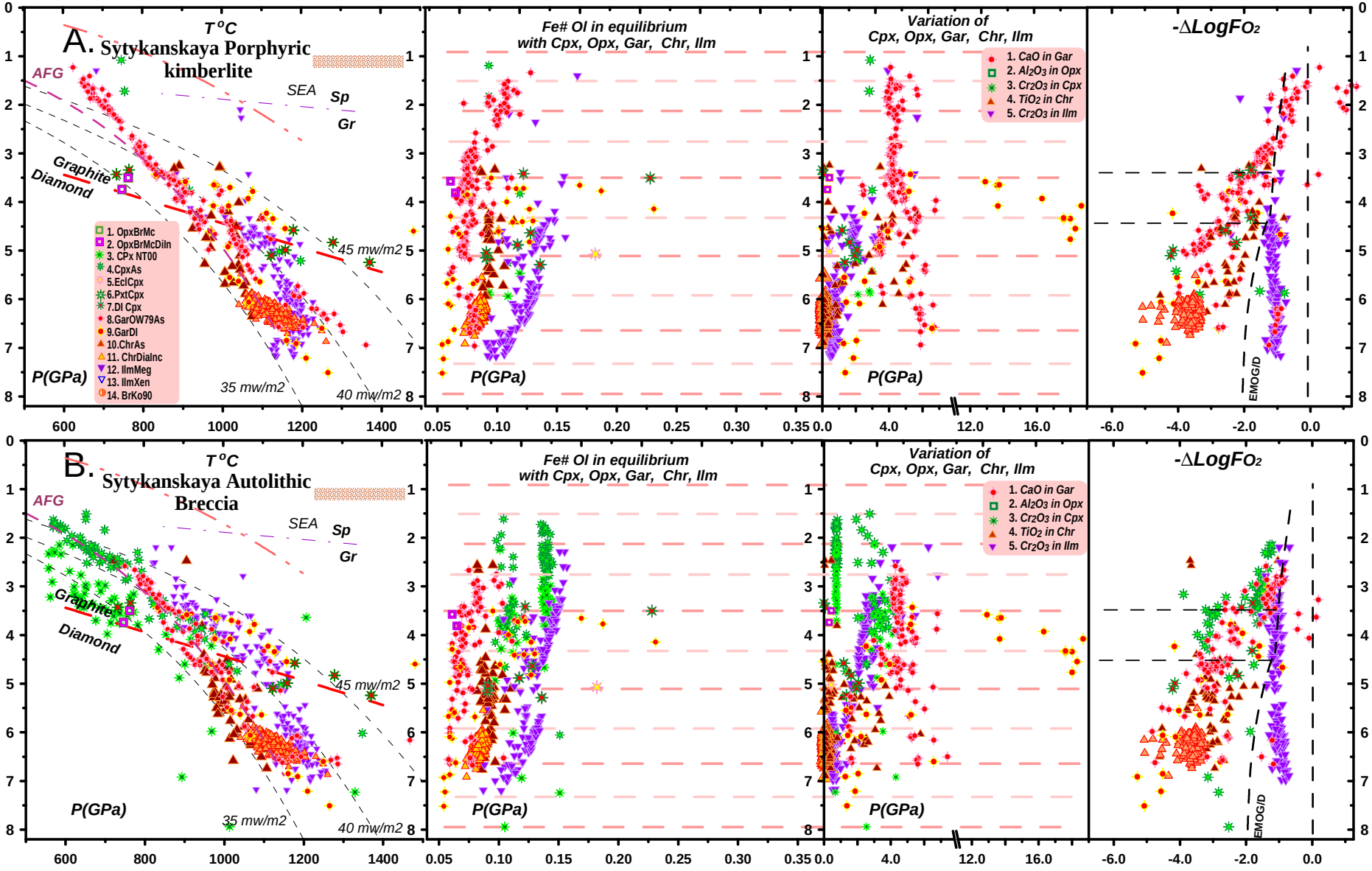
A. Sytykanskaya Porphyric kimberlite
B. Sytykanskaya Autolithic Breccia
T °C
AFG
SEA
Sp
Gr
Graphite
Diamond
45 mw/m2
35 mw/m2
40 mw/m2
P(GPa)
1. OpxBrMc
2. OpxBrMcDiln
3. CPx NT00
4.CpxAs
5.EclCpx
6.PxtCpx
7.DI Cpx
8.GarOW79As
9.GarDI
10.ChrAs
11. ChrDialnc
12. IlmMeg
13. IlmXen
14. BrKo90
Fe# Ol in equilibrium with Cpx, Opx, Gar, Chr, Ilm
Variation of Cpx, Opx, Gar, Chr, Ilm
1. CaO in Gar
2. Al2O3 in Opx
3. Cr2O3 in Cpx
4. TiO2 in Chr
5. Cr2O3 in Ilm
-ΔLogFO2
EMOG/D

Fig.11

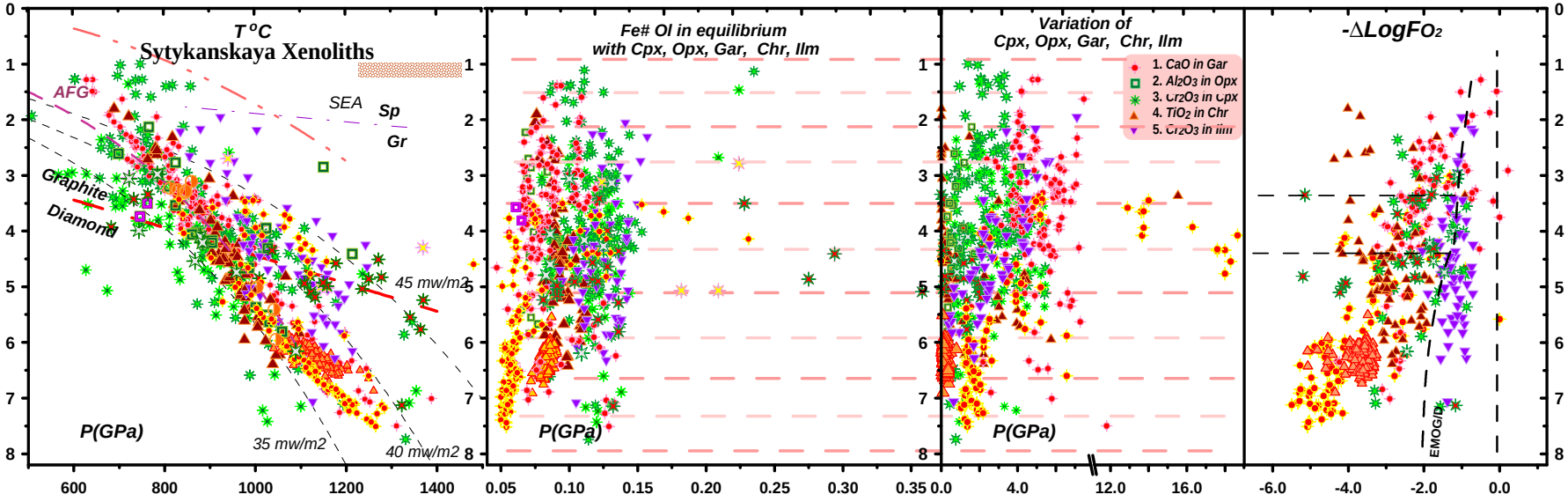
T °C
Sytykanskaya Xenoliths
AFG
SEA
Sp
Gr
Graphite
Diamond
45 mw/m2
35 mw/m2
40 mw/m2
P(GPa)
Fe# Ol in equilibrium
with Cpx, Opx, Gar, Chr, Ilm
P(GPa)
Variation of
Cpx, Opx, Gar, Chr, Ilm
1. CaO in Gar
2. Al2O3 in Opx
3. Cr2O3 in Cpx
4. TiO2 in Chr
5. Cr2O3 in Ilm
P(GPa)
-ΔLogFO2
EMOG/D

Fig.12

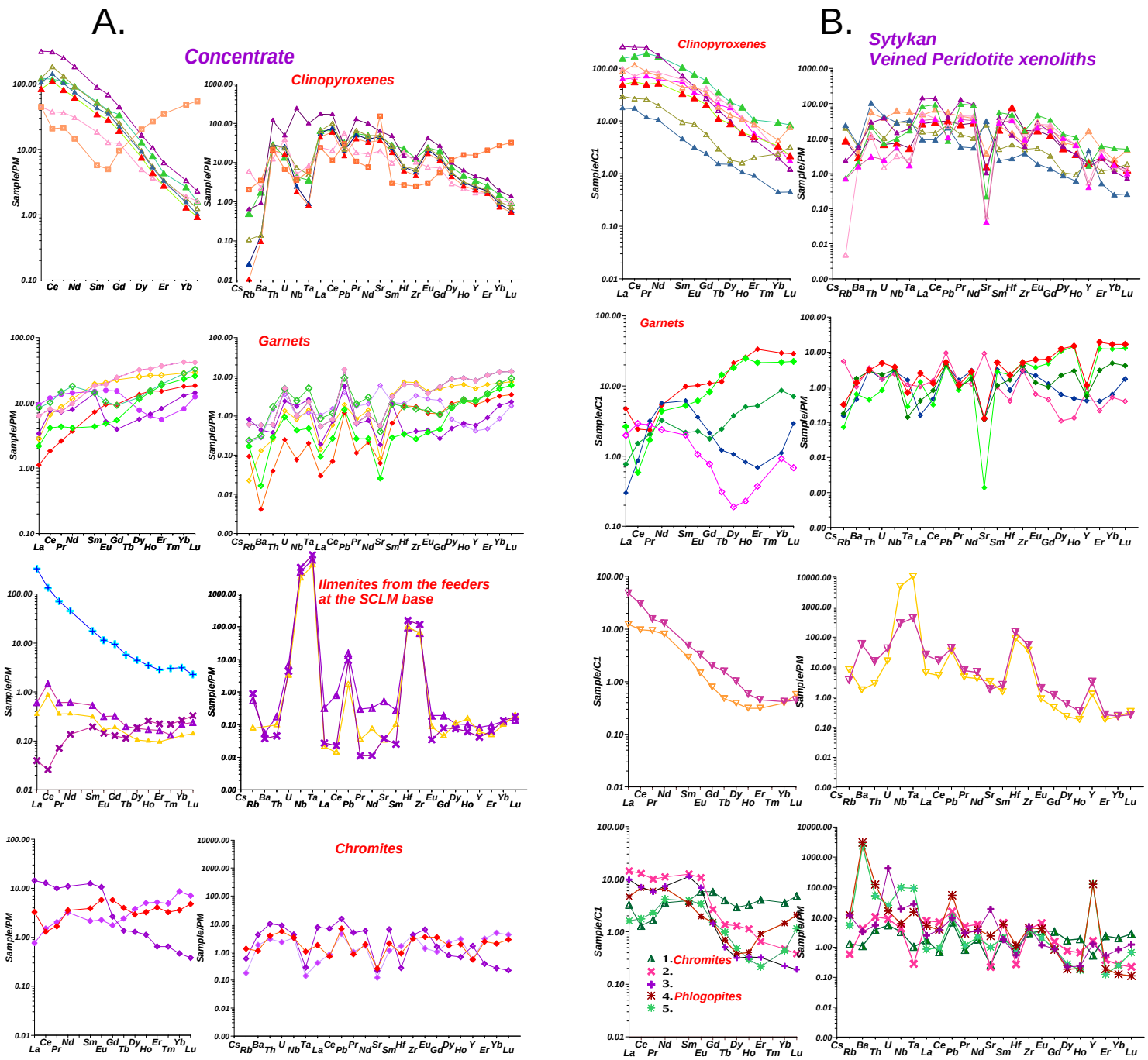
A.
B.
Concentrate
Clinopyroxenes
Sytykan
Veined Peridotite xenoliths
Garnets
Ilmenites from the feeders
at the SCLM base
Chromites
1.Chromites
2.
3.
4.Phlogopites
5.
Sample/PM
Sample/C1

Fig.13

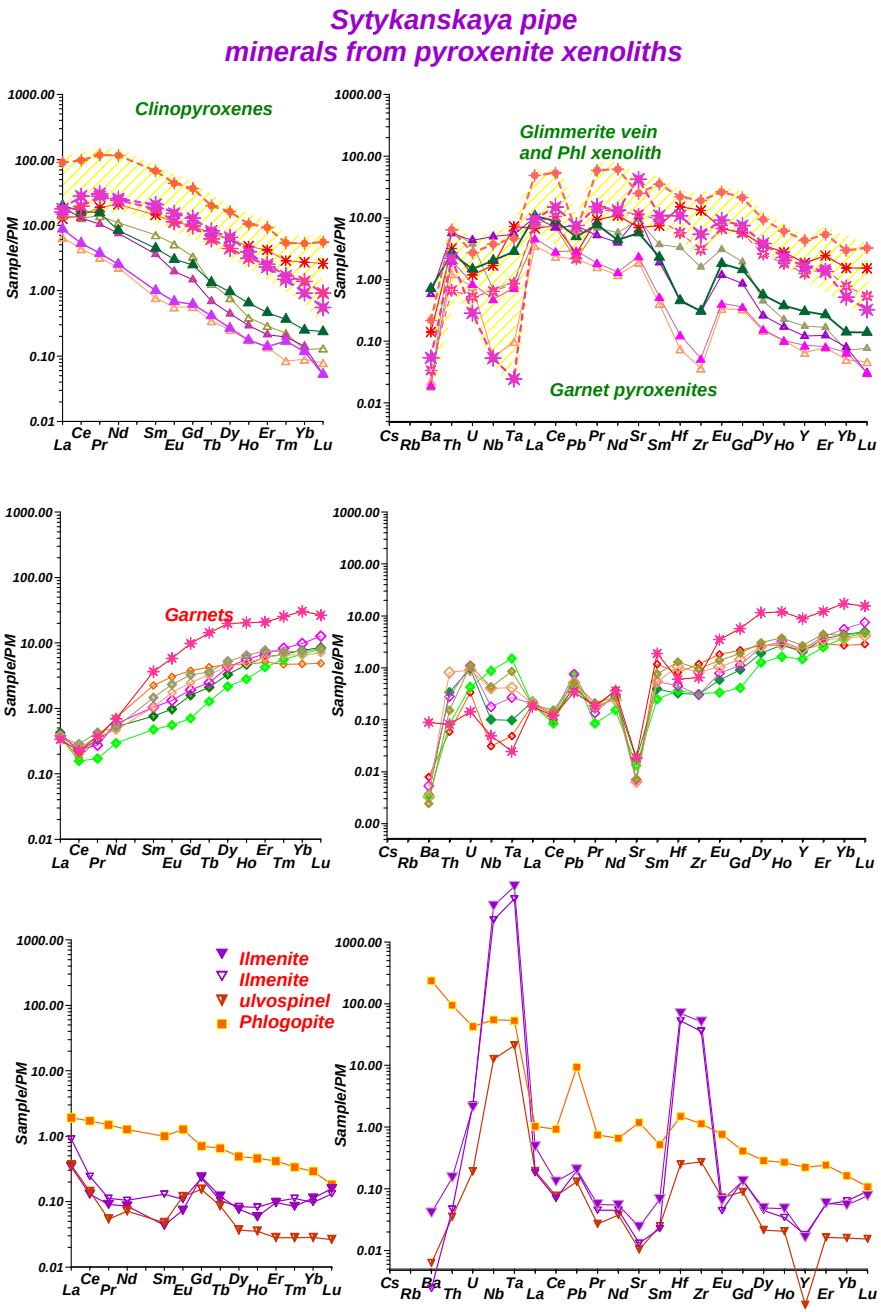
Sytykanskaya pipe
minerals from pyroxenite xenoliths
Clinopyroxenes
Glimmerite vein
and Phl xenolith
Garnet pyroxenites
Garnets
Ilmenite
Ilmenite
ulvospinel
Phlogopite
Sample/PM
1000.00
100.00
10.00
1.00
0.10
0.01
0.00
La Ce Pr Nd Sm Eu Gd Tb Dy Ho Er Tm Yb Lu
Cs Rb Ba Th U Nb Ta La Ce Pb Pr Nd Sr Sm Hf Zr Eu Gd Dy Ho Y Er Yb Lu

Fig.14

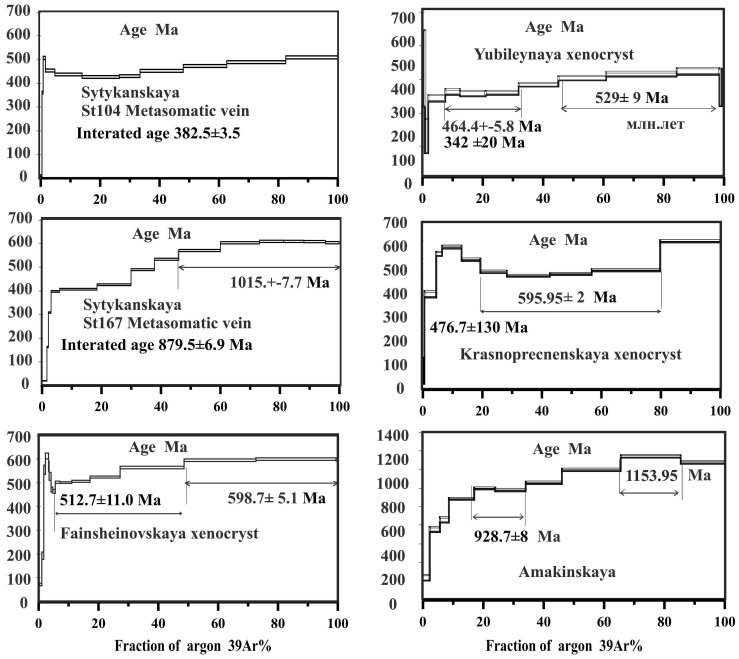

Fig.15

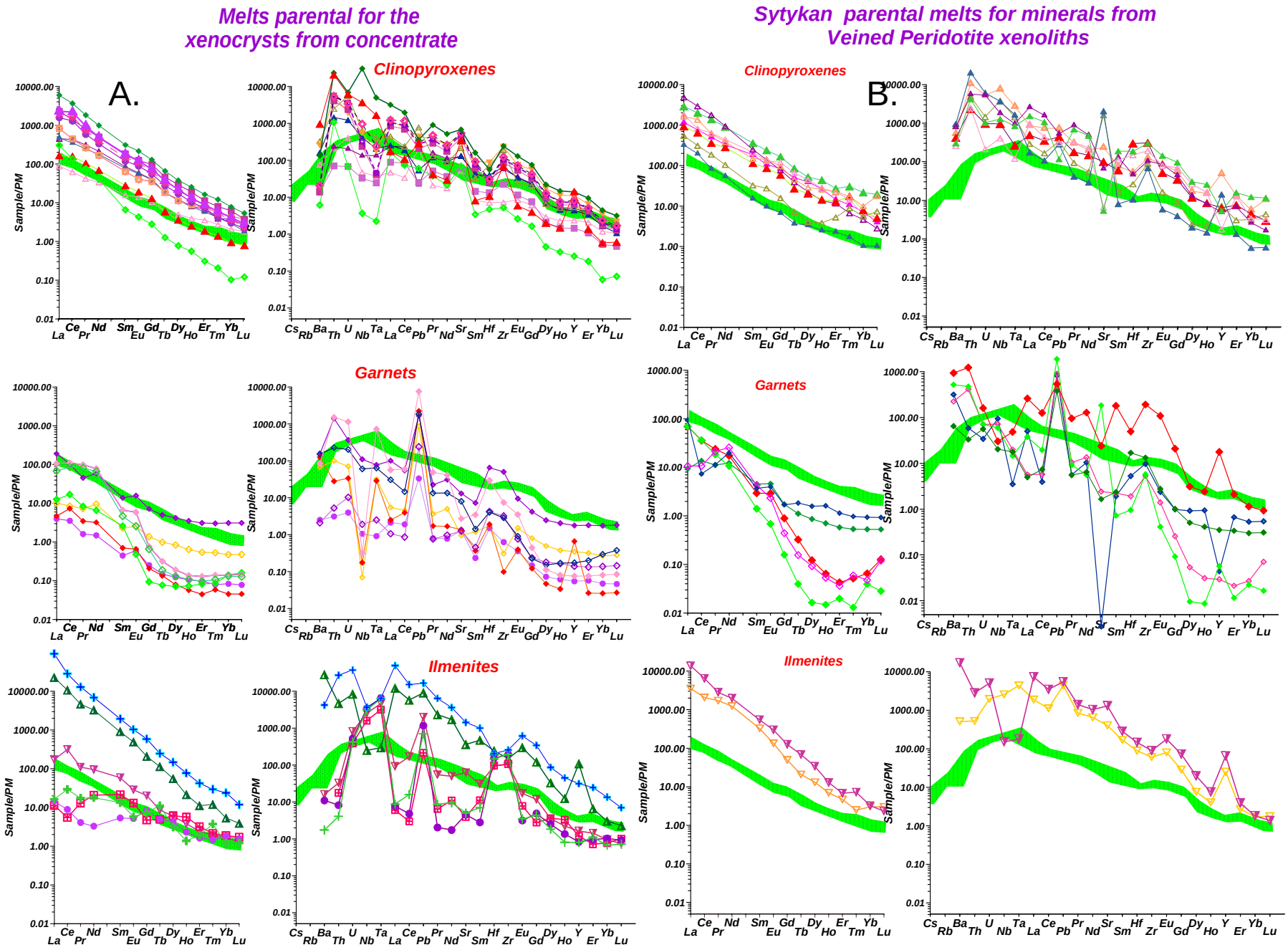
Melts parental for the xenocrysts from concentrate
Sytykan parental melts for minerals from Veined Peridotite xenoliths
A.
B.
Clinopyroxenes
Clinopyroxenes
Garnets
Garnets
Ilmenites
Ilmenites
Sample/PM
10000.00
1000.00
100.00
10.00
1.00
0.10
0.01
La Ce Pr Nd Sm Eu Gd Tb Dy Ho Er Tm Yb Lu
Cs Rb Ba Th U Nb Ta La Ce Pb Pr Nd Sr Sm Hf Zr Eu Gd Dy Ho Y Er Yb Lu

Fig.16

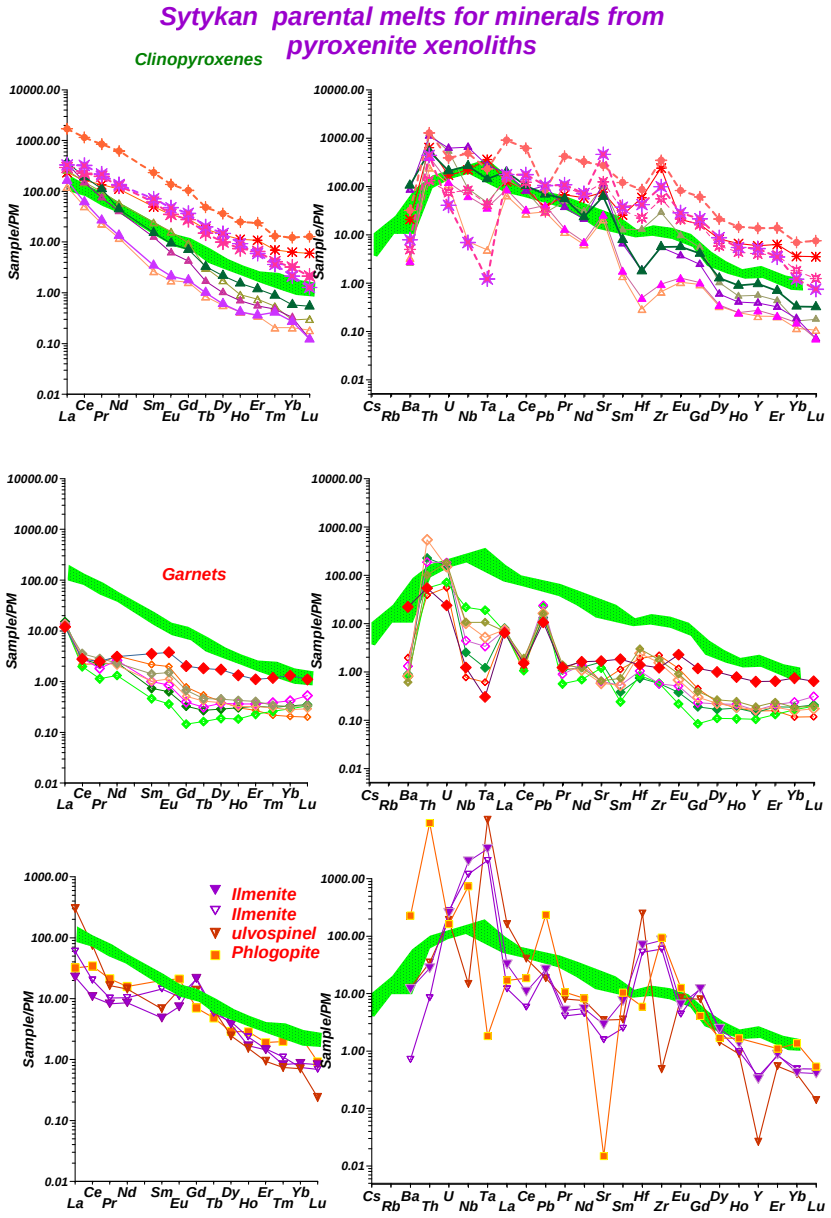
Sytykan parental melts for minerals from pyroxenite xenoliths
Clinopyroxenes
Garnets
Ilmenite
Ilmenite
ulvospinel
Phlogopite
Sample/PM
10000.00
1000.00
100.00
10.00
1.00
0.10
0.01
La Ce Pr Nd Sm Eu Gd Tb Dy Ho Er Tm Yb Lu
Cs Rb Ba Th U Nb Ta La Ce Pb Pr Nd Sr Sm Hf Zr Eu Gd Dy Ho Y Er Yb Lu

Fig.17

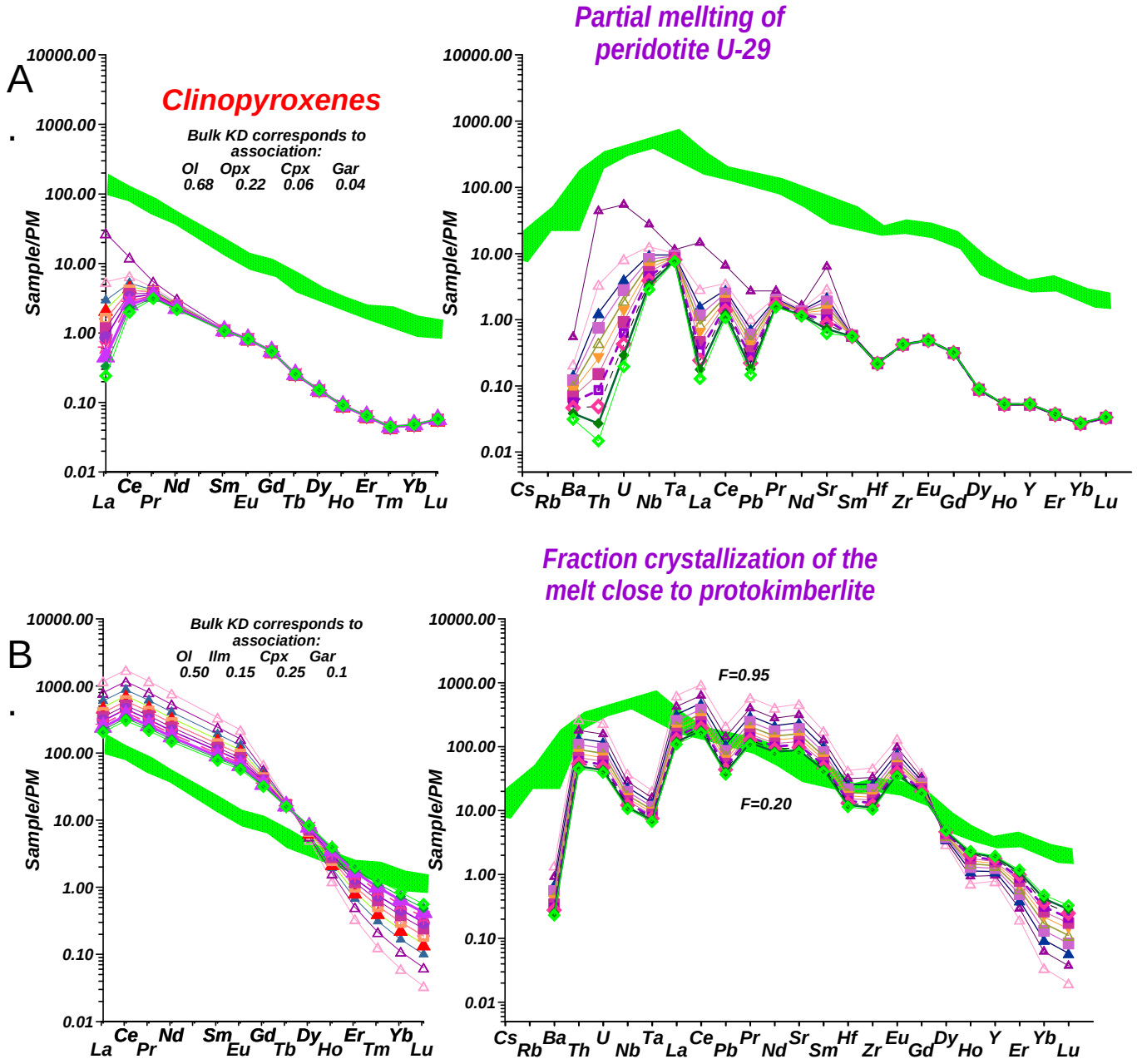
A
Clinopyroxenes
Bulk KD corresponds to association:
Ol Opx Cpx Gar
0.68 0.22 0.06 0.04
Partial mellting of peridotite U-29
Sample/PM
10000.00
1000.00
100.00
10.00
1.00
0.10
0.01
La Ce Pr Nd Sm Eu Gd Tb Dy Ho Er Tm Yb Lu
Cs Rb Ba Th U Nb Ta La Ce Pb Pr Nd Sr Sm Hf Zr Eu Gd Dy Ho Y Er Yb Lu
B
Bulk KD corresponds to association:
Ol Ilm Cpx Gar
0.50 0.15 0.25 0.1
Fraction crystallization of the melt close to protokimberlite
F=0.95
F=0.20

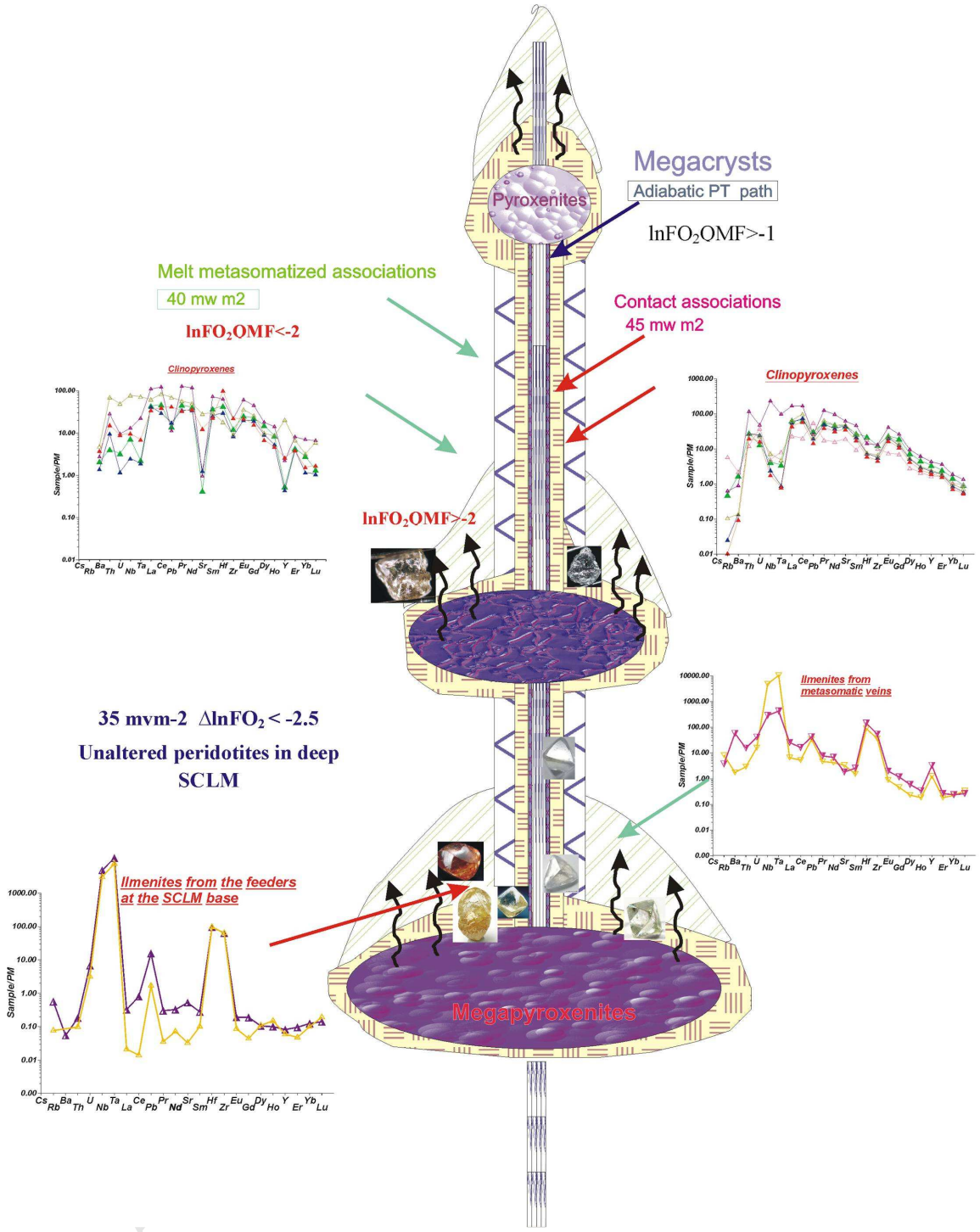
Megacrysts
Adiabatic PT path
Pyroxenites
lnFO2QMF>-1
Melt metasomatized associations
40 mw m2
lnFO2QMF<-2
Contact associations
45 mw m2
Clinopyroxenes
Clinopyroxenes
lnFO2QMF>-2
35 mvm-2 ΔlnFO2 < -2.5
Unaltered peridotites in deep SCLM
Ilmenites from metasomatic veins
Ilmenites from the feeders at the SCLM base
Megapyroxenites
Sample/PM

Alakit filed Opx – Gar and monomineral Gar and Px geotherms are close to 35mwm-2 at SCLM base and 600^{o}C near Moho

Mantle xenoliths from Sytykan pipe represent highly metasomatized mantle column created according to $^{40}Ar/3^{9}Ar$ 1120,1050, 600, 385 Ma

Xenocryst of Cr- diosides are close in TRE to protokimberlites while veined xenoliths show inflected patterns and

Layered structure of the mantle column consists of 5 large units showing evolution between the kimberlite stages

Pyroxenite horizon 3.5-4.5 GPa is most metasomatized alkaline amphibole, Cpx-Phl and Cr- Ilm veins from different stages

Fig.1

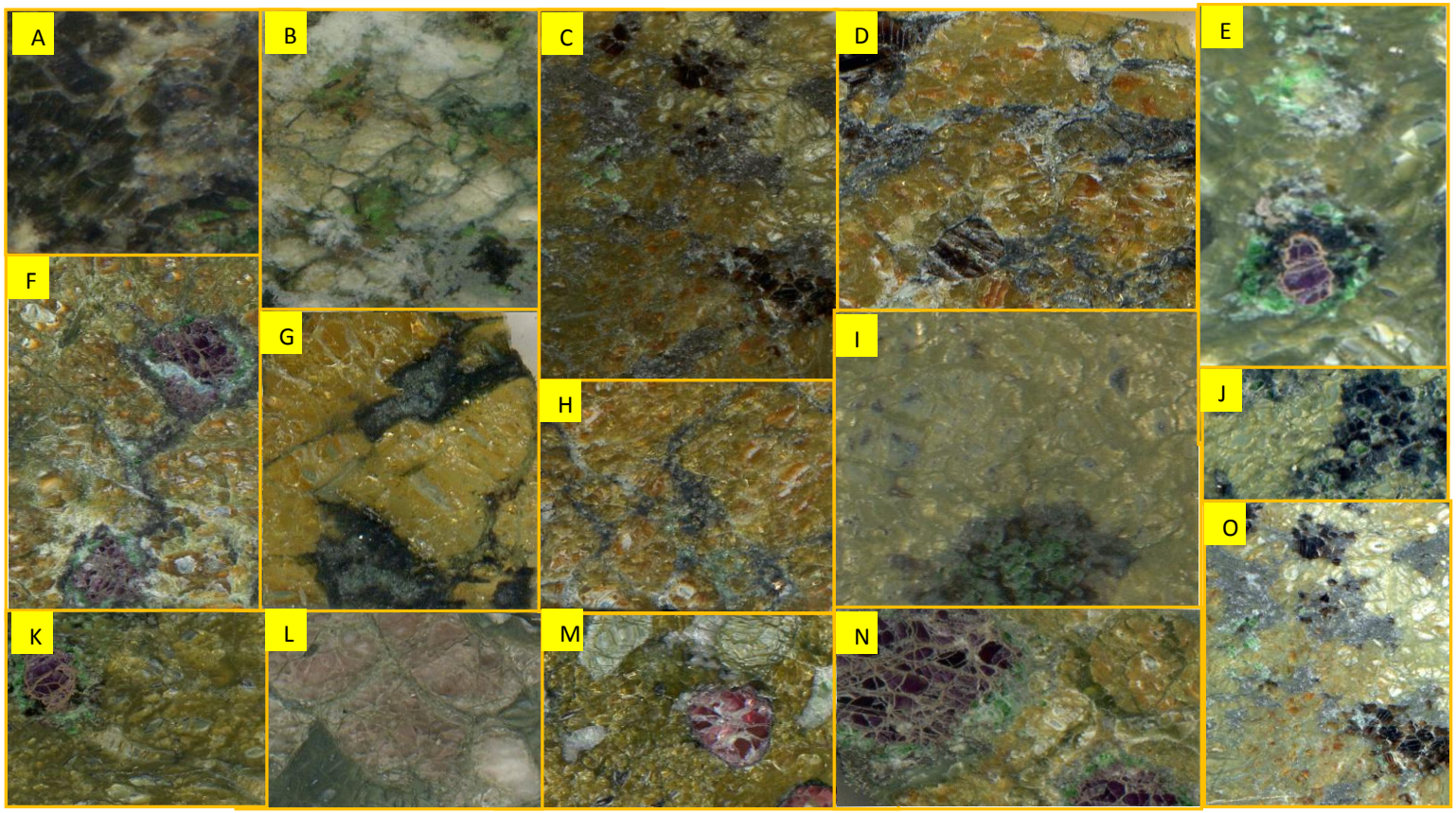

Fig.1. Photo images of the mantle xenoliths from Sytykanskaya pipe.

A. Glimmerite like veins in peridotites. B. Stock work of the metasomatic veins in the peridotite . C. Nest of the metasomatic Cpx, Phl , Ilm in peridotites. D. The nets of the metasomatic Ilm – Cr- Di and Phl in peridotite. E. Coronas of Phl –Cpx and Ulvospinels in garnets. F. The metasomatic microveins and coronas of Cpx and Phl on garnets. G. Ilm – Cpx , Phl and carbonates on garnets. H. Microveins of Ilm – Cpx and carbonates in peridotites. I. Symplectites of Ti – rich spinels, Cpx and Phl after garnets. J. Sp –Ilm – Cpx aggregates in peridotites. K. Coronas of Cpx and Phl on garnets. L. Substituted eclogite. M. Gar garzburgite. N. Cpx corona on garnets. O. Disseminated nests of Phl and Cpx in peridotite.

Fig.2

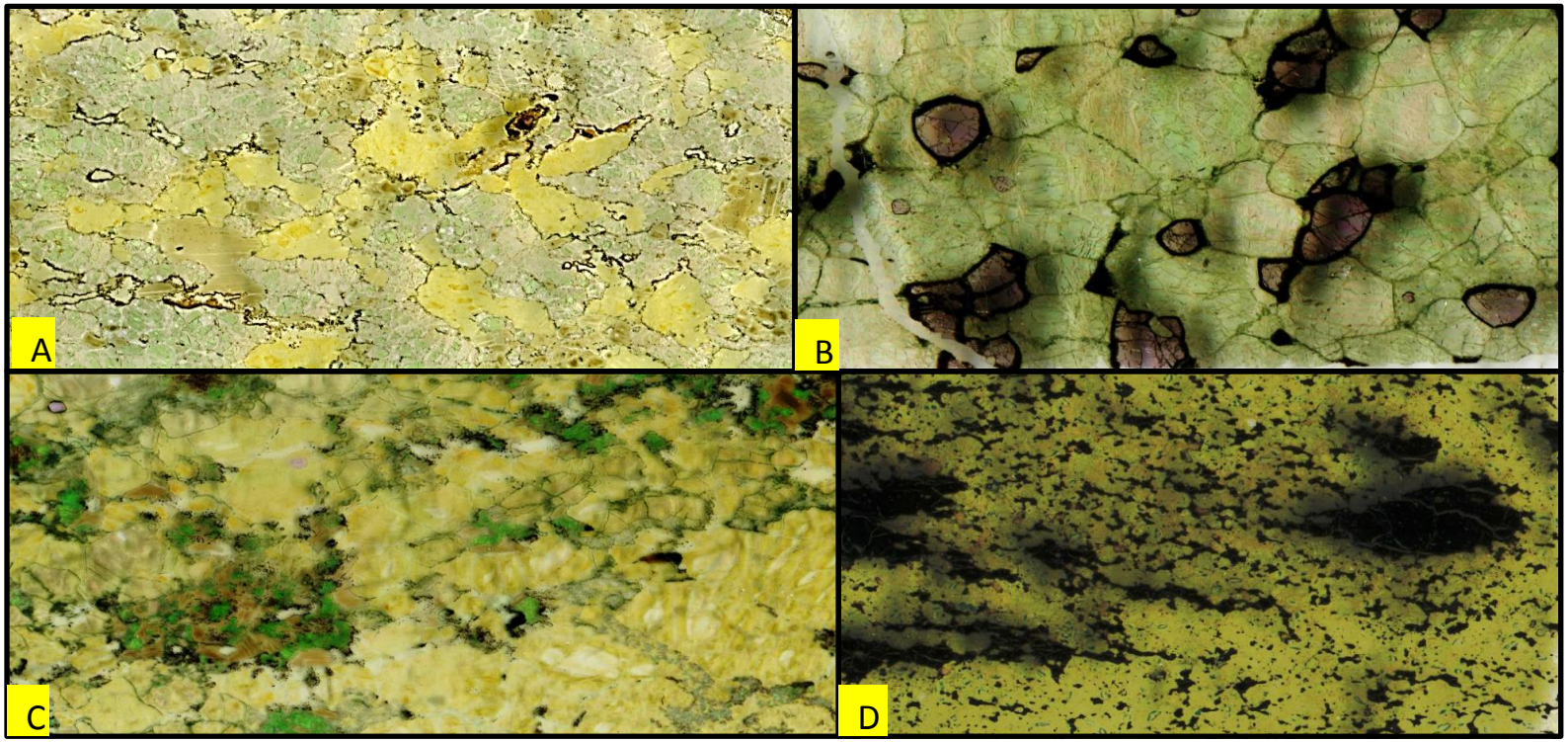

Fig. 2. Photo of the Thin sections of mantle xenoliths from Sytykanskaya pipe A. Details of the Cpx- Phl veins. B. Garnet websterite. C. Glimmerite nests with the alkaline amphibole, Cr –diopside, phlogopite, ulvospinel, ilmenite in peridotite. D. Ilmenite – bearing peridotite with Cr- diopside and relics of garnets.

Fig.3

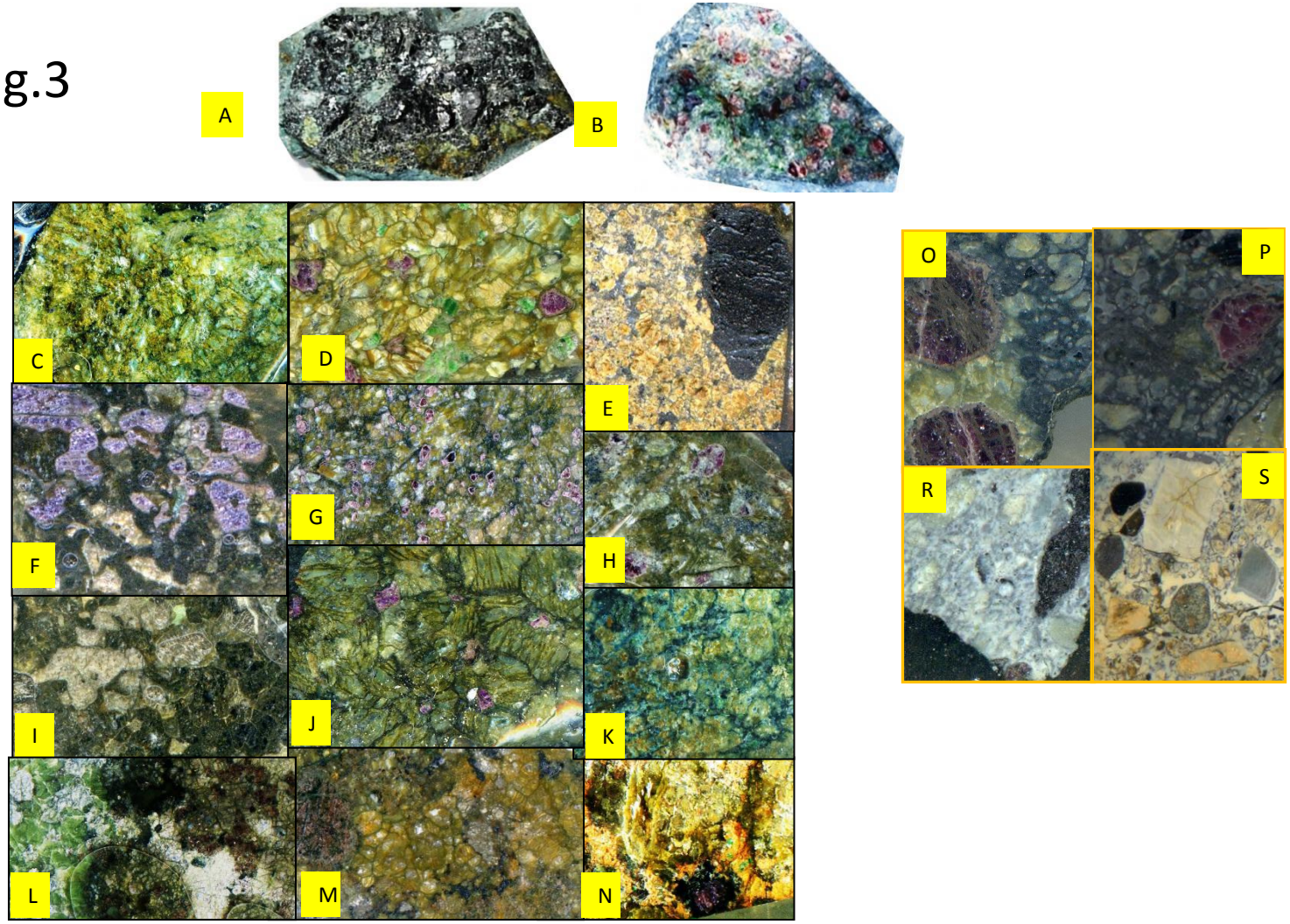

Fig. 3. Photo images of the mantle xenoliths from Sytykanskaya pipe. A. Picroilmenite nodule in contact with the lherzolite ; B. Garnet websterite; C. Sp – lherzolite with the Ilm – Cpx veinlets. D. Granular garnet lherzolite; E. Serpentinizied harzburgite with large Ilm grain and veinlets. F. Serpentinized garnet lherzolite coarse grained; G. Serpentinized garnet lherzolite fine grained; H. Serpentinized garnet lherzolite coarse grained with Ilm-Phl nests; I. Sp harzburgite; J. Gar harzburgite; K. Peridotite with intergranular Ilm –Cpx veinlets; L. Contact zone of orthopyroxenite with depleted Sp lherzolite; M. Lherzolite with the garnets substituted by secondary Phl – SP – Gar pyroxene aggregate. N. Peridotite with the Gar grains surrounded by ilmenites and secondary Cr- diopside. O. - P. Porphyric kimberlite with the fragments of microxenoliths. R.-S. Autolithoc breccia